Aus dem
Helmholtz-Zentrum München
Comprehensive Pneumology Center (CPC)

Clinical proteomics of pneumonia – antibody-mediated immunopathology in COVID-19

Dissertation
zum Erwerb des Doctor of Philosophy (Ph.D.) an der Medizinischen Fakultät der Ludwig-Maximilians-Universität München

vorgelegt von
Anna Semenova

aus
Seversk / Russische Föderation

Jahr
2024

Mit Genehmigung der Medizinischen Fakultät der
Ludwig-Maximilians-Universität München

Erstes Gutachten:	Prof. Dr. Jürgen Behr
Zweites Gutachten:	Prof. Dr. Andreas Pichlmair
Drittes Gutachten:	Prof. Dr. Axel Imhof
Viertes Gutachten:	Priv. Doz. Dr. Leo Nicolai

Dekan: Prof. Dr. med. Thomas Gudermann

Tag der mündlichen Prüfung: 09.12.2024

Table of contents

Table of contents **1**

Abstract **4**

List of figures **6**

List of tables **7**

List of abbreviations **8**

1. Introduction **12**

1.1. Overview of the coronavirus disease 2019 12

1.2. SARS-CoV-2 structure and mechanism of the host cell entry 13

1.3. Clinical manifestations and pathophysiology of COVID-19 18

1.3.1. Endothelial dysfunction and thromboinflammation 19

1.3.2. Dysregulation of the complement system 20

1.3.3. Extrapulmonary manifestations 21

1.4. Immunopathology of severe COVID-19 23

1.4.1. B cell-mediated immunopathology 24

1.4.2. Role of autoantibodies in the development of severe COVID-19 27

1.5. Pathophysiology of long COVID 31

Main question **34**

2. Material and Methods **35**

2.1. Human participants and sample availability: Chicago cohort 35

2.1.1. Definition of pneumonia subgroups 35

2.1.2. Sample collection 36

2.1.3. Visualization of the clinical metadata 37

2.2. Human participants and sample availability: Munich cohort 38

2.2.1. Experimental design 38

2.2.2. Selection of the control samples: Munich cohort 39

2.3. Sample processing methods 41

2.3.1. Protein extraction from donor lung tissue 41

2.3.2. Differential antigen capture assay (DAC) 41

2.3.3. Fluid sample preparation 42
2.3.4. LC-MS/MS analysis 43
2.3.5. Proteomics raw data processing 43
2.4. Proteomics data analysis 44
2.4.1. Principal component analysis (PCA) 44
2.4.2. Co-expression network analysis 44
2.4.3. Over-representation analysis (ORA) 45
2.4.4. Gene set variation analysis (GSVA) 45
2.4.5. Analysis of protein circulation between plasma and BALF in pneumonia patients . 46
2.4.6. Analysis of the autoreactivity data 46
2.4.7. Modeling of time and severity effects on the autoreactivities in the Munich cohort . 47
1.1.1 Calculation of the autoantigen score 48
1.1.2 Analysis of the associations between autoantigens and clinical parameters 48
2.5. Single-cell RNA sequencing data analysis 49
2.5.1. Pre-processing 49
2.5.2. Downstream analysis of single-cell data 49
2.5.3. Annotation of B and plasma cells 50
2.5.4. BCR-seq analysis 53
2.5.5. B cell clone/clonotype definition 53
3. Results 55
3.1. Proteomic analysis of biofluids of patients with infectious lung diseases 55
3.1.1. Demographics of the SCRIPT cohort 55
3.1.2. Identification of pneumonia-specific molecular signatures upon the intubation 59
3.1.3. Dynamics of pneumonia-specific molecular signatures in BALF 63
3.1.4. Presence of plasma proteins in the lung environment in COVID-19 patients is associated with a decreased P/F ratio 66
3.1.5. The COVID-19-specific signature consists of lung-abundant and plasma-abundant proteins 69
3.2. Single-cell multi-omic analysis of COVID-19-induced B cell populations 73
3.2.1. Molecular mechanisms of self-tolerance in B cells 73
3.2.2. COVID-19-specific antibody variable domains are associated with disease severity 77
3.2.3. Revealing cellular identities of COVID-19-specific B cell clones 80

3.3. Study of autoantibody binding repertoire of acute COVID-19 patients 85

3.3.1. COVID-19 and autoimmunity 85

3.3.2. Demographics of the Munich cohort 86

3.3.3. Comparative analysis of autoantibody repertoire of two independent COVID-19 cohorts 89

3.3.4. Dynamics of the autoimmune response in COVID-19 patients 94

3.3.5. Associations between putative autoantigens and clinical parameters 98

Limitations of the study 104

Discussion 106

Appendix 108

Acknowledgments 110

Affidavit 111

Confirmation of congruency 112

Curriculum vitae 113

List of publications 115

Bibliography 116

Abstract

Infectious respiratory diseases comprise the 4th most fatal group of diseases worldwide. COVID-19 patients exhibit unique pathophysiology, which is not observed in pneumonia caused by other respiratory viruses or bacterial pathogens with similar severity. Most COVID-19 studies lack appropriate comparisons to other viral types of pneumonia, hindering the development of biomarkers for early identification of high-risk COVID-19 patients. This study aims to investigate the humoral immune responses and identify distinct proteomics signatures associated with COVID-19 compared to influenza and bacterial pneumonia. Moreover, the project specifically focuses on unraveling autoimmune aspects of severe COVID-19.

I applied proteomic profiling to bronchoalveolar lavage fluid (BALF) and plasma samples from pneumonia patients of the SCRIPT cohort at Northwestern Memorial Hospital (NMH) Chicago and assessed the enrichment of molecular signatures unique to COVID-19 (n=13), influenza (n=7), and bacterial pneumonia (n=6) patients at up to five time points after intubation in the intensive care unit. Emphasizing persistent proteomic signatures during hospitalization, I outlined plasma- and lung-abundant proteins and revealed upregulation of immunoglobulin production in the bronchoalveolar environment specific to SARS-CoV-2 infection.

Secondly, utilizing a single-cell multi-omic dataset of COVID-19 patients (n=102) at mild and severe stages, I identified the overrepresentation of immunoglobulin V-domains connected to COVID-19 severity. Furthermore, my findings elucidated the transcriptomic and surface protein markers of plasma cell populations, contributing to COVID-19-specific humoral immune responses observed in the BALF of Chicago cohort.

Lastly, I applied a Differential Antibody Capture (DAC) assay on two independent cohorts of acute COVID-19 patients to capture plasma antibodies that show affinity to native lung proteins. I identified 93 putative autoantibody targets specific to COVID-19 patients, with 19 targets in common in both cohorts. Among the putative autoantigens, I observed extracellular matrix, complement regulation, nuclear antigens, and immune regulatory proteins. Besides that, the dynamic changes in autoantibody patterns were correlated with clinical parameters, revealing the effect of individual autoantibodies and overall autoreactivity on severe COVID-19 immunopathology. This was demonstrated by the significant correlation of the cumulative autoantigen coefficient with a length of intubation, aspartate transaminase (AST), alanine transaminase (ALT), Troponin I, and procalcitonin, indicating prolonged recovery periods, multi-organ damage, and increased susceptibility to secondary bacterial infections.

My work improves the understanding of unique proteomic features specific to COVID-19 pneumonia, revealing the upregulation of complement cascade, platelet degranulation proteins, and immunoglobulins in the lung environment. Besides that, the research sheds light on the develop-

ment of autoantibody responses during the acute phase of infection, thus providing potential biomarkers to improve the diagnosis in uncertain cases and identify severe COVID-19 trajectories at an early stage.

List of figures

Figure 1.2: Mechanisms of SARS-CoV-2 entry to the host cells.

Figure 1.3: Underlying mechanisms of COVID-19 pathophysiology.

Figure 1.4.1: The immunopathology of COVID-19.

Figure 1.4.2: Potential mechanisms and examples of aABs in COVID-19.

Figure 1.5: Immunopathology of long COVID.

Figure 2.2.2: Schema of control cohort selection (the Munich cohort).

Figure 3.1.1: The SCRIPT cohort demographics.

Figure 3.1.2: Pneumonia-specific protein signatures can be detected in BALF and plasma on the day of intubation.

Figure 3.1.3: Pneumonia-specific signatures detected in BALF during intubation persist longitudinally.

Figure 3.1.4: Elevated levels of plasma proteins in the bronchoalveolar environment of COVID-19 patients are associated with a decreased P/F ratio.

Figure 3.1.5: COVID-19 patients contain both plasma-abundant and lung-abundant immunoglobulins, distinguishing them from patients with other types of pneumonia.

Figure 3.2.1: B cell development.

Figure 3.2.2: Variable fragments of BCR are predictive of the COVID-19 severity.

Figure 3.2.3: COVID-19-specific B cells display antibody-producing and autoimmune-like phenotypes.

Figure 3.3.2: Demographics of the Munich cohort.

Figure 3.3.3: Comparative analysis of the putative auto-antigen repertoire of two independent COVID-19 cohorts.

Figure 3.3.4: Longitudinal profiling of autoreactivities in mild and severe COVID-19 patients.

Figure 3.3.5: Associations between the presence of putative autoantigens and clinical parameters of two independent severe COVID-19 cohorts.

List of tables

Table 2.5.3: Transcriptomic markers of B and plasma cell subsets.

Table 3.2.3: Transcriptomic markers of dividing plasmablast and IgA high plasma cell clusters.

Table A1: Baseline characteristics of the Chicago cohort on the initial day of the intubation.

Table A2: Baseline characteristics of the Munich cohort at the first time window (0-11 days).

List of abbreviations

ARDS Acute respiratory distress syndrome

aAB Autoantibodies

ABCC3 Canalicular multispecific organic anion transporter 2

ACE2 Angiotensin-converting enzyme

AFF3 AF4/FMR2 family member 3

AKI Acute kidney injury

ALAD Delta-aminolevulinic acid dehydratase

ANAs Antinuclear antibodies

ANCAs Anti-cytoplasmic neutrophil antibodies

APOC3 Apolipoprotein C-III

APOE Apolipoprotein E

APOH Beta-2-glycoprotein 1

APS Anti-phospholipid syndrome

BAL Bronchoalveolar lavage

BASP1 Brain abundant membrane attached signal protein 1

BCR B cell receptor

CCDC178 Coiled-coil domain containing 178.

CCT6B T-complex protein 1 subunit zeta-2

CD69 Early activation antigen CD69

CD83 CD83 antigen

CFHR1 Complement factor H-related protein 1

CFHR2 Complement factor H-related protein 2

CFHR5 Complement factor H-related protein 5

CITE-seq Cellular indexing of transcriptomes and epitopes

COLEC10 Collectin-10

COLEC11 Collectin-11

COVID-19 Coronavirus disease 2019

CPS1 Carbamoyl-phosphate synthase

CRP C-reactive protein

DAC Differential antigen capture assay

DEGs Differentially expressed genes

E Envelope protein

ECMO Extracorporeal Membrane Oxygenation

EPCR Endothelial cell protein C receptor

FCN2 Ficolin-2

FGL1 Fibrinogen-like protein 1

FN1 Fibronectin

FTLFerritin light chain

GCNA Gene co-expression network analysis

GM-CSF Granulocyte-macrophage colony-stimulating factor

GOT Aspartate aminotransferase

GPCR G protein-coupled receptors

GPT Alanine aminotransferase

GPX3 Glutathione peroxidase 3

GR Glucocorticoid receptor

GSTO1 Glutathione S-transferase omega-1

GSVA Gene set variation analysis

HLA-DMB HLA class II histocompatibility antigen, DM beta chain

HLA-G Soluble HLA class I histocompatibility antigen, alpha chain G

HMBS Porphobilinogen deaminase

HSPA12B Heat Shock Protein Family A (Hsp70) Member 12B

HSPA2 Heat shock-related 70 kDa protein 2

HVGs Highly variable genes

IFIT1 Interferon-induced protein with tetratricopeptide repeats 1

IGF1R Insulin-like growth factor 1 receptor alpha chain

IGFBP6 Insulin-like growth factor-binding protein 6

IL1RAP Interleukin-1 receptor accessory protein

Il-6 Interleukin-6

IL6R Interleukin-6 receptor subunit alpha

ITIH4 35 kDa inter-alpha-trypsin inhibitor heavy chain H4

KLF6 Krueppel-like factor 6

KLKB1 Plasma kallikrein heavy chain

KMT2C Histone-lysine N-methyltransferase 2C

KRT31 Keratin, type I cuticular Ha1

KRT84 Keratin, type II cuticular Hb4

KRT86 Keratin, type II cuticular Hb6.

LC long COVID

LFQ Label-free quantification

LTB Lymphotoxin-beta

LTBP1 Latent-transforming growth factor beta-binding protein 1

LY96 Lymphocyte antigen 96

LYVE1 Lymphatic vessel endothelial hyaluronic acid receptor 1

M Membrane protein

MASP2 Mannan-binding lectin serine protease 2 A chain

MBL Mannose-binding lectin

MFAP5 Microfibrillar-associated protein 5

MS4A1 B-lymphocyte antigen CD20

N Nucleocapsid protein

NK natural killer

NR4A2 Nuclear receptor subfamily 4 group A member 2

NTD N-terminal domain

PACSIN2 Protein kinase C and casein kinase substrate in neurons protein 2

PaO2/FiO2 Partial pressure of arterial oxygen to fraction of inspired oxygen

PASC Post-acute sequelae of SARS-CoV-2 infection

PBMCs Peripheral blood mononuclear cells

PEBP1 Hippocampal cholinergic neurostimulating peptide

PEEP Positive end-expiratory pressure

POSTN Periostin

PPL Periplakin

PRDX1 Peroxiredoxin-1

PRDX5 Peroxiredoxin-5

pre-B cell Precursor B cell

pro-B cell Progenitor B cell

RAAS Renin-angiotensin-aldosterone system

RBD Receptor-binding domain

RBP4 Plasma retinol-binding protein

RELN Reelin

ROS Reactive oxygen species

S Spike protein

SAA2 Serum amyloid A-2 protein

SAA4 Serum amyloid A-4 protein

SAMM50 Sorting and assembly machinery component 50 homolog

scBCR-seq Single-cell B-cell receptor sequencing

SELENOP Selenoprotein P

SERPINA10 Protein Z-dependent protease inhibitor

SERPINF2 Alpha-2-antiplasmin

SLE Systemic Lupus Erythematosus

SOFA Sequential Organ Failure Assessment

SPTB Spectrin beta chain, erythrocytic

ST3GAL6 Type 2 lactosamine alpha-2,3-sialyltransferase

SVEP1 Sushi, von Willebrand factor type A, EGF and pentraxin domain-containing protein 1

TEM T effector memory

TEP1 Telomerase protein component 1

TFPI Tissue factor pathway inhibitor

TSKU Tsukushin

t-SNE t-distributed Stochastic Neighbor Embedding

TUBB1 Tubulin beta-1 chain

TXN Thioredoxin

UMAP Uniform Manifold Approximation and Projection

YWHAG 14-3-3 protein gamma, N-terminally processed

1. Introduction

1.1. Overview of the coronavirus disease 2019

According to the National Health Institutes, pneumonia is defined as a lung infection in which alveoli become filled with fluid or pus (1). Pneumonias can be caused by molecular pathogens of bacterial, viral, or fungal origin and common symptoms can vary from mild to severe, including cough, fever, chills, and difficulty respiring.

One of the most recent examples of acute pneumonia is severe acute respiratory syndrome coronavirus 2 (SARS-CoV-2), which emerged in Wuhan, China, in December 2019 and rapidly caused a worldwide pandemic, leading to more than 5.4 million deaths and 287 million individuals affected by December 31, 2021 (2).

This became possible due to the wide range of SARS-CoV-2 transmission mechanisms. Among them are direct contact, and airborne transmission through droplets (2). The primary mechanism for SARS-CoV-2 was shown to be droplets or aerosols and direct contact with infected individuals (3). The median incubation period of SARS-CoV-2 is estimated to reach 5.1 days, and most patients develop symptoms within 11.5 days of infection (4). Infected with SARS-CoV-2 individuals develop respiratory illness ranging from mild to severe and lethal outcomes characterized by acute respiratory failure, septic shock, and multiorgan failure. Besides that, 17.9% to 33.3% of infected individuals never develop symptoms (5). A recently published meta-analysis reported that severe disease course was noted in 23% of the infected patients, while 6% were deceased (6).

The virus targets the respiratory system, leading to the increased influx of immune cells, endothelial cell activation, and accumulation of fluid in the lungs, resulting in breathing complications and, in critical cases, acute respiratory distress syndrome (ARDS). Among common manifestations of COVID-19 include fever, fatigue, dry cough, alternations of smell and taste, and shortness of breath (7). COVID-19 is not limited to the respiratory system, and multiple studies have reported extrapulmonary symptoms (8). Additionally, COVID-19 clinical manifestations can persist after the acute phase of the disease in approximately 10% of the infected individuals, characterized as long COVID-19 (9).

The main risk factor for susceptibility to severe pneumonia caused by COVID-19 is age; life-threatening cases become more common in patients aged 65 years onward (6). Another critical factor is sex, and a retrospective evaluation of the mortality rates in acute care hospitals in the United States of America (USA) in 2020 revealed a higher mortality rate in male (12.5%) compared to female patients (9.6 %) (10). Higher mortality in SARS-CoV-2-infected male patients is

hypothesized to be caused by impaired T cell activation and higher levels of fucosylated anti–SARS–CoV–2 antibodies (ABs) (11). Additionally, patients with pre-existing medical conditions had six times higher hospitalization rates than those without medical conditions (45.4% vs. 7.6%) based on the reported cases in January-May 2020 (7). Main comorbidities imposing risk of developing severe COVID-19 included diabetes, hypertension, obesity, chronic lung disease, cardiovascular disease, chronic kidney disease, and chronic liver disease.

Several measures have been implemented to prevent the active spread of the virus, including social distancing and everyday use of medical masks (5). In 2020-2021, many countries established lockdown protocols, which reduced infection rates and decreased hospital loads, providing necessary care for severe and critical COVID-19 patients (12). More importantly, the pandemic significantly impacted global healthcare systems and the economy. During 2020-2022 several governments imposed traveling restrictions and quarantine, resulting in the service industry suffering from reduced customer activity, which led to financial difficulties and massive job loss. Furthermore, the COVID-19 pandemic-imposed challenges to the management of health workers and medical supplies, as well as facility usage (13). Finally, the pandemic, besides its direct effects on the health of individuals, increased morbidity risk for other treatable diseases, which lead to notable disruption in healthcare services (12). These factors lead to long-term economic consequences triggering fears of financial crisis and recession and strong socio-economic effects on many aspects of human life.

1.2. SARS-CoV-2 structure and mechanism of the host cell entry

SARS-CoV-2 is a positive-sense, single-stranded RNA virus, which belongs to the Coronoviridae family (16). It structurally and phylogenetically resembles SARS-CoV and MERS-CoV and consists of four main proteins: spike (S), envelope (E) glycoprotein, nucleocapsid (N), and membrane (M) protein. Additionally, it includes 16 nonstructural proteins and 5-8 accessory proteins (14).

The S, E, and M proteins form the virion membrane, while N interacts with viral genomic RNA to remain confined in the virion. The S protein facilitates virus entry and consists of two subunits: S1 and S2, which are cleaved by the furin protein convertase in the Golgi apparatus during the virus maturation process in the host cell. The primary function of S1 is to bind to the host cell receptor in the new cell, and S2 mediates membrane fusion, allowing virus entry.

Additionally, the S1 subunit can be further divided into a receptor-binding domain (RBD) and an N-terminal domain (NTD), facilitating viral entry into the host cell and serving as a potential target for neutralization in response to vaccines.

The primary host receptor utilized by SARS-CoV-2 for cell entry is angiotensin-converting enzyme (ACE2), a carboxypeptidase in the renin-angiotensin-aldosterone system (RAAS). This receptor is ubiquitously expressed in the lower respiratory tract, making it a primary site of COVID-19 infection. Besides the respiratory system, ACE2 is also detected in other organs, specifically the heart, liver, kidney, small intestine, and brain (15), which is believed to account for multi-organ involvement in some COVID-19 patients (16).

Upon interaction with ACE2, the S1 subunit changes its conformation and binds the receptor via the RBD, followed by the fusion between viral and cellular membranes and the entrance of the virus into the host cell. The virus attachment process is followed by interaction between the S2 subunit and the host transmembrane serine protease 2 (TMPRSS2), which governs cell entry and viral replication (17).

The replication process starts with the translation of the SARS-CoV-2 genome into two large polyproteins, ORF1a and ORF1b (Fig.1.2). These polyproteins undergo proteolytic cleavage by the viral proteases PLpro and Mpro, yielding 16 non-structural proteins (nsp) (18). These proteins are essential in mediating viral replication and transcription by interfering with host translation and innate immune responses, establishing viral replication complexes, and modulating host cell functions (19). As a next step, SARS-CoV-2 modifies the host cell membrane to create a replication organelle, which shields viral RNA and enzymes and protects them from the host immune system. These organelles are built primarily using double-membrane vesicles (DMVs) formed from the endoplasmic reticulum (ER) (20). The formation of DMVs is guided by viral proteins nsp3, nsp4, and nsp6, which remodel ER and connect DMVs with other cellular structures (21). Within the organelles, viral non-structural proteins assemble into the replication and transcription complex (RTC), which also contains an RNA-dependent RNA polymerase (RdRp), RNA helicase, and a proofreading enzyme to ensure the fidelity of RNA replication. RdRp synthesizes full-length copies of the viral genome and shorter subgenomic messenger RNAs (sgRNAs) (22). These sgRNAs are then translated into S, M, E, and N viral proteins essential for viral replication and assembly. The replication in the organelles enables efficient viral replication and transcription, contributing to the pathogenicity of SARS-CoV-2.

Finally, viral RNA and N proteins undergo assembly into ribonucleoprotein (RNP) complexes, which are then included in new virus particles. Recent studies demonstrated that RNPs assemble into a "beads-on-a-string" structure with several RNP complexes wrapped around the viral RNA (23). As a next step, the N and the M viral proteins are transported to the ER-to-Golgi intermediate compartment (ERGIC), where they incorporate RNP complexes into new virions (24). These virions mature while passing through the Golgi apparatus and later exit the cell via a process of fusion of lysosomes with the cellular membrane, lysosomal exocytosis (25). This process requires

various factors, including calcium ions and members of the SNARE complex. The new viral particles invade respiratory epithelial cells, providing new infectious material for the infection transmission via respiratory droplets.

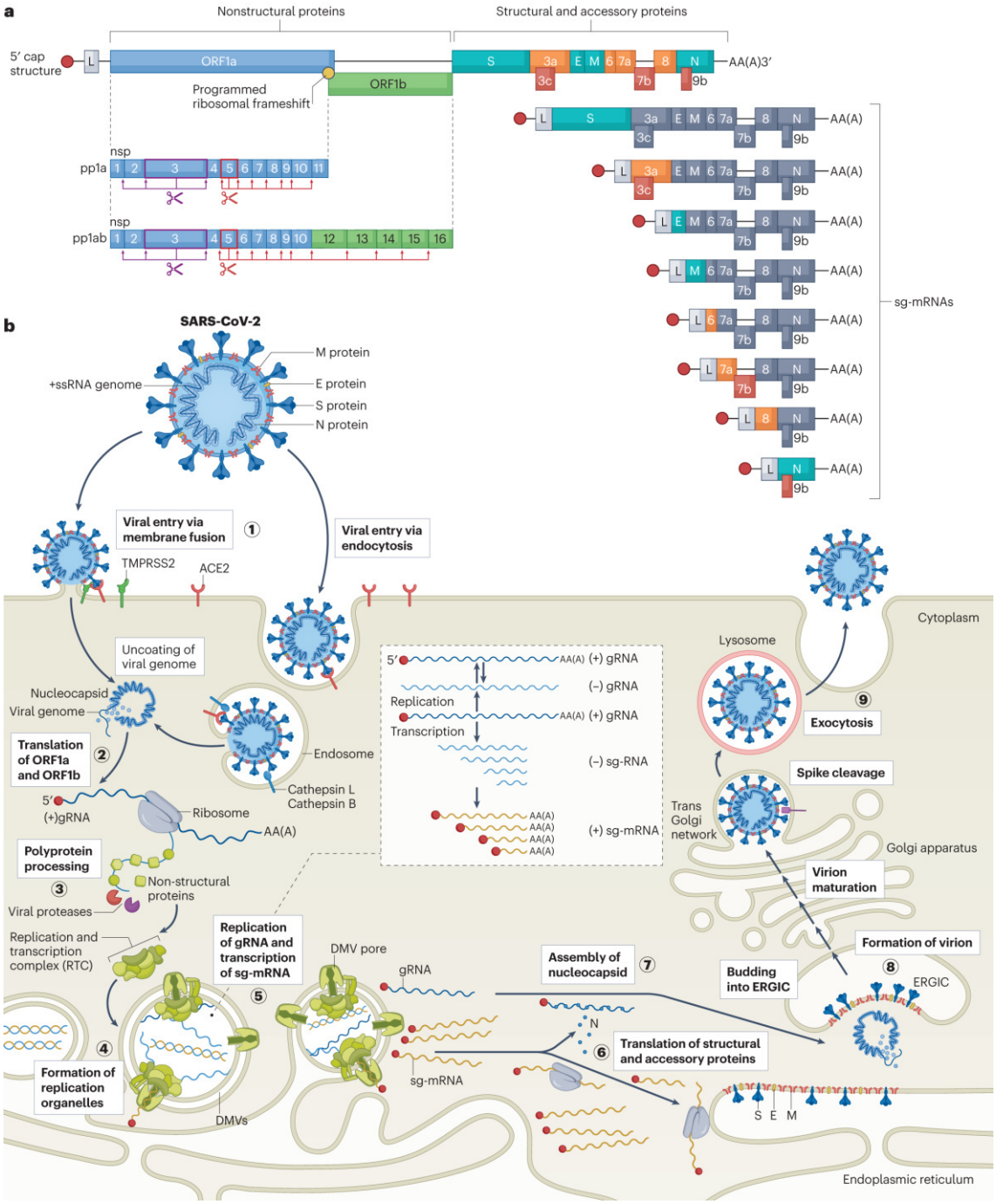

Figure 1.2: Mechanisms of SARS-CoV-2 entry to the host cells. The SARS-CoV-2 virus contains the spike (S), membrane (M), and envelope (E) proteins, as well as a single-stranded RNA that surrounds nucleocapsid (N) proteins. The virus life cycle begins with the interaction of the S protein and the ACE2 receptor on the host cells (step 1). The cell protease TMPRSS2 facilitates the fusion of the viral envelope with the cell membrane, leading to the virus's entry into the cell. Once inside the host cell, the viral RNA is released and translated into polyproteins ORF1a and ORF1b (step 2), which are then processed into non-structural proteins (nsp1–16) that form the replication and transcription complex (RTC) (step 3). The host cell's endoplasmic reticulum (ER)

membranes are altered to form double-membrane vesicles (DMVs), which serve as replication sites (step 4). The RTC replicates the viral RNA and produces subgenomic mRNAs (sg-mRNA) (step 5), which are then translated into viral proteins (S, M, E, and N) (step 6). The newly synthesized RNA binds with N proteins to form the nucleocapsid (step 7). Structural proteins are transported to the ER-to-Golgi intermediate compartment (ERGIC), where they combine with the nucleocapsid to create new virus particles (step 8). These particles mature as they pass through the Golgi apparatus and are later released from the cell through lysosomal exocytosis (step 9). The figure is taken from (26), copyright permission is acquired from the publisher.

1.3. Clinical manifestations and pathophysiology of COVID-19

Although COVID-19 is considered a respiratory infection, patients infected with SARS-COV-2 display many symptoms, many of which also involve other organ systems besides the lung. This rendered COVID-19 patient management and made the development of the markers and treatment strategies for all involved organ systems particularly challenging. At the pandemic's beginning, clinicians implemented severity assessment parameters as part of the screening routine to assess COVID-19 severity and mortality and the potential high risk of requiring critical care. Among them were C-reactive protein (CRP), Sequential Organ Failure Assessment (SOFA), Interleukin-6 (Il-6), and leukocyte count. CRP and IL-6 levels were demonstrated to be predictive of the patients' inflammation backgrounds, while the SOFA score and leukocyte count were implemented to predict multi-organ failure and high mortality risk (27,28).

Additionally, the NIH classified COVID-19 into five distinct severity types based on clinical symptoms, laboratory tests, radiographic abnormalities, and organ functions (29). The severity categories included asymptomatic, mild, moderate, severe, and critical illness. Asymptomatic patients are SARS-CoV-2 positive; however, they do not exhibit any clinical symptoms consistent with COVID-19. Mild cases were characterized by the detection of symptoms such as fever, cough, sore throat, malaise, headache, muscle pain, nausea, vomiting, diarrhea, anosmia, or dysgeusia without shortness of breath or abnormal chest imaging. Patients with moderate severity present clinical symptoms or radiologic evidence of lower respiratory tract disease and reduced oxygen saturation (SpO2) ≥94%. Severe COVID-19 cases are defined by SpO2 less than 94%, and a ratio of partial pressure of arterial oxygen to fraction of inspired oxygen (PaO2/FiO2) of less than 300, together with increased frequency of breathing greater than 30 breaths/min, or lung infiltrates taking more than 50% of the total lung volume. Finally, critical cases are distinguished by acute respiratory failure, septic shock, or multiple organ dysfunction. Additionally, severe and critical COVID-19 patients undergo endotracheal intubation, which is installed to present a respiratory crisis, remove accumulated liquids from the lungs, and improve therapy administration. For the parameters defining respiration failure or ARDS in severe and critical COVID-19 patients, clinicians commonly use PaO_2/FiO_2 (P/F) ratio and positive end-expiratory pressure (PEEP) to classify severity (30). PEEP is the pressure applied to the mechanical ventilator used to stabilize the lungs and improve oxygenation; higher values represent increased respiratory failure. The P/F ratio displays the partial pressure of oxygen in arterial blood (PaO2) to the fraction of inspiratory oxygen concentration (FiO2), which indicates reduced oxygenation and more severe ARDS. In severe cases, patients are connected to an Extracorporeal Membrane Oxygenation (ECMO) device, which provides heart and lung support to patients with decreased organ functions.

Apart from having a substantial respiratory pathology compared with diseases caused by other viral respiratory pathogens, COVID-19 patients exhibit a distinct pathophysiology that is charac-

terized by increased extrapulmonary manifestations. These conditions include thrombotic complications, acute kidney injury, myocardial injury, acute coronary syndromes, hepatocellular injury, gastrointestinal symptoms, hyperglycemia and ketosis, neurologic illnesses, ocular symptoms, and dermatologic complications. One of the features of COVID-19 pathophysiology was the increased frequency of blood clotting events, corresponding to increased levels of D-dimer, C-reactive protein (CRP), P-selectin, and fibrinogen (31,32). For example, D-dimer is a product of cross-linked fibrin cleavage and a marker of elevated coagulation events (33). A recent study revealed increased D-dimer levels in 10% of all COVID-19 patients, corresponding to the high coagulation pathology frequency (34) and several lines of evidence support the hypothesis of the involvement of inflammatory, immune, coagulation, and complement pathways in COVID-19 coagulopathy (35). Associations of the innate immune response and coagulation, leading to clot formation promoted by endothelial cell dysfunction and inflammation, have been named 'immunothrombosis'.

1.3.1. Endothelial dysfunction and thromboinflammation

Under normal conditions, the vascular endothelium maintains its homeostasis by expressing antithrombotic molecules that inhibit platelet activation (e.g. nitric oxide, prostacyclin, and ectonucleotidases) and coagulation (e.g. tissue factor pathway inhibitor (TFPI)). In addition, expression of thrombomodulin, and endothelial cell protein C receptor (EPCR) ensures negative regulation of blood coagulation. Besides that, vascular endothelium carbohydrate-rich glycocalyx lining has an anticoagulant property and protects against pathogen invasion (36).

In contrast, SARS-CoV-2 infection was reported to disrupt vascular endothelium, which is believed to be one of the main contributors to the disease pathogenesis (37,38). ACE2, a regulator protein in the renin-angiotensin-aldosterone and kallikrein-kinin systems (39,40), plays an important role in this process. The first system maintains blood pressure and electrolyte balance, and the second regulates the relaxation of smooth muscle cells and vascular permeability. SARS-CoV-2 has a unique interaction mechanism with its receptor ACE2, which induces endothelial cell dysfunction at the early stage of the infection in the lung. This leads to the activation of both regulatory systems during COVID-19 resulting in increased vascular permeability, inflammation, and organ damage (41,42).

Additionally, the innate immune system can also enhance COVID-19-induced pathogenic mechanisms and contribute to clot formation via neutrophils, which are recruited early after the beginning of the infection in response to chemoattractants released at sites of virus-mediated injury. Neutrophils play an essential role in the phagocytosis and formation of the neutrophil extracellular traps (NETs), as well as the release of the proteolytic enzymes, chemokines, and reactive oxygen and nitrogen species (RONS), contributing to the first-line of immune response to the virus. NETs are released when neutrophils undergo programmed cell death (43). They consist of network-like

structures with the inclusion of DNA, histones, oxidant enzymes, coagulant factors, and complement factors. NETs were also reported to promote clotting in COVID-19 by retaining platelets and expressing functional tissue factors (TF), having an increasing tendency in more severe and deceased patients (44).

1.3.2. Dysregulation of the complement system

In addition to neutrophils, the complement system is another critical component of the COVID-19 patients' pathophysiology (45). COVID-19 patients exhibit elevated serum levels of C5a and C5b-C9 complement components, which correlate with disease severity (46,47). Several reports suggest that SARS-CoV-2 activates the complement in two ways directly and indirectly. Direct activation occurs through the classical, lectin, and alternative pathways. The classical pathway of complement activation is triggered by the formation of complement-fixing antibody immune complexes (IgG or IgM) (46). Secondly, the alternative pathway activation relies on the competitive interaction of C3 and C5 convertase with negative regulation factor H (48). Notably, the cleavage of component C5 leads to the release of pro-thrombotic factors from platelets, activation of TF, and induction of P-selectin expression on endothelial cells, promoting leukocyte recruitment (35). Lastly, the lectin pathway becomes activated by the direct interaction of S protein with mannose-binding lectin (MBL), FCN2, and COLEC11 and by the N-protein mediated enhanced C4 cleavage by MASP2 (49). Additionally, damaged epithelial and endothelial cells release complement factors, mediating the indirect complement activation.

Lastly, complement activation is tightly connected to platelet homeostasis. Platelet activation can be triggered by multiple factors, specifically C3a and C5a complement proteins, inflammatory cytokines, anti-SARS-CoV-2 antibodies, and messengers produced by activated endothelial cells (50), which is another important factor in COVID-19 pathophysiology. One of the reported mechanisms triggering platelet activation in COVID-19 involves increased MAPK signaling and thromboxane A2 (TXA2) in platelets (51). Additionally, patients with COVID-19 demonstrate increased levels of circulating platelet activation markers CCL5 and platelet factor 4 (PF4) and platelet-monocyte and platelet-neutrophil aggregates (52). Due to the activation of the endothelium, these aggregates can adhere to the vessel walls and promote hypercoagulability (53). Moreover, dysregulated coagulation and inflammatory pathways, constantly activated through the positive feedback loop between complement, NETs, and coagulation impose secondary tissue damage in critical COVID-19 patients (54). Thus, activated platelets, neutrophils, and complement play complementary roles in increased thrombotic events in COVID-19 patients and predict more severe patient conditions.

1.3.3. Extrapulmonary manifestations

Another important hallmark of COVID-19 is the extrapulmonary symptoms affecting the gastrointestinal, renal, and cardiac systems. Firstly, the most frequently encountered extrapulmonary manifestation of COVID-19 is acute kidney injury (AKI), which is also associated with increased mortality risk (55). According to recent reports, >20% of hospitalized and >50% of ICU COVID-19 patients are likely to develop AKI (56). The pathophysiology of COVID-19 AKI originates from several factors, including cardiovascular comorbidity, the direct effect of the virus on the kidney, and upregulated inflammatory responses (57). However, endothelial injury and dysregulation of the complement and coagulation system are considered to be the main drives of this process (58). Several research groups have also reported the presence of the virus in renal endothelial cells, where they can promote endothelial damage and vasoconstriction, followed by the formation of microthrombi and renal microvasculature injury (56). However, further studies must be initiated to determine biomarkers capable of more accurately predicting COVID-19-mediated kidney injury.

Myocardial injury in COVID-19 patients commonly manifests as myocardial ischemia (MI), blood flow obstruction in coronary arteries to the heart, and myocarditis, inflammation of the heart muscle. A retrospective study of 187 patients with COVID-19 from a single center revealed that 27.8% exhibited elevated troponin levels, indicative of myocardial injury (59). Additionally, a meta-analysis of published studies showed that acute myocardial injury and pre-existing cardiovascular diseases were highly associated with increased mortality and ICU admission in COVID-19 patients (60). Among the potential mechanisms driving myocardial injury in COVID-19 patients, researchers suggested multiple mechanisms, including direct injury from the viral infection, mediated by ACE2 receptors expressed in myocardiocytes, endothelial cell injury and hypercoagulability, and cytokine storm, which induces systemic inflammation and potentially leads to myocardial injury without direct viral infiltration (61).

To summarize, besides profound lung damage phenotype, COVID-19 patients, also display several extrapulmonary manifestations, which develop due to the ubiquitous expression of ACE2, in multiple extrapulmonary tissues. Other important drivers, such as immunothrombosis, endothelial damage, and dysregulation of immune responses, all might contribute to the broad spectrum of manifestations observed in COVID-19 patients.

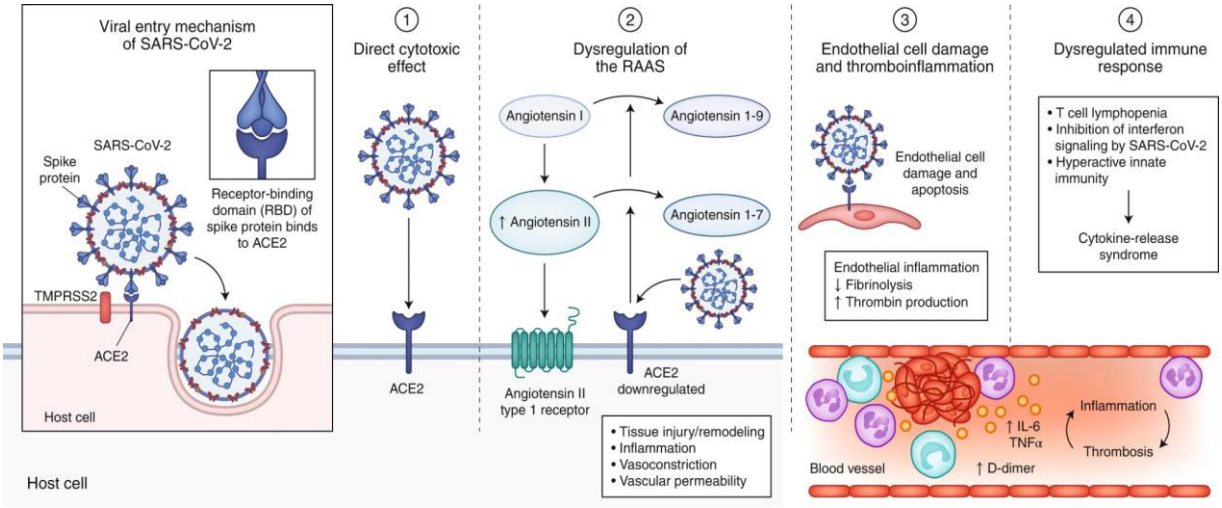

Figure 1.3: Underlying mechanisms of COVID-19 pathophysiology. The infection process begins with SARS-CoV-2 entry into the cell via its interaction with ACE2 in the presence of TMPRSS2.

Proposed mechanisms for COVID-19 caused by infection with SARS-CoV-2 include (1) direct virus-mediated cell damage; (2) dysregulation of the RAAS as a consequence of downregulation of ACE2 related to viral entry, which leads to decreased cleavage of angiotensin I and angiotensin II; (3) endothelial cell damage and thromboinflammation; and (4) dysregulation of the immune response and hyperinflammation caused by inhibition of interferon signaling by the virus, T cell lymphodepletion, and the production of proinflammatory cytokines, particularly IL-6 and TNFα (Gupta et al., 2020, p. 1018).

The figure is taken from (59), copyright permission is acquired from the publisher.

1.4. Immunopathology of severe COVID-19

One of the critical hallmarks of SARS-CoV-2-induced pneumonia is the dysregulation of the immune response, which results in the impairment of defense mechanisms. This leads to irreversible inflammatory responses, autoimmune-like manifestations in the patients, and tissue damage. The most notable differences were observed in dysregulations of the adaptive immune responses in COVID-19 patients. In the mild COVID-19 stage, SARS-CoV-2-specific $CD4^+$ and $CD8^+$ T cells are activated and provide a rapid viral clearance (62). $CD4^+$ T cells contribute to the production of neutralizing antibodies (ABs) and have been studied in great detail to improve the production of vaccines for COVID-19 (63),(64). In contrast, in severe COVID-19, impaired T-cell mechanisms are responsible for the disease progression. For example, polyfunctional antigen-specific T cells were shifted to the dominating cytotoxic phenotype, resulting in increased tissue damage (65). Besides that, activated $CD4^+$ and $CD8^+$ cells have been detected in elevated proportions in the lungs of severe COVID-19 patients, promoting inflammation, endothelial dysregulation, and fibrosis (66). Additionally, several studies reported the presence of SARS-CoV-2-specific regulatory T cells (T regs) in patients with critical disease stages connected to overall poor T cell responses (67). Finally, T cells in patients with COVID-19 demonstrated exhaustion phenotypes, characterized via upregulated surface PD-1 and TIM-3, which can impact the patients' long-term recovery. Thus, elevated exhaustion levels and reduced functional diversity of T cells predict severe progression in patients with COVID-19 (68).

Clinicians have also reported lymphopenia, a reduction in white blood cell count, as a critical feature of patients with COVID-19, especially in severe cases (69). $CD4^+$ and $CD8^+$ T cells and natural killer (NK) cells were considered the most affected immune cell types (69,70). Additionally, reduced frequencies of helper T cell subsets have been observed in severe cases, coupled with insufficient humoral immune response. Notably, B cell numbers were also reduced in some COVID-19 patients requiring intensive care, which has been used as an indicator of disease severity and prognosis (71).

Lastly, alterations in neutrophil and monocyte counts have been broadly observed in patients with COVID-19. Increased neutrophil numbers were reported in 38% of the patients from the Wuhan study (72). The neutrophil count and neutrophil-to-lymphocyte ratio have been used to predict the severity of the disease and potentially poor clinical outcomes (44). At the same time, severe COVID-19 patients also demonstrate reduced levels of eosinophils, basophils, and monocytes (69).

Finally, increased cytokine production is another key feature of severe COVID-19. Already at the beginning of the pandemic, it was noted that critical and severe COVID-19 patients demonstrate an increase in inflammatory cytokines, specifically IL-1β, IL-2, IL-6, IL-7, IL-8, IL-10, G-CSF, granulocyte macrophage-colony stimulating factor (GM-CSF), interferon-inducible protein-10 (IP10),

monocyte chemotactic protein 1 (MCP1), macrophage inflammation protein-1α, IFN-γ, and TNF-α, named ‘cytokine storm’ (16,44,73,74). This uncontrolled release of cytokines often leads to the hyperactivated state of the immune system and multi-organ failure.

1.4.1. B cell-mediated immunopathology

B cell-mediated immunopathology is an important contributor to the clinical picture of COVID-19 patients. In the context of humoral immunity, antigen-specific B cell activation is required to develop virus-specific antibodies, followed by the formation of germinal centers (GCs) in lymph nodes and the development of long-lived antibody-producing cells (75).

The GC reaction is vital in providing antibody diversity via the interaction of T and B cells and ultimate expression of the adaptive immune response. During the early stages of the immune response, B cells recognize foreign antigens and migrate to the GC, where they interact with T cells on the border between B and T cell zones, which leads to their activation and differentiation into GC B cells and T follicular helper cells (Tfh)(76). The maturation of B cells in the GC is facilitated by the transcriptional factor Bcl-6. GC B cells move into the dark zone, where they undergo somatic hypermutation (SHM) and class switch recombination (CSR) proliferate. SHM is responsible for providing diversity to the antibody pool, introducing random mutations in the V-region of the BCR. Another important reaction is CSR, which allows the production of antibodies of different isotypes. Subsequently, GC B cells move to the light zone, interacting with Tfh cells and getting positively selected based on their affinity to the antigen. Transcriptional factors Myc and Rel drive the GC reaction, enabling the continuous circulation of B cells between light and dark zones (75).

The humoral immune response induced by SARS-CoV-2 infection emerges with non-specific IgM antibodies appearing on day six during the acute phase of infection (77). This is followed by an increase in virus-specific IgG and IgA isoforms, produced by the GC reaction, peaking at 23 days from symptom onset and residing in the circulation for up to 16 months after the infection (78). As COVID-19 infects the respiratory system, mucosal IgA is also increased in serum and saliva samples (79). According to structural studies, most neutralizing antibodies detected in patients are directed to the viral S protein and bind distinct epitopes of the RBD, blocking viral interaction with the ACE2 receptor (80). Importantly, in COVID-19 patients, increased IgG levels are associated with disease severity. Severe and critical cases demonstrate high antibody titers in the first seven days of the disease and humoral immune responses in milder cases peak on day 15 (81). Additionally, a higher titer of total antibodies is associated with a worse clinical outcome in COVID-19 patients (82).

Despite the major protective functions of the antibodies, malfunction of the humoral immune response has been reported to contribute to the pathology of severe COVID-19. Several studies have reported the initiation of extrafollicular B cell responses in critical and severe COVID-19

patients in the absence of GCs in lymphatic organs as well as low levels of SHM among B cells (83). Critical patients demonstrate excessive humoral responses with low levels of SHM, which facilitate disease exacerbation (84). Moreover, several studies have shown that IgG complexes (virus-specific antibodies) undergo glycosylation or fucosylation of the Fc region, which further leads to the activation of the FcyRs on myeloid cells and amplifies the production of proinflammatory cytokines, specifically IL-6 and TNF. This mechanism was observed in critical but not mild COVID-19 patients, leading to excessive lung damage (11). Additionally, many studies have reported auto-reactive antibodies towards IFNs and cytokines, which are more prevalent in severe patients and are associated with unfavorable disease prognosis (85,86).

Considering the significant role of the adaptive immune response in COVID-19 pathogenesis, many of the recently approved treatment agents for severe COVID-19 cases are immunomodulators (29). Besides commonly used corticosteroids, such as dexamethasone, which interacts with glucocorticoid receptors (GR) and suppresses the immune system, using a more targeted approach was proven beneficial for severe and critical COVID-19 cases. This was achieved by using monoclonal antibodies counteracting with the IL-6 pathway, such as tocilizumab and sarilumab, inhibitors of the JAK-STAT signaling pathway (baricitinib and tofactinib), and IL-1 targeted agents (anakinra and canakinumab) (29). All these agents were successfully applied to hospitalized patients with a rapidly worsening disease trajectory, turning down the ‘cytokine storm’ and changing the disease outcome.

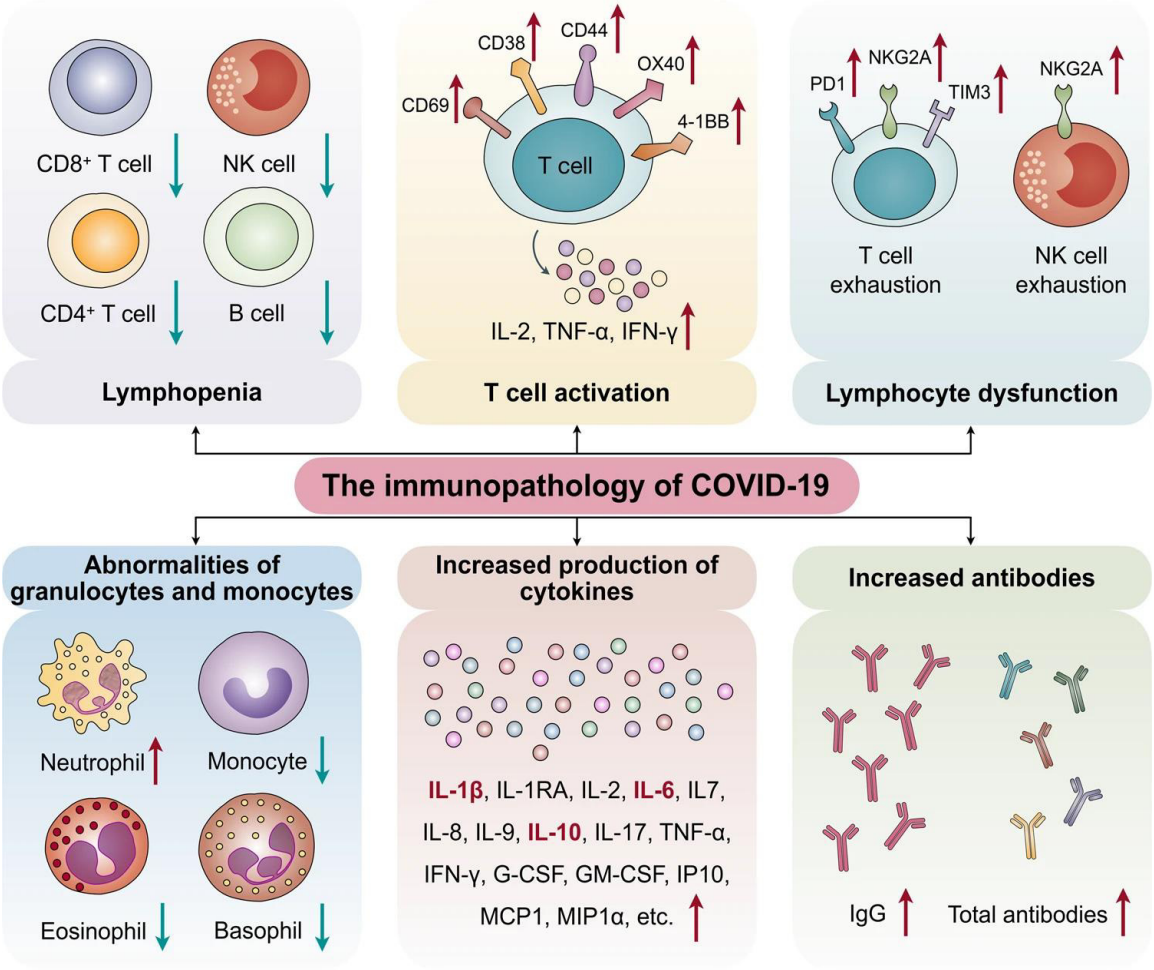

Figure 1.4.1: The immunopathology of COVID-19. Lymphopenia is a crucial feature of patients with COVID-19, specifically in severe cases. Activation of CD4+ and CD8+ T cells in severe patients with a central memory phenotype, accompanied by high levels of IFN-γ, TNF-α, and IL-2, is a hallmark of COVID-19. Another mechanism of COVID-19 immunopathology is the accumulation of exhausted T cells, characterized by programmed cell death protein-1 (PD1), T cell immunoglobulin domain, and mucin domain-3 (TIM3) upregulation. Lastly, neutrophil levels are significantly higher in severe patients, while the percentage of eosinophils, basophils, and monocytes are reduced. 'Cytokine storm' denotes the increased cytokine production, especially IL-1β, IL-6, and IL-10, and indicates hyperactivation of the immune system accompanied by uncontrolled release of signaling molecules. Finally, increased overall antibody titers, particularly IgG levels are observed in severe patients suggesting early seroconversion and possible B-cell-mediated immunopathology. The figure is taken from (87), copyright permission is acquired from the publisher.

1.4.2. Role of autoantibodies in the development of severe COVID-19

Several studies investigating mechanisms of immune dysregulation in acute COVID-19 reported induction of aABs with the potential implications for disease severity and long COVID. Besides that, severe COVID-19 patients demonstrated extrafollicular B cell activation, suggesting a potential auto-reactive B cell emergence mechanism similar to one in autoimmune diseases. Moreover, a broad spectrum of autoantibodies have been identified in COVID-19 patients with an acute course of the disease, targeting antigens of pulmonary, vascular, renal, gastrointestinal, and central nervous systems. Notably, COVID-19-induced autoimmunity is not the first instance of autoreactivity caused by viral infections; similar cases have been previously reported in individuals infected with parvovirus B19, Epstein-Barr virus, and hepatitis A and B (88).

In addition, electronic health records demonstrate an increase in new-onset autoimmune diagnoses in individuals with SARS-CoV-2 infection compared to ones without infection (89,90). A new report on the German cohort consisting of 642,000 patients with COVID-19 suggests that 43% of individuals exhibited an increased likelihood of new-onset autoimmunity (91).

Molecular mimicry (92), bystander activation (93), and epitope spreading are discussed among the hypothesized molecular mechanisms underlying aAB production in acute COVID-19 (94). Firstly, increased levels of circulating self-antigens, released due to extensive tissue damage and the impaired generation of pro-inflammatory cytokines lead to B cells' bystander activation (activation without antigen recognition) targeting host tissues (95,96). The second hypothesis considers the possibility of SARS-CoV-2 proteins/RNA products and host molecule interactions. In a highly inflammatory environment, the innate immune system reacts against self-antigens, a tenet coined as intermolecular epitope spreading (94). Finally, molecular mimicry theory, which describes viral epitopes cross-reacting with host proteins, leads to the breach of the tolerance mechanism and autoimmunity (92). Cross-reactive epitopes have been identified on domain 2 of the SARS-CoV S protein that shares similarities with specific proteins found in human lung epithelial cells (92). Additionally, it has been observed that the antibodies against SARS-CoV S protein can lead to increased adherence of human peripheral blood mononuclear cells to A549 cells (97).

One of the first reports describing autoimmune pathology in severe COVID-19 patients was a study conducted by Bastard et al., which highlighted autoantibodies against type I IFNs detected in 10% of COVID-19 patients and contributing to a more severe disease course (91). Subsequently, autoantibodies became a solid concept in COVID-19 research, with a growing number of studies describing new autoantibodies in severe patients. One of them demonstrated that 45.4% of COVID-19-positive patients have at least one of three common autoantibodies assessed in the clinics: antinuclear (ANAs), anti-antiphospholipid, or anti-cytoplasmic neutrophil antibodies (ANCAs) (98).

Furthermore, human protein arrays screened for aABs in hospitalized COVID-19 patients (either in the ICU or regular ward) compared to other ICU patients who did not have COVID-19 (99) and revealed 260 candidate autoantigens, which were more abundant, but not limited to severe COVID-19 cases. Subsequently, several research groups described autoantibodies targeting various other proteins, such as immune signaling molecules (cytokines, chemokines, and their receptors) (85), G protein-coupled receptors (GPCR) (100), anti-cardiolipin (101,102), cardiac antigens (103), ribosomal and chromatin proteins, thyroid antigens (104), acute phase proteins and platelet surface proteins. Most of the studies claim the association of autoantibodies with the severity of disease and age (101). Notably, increased levels of autoantibodies are strongly associated with increased mortality in elderly COVID-19 patients (105), as elderly patients are more prone to develop autoimmune reactions due to increased amounts of free DNA in the circulation, and thus increased autoantibodies, and immunosenescence (106).

Additionally, clinical evidence has shown that severe COVID-19 patients develop profound organ damage, myopathy, inflammation of the joints, anti-phospholipid syndrome, manifesting by deep vein thrombosis, pulmonary embolism as well as neurological symptoms, which were partially supported by the presence of aABs. For example, antibodies targeting cardiolipin, platelet glycoprotein, C1q, and beta-glycoprotein (APOH) were described to significantly increase the probability of developing severe disease by increasing the risk of thrombotic events specific to the COVID-19 clinical picture, such as deep vein thrombosis and pulmonary thromboembolism (107),(108).

Whether the presence of autoantibodies in the course of infectious disease is always associated with less favorable outcomes is an open question. For example, autoantibodies against chemokines, specifically CCL19 in post-COVID-19 patients were associated with better disease prognosis and prevented the development of PASC at one year post-infection(85). Despite the multiple studies describing a broad array of aABs induced in the acute COVID-19 phase, only a few studies outlined an association with a progression of long COVID-19 (85,109). Noteworthy, autoantibodies are also detected in healthy individuals at physiological levels (109–113) and can be affected by age, sex, and disease conditions.

The induction of aABs and their potential role in disease severity and long COVID demonstrates the complexity of immune responses to COVID-19. This emphasizes the necessity for further research to uncover the mechanisms driving aAB production and the implications of aABs for clinical management.

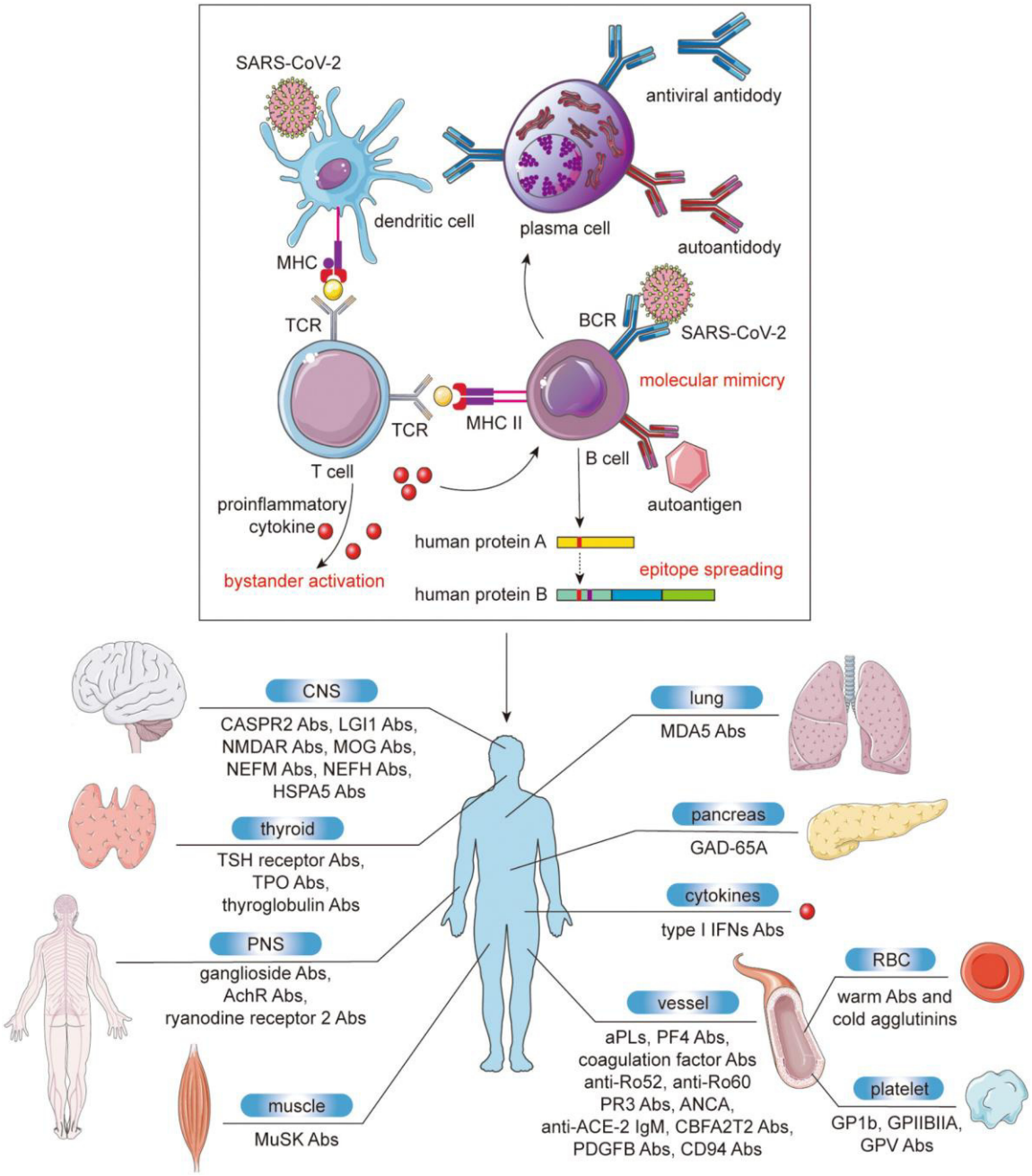

Figure 1.4.2: Potential mechanisms and examples of aABs in COVID-19. During the acute phase of COVID-19 infection, autoantibodies can be generated via three possible mechanisms. Molecular mimicry between the S SARS-COV-2 protein and human proteins can induce autoantibodies that cross-react with human proteins. In addition, autoreactive T and B cells are activated by the release of proinflammatory cytokines, and these autoimmune responses are perpetuated and amplified by epitope spreading which emerges during chronic autoimmune or inflammatory conditions.

The wide distribution of autoantigens across different tissues (CNS, PNS, endocrine system, muscle, blood and vascular system) accounts for the systemic manifestations of post-COVID-

19 patients. Abs, autoantibodies; ACE-2, angiotensin-converting enzyme-2; AChR, anti-acetylcholine receptor; ANCA, anti-neutrophilic cytoplasmic antibodies; APLs, antiphospholipid antibodies; BCR, B cell receptor; CASPR2, contactin-associated protein-like 2; CBFA2T2, CBFA2/RUNX1 partner transcriptional co-repressor 2; CNS, central nervous system; GAD-65A, glutamic acid decarboxylase-65 autoantibodies; HSPA5, heat shock protein family A member 5; IFNs, interferons; LGI1, leucine-rich glioma inactivated protein 1; MDA5, melanoma-differentiation-associated gene 5; MHC, major histocompatibility complex; MOG, Myelin oligodendrocyte glycoprotein; MuSK, anti-muscle-specific kinase; NEFH, neurofilament heavy; NEFM, neurofilament medium; NMDAR, N-Methyl-D-Aspartate Receptors; PDGFB, platelet-derived growth factor subunit B; PF4, platelet factor 4; PNS, peripheral nervous system; PR3, protease 3; RBC, red blood cell; TCR, T cell receptor; TPO, thyroperoxidase; TSH, thyroid stimulating hormone (Ding et al., 2023, p.7).

The figure is taken from (114), copyright permission is acquired from the publisher.

1.5. Pathophysiology of long COVID

Alongside the acute manifestations of COVID-19, there is growing evidence of chronic pulmonary and extra-pulmonary complications following the resolution of the primary infection. These manifestations are termed the post-acute sequelae of SARS-CoV-2 infection (PASC) or long COVID (LC). According to the WHO, PASC occurs in individuals with confirmed SARS-CoV-2 infection in the following three months from the onset of COVID-19 (115). The symptoms should last at least two months and cannot be explained by an alternative diagnosis. Symptoms may persist from the initial illness or be a new onset. According to current statistics, PASC is observed in approximately 10-20% of the SARS-CoV-2 infected individuals (115). Moreover, a systematic review of COVID-19 survivors who developed PASC showed that the median age of the patients is 54.4 years, with 56% of males and 79% of patients being hospitalized during COVID-19 infection (116). Additionally, among non-hospitalized COVID-19 survivors with PASC, most of the individuals were middle-aged women (117).

Similar to acute COVID-19, PASC patients demonstrate a broad spectrum of manifestations with affected pulmonary and extrapulmonary organ systems (118). Additionally, an online survey covering 4,000 individuals from 56 countries reported a wide range of symptoms covering neuropsychiatric, systemic, reproductive, musculoskeletal, immunological, and cardiovascular systems (119). Among the most common symptoms are weakness, fatigue, general malaise, and impaired concentration and breathlessness (120).

Ongoing clinical research focuses on stratifying PASC patients into specific categories based on symptom patterns to derive more tailored patient treatment approaches and avoid the heterogeneous nature of the disease. A recent report, where machine learning techniques were employed, suggested that the classification of PASC patients should be divided into eleven clinical outcome categories based on the common symptoms (121). With emerging consensus stratifications for PASC, the next challenge would be understanding key mechanisms and pathologies associated with different symptoms of the disease and developing clinical biomarkers capable of successfully guiding clinical treatment strategies. Unfortunately, to date, PASC-specific immunobiology and associated risk factors remain elusive.

As a potential mechanism of PASC, researchers highlight the persistence of viral copies and RNA in multiple tissues after acute infection, excessive tissue damage, the imbalance of microbiome and virome, and the emergence of autoimmune reactions triggered by the virus (122). One of the leading hypotheses of PASC development is the presence of remaining SARS-CoV-2 reservoirs in the body after the acute phase of the infection. Specifically, viral proteins and RNA products have been ubiquitously detected in the respiratory, cardiac, and renal systems and the patients' brains, muscles, and eyes (123,124). This may be one of the triggers for constantly elevated pro-inflammatory cytokines levels, specifically IL-6, TNF-α, and IL-1β, IFN-β and IFN-λ1, detected in

PASC patients (125). Additionally, the gastrointestinal tract has been proposed as a site for viral reservoirs, with evidence of the virus detection in stool samples and colon biopsies (123).

Further, evidence has been accumulated since the onset of the COVID-19 pandemic, suggesting multiple organ damage caused by the infection, which persisted even after the resolution of the acute symptoms (126–128). Re-analyzed multi-organ MRI data from 201 non-hospitalized individuals with PASC revealed that 70% of patients in the group exhibited impairment in one or more organs four months after the initial COVID-19 onset (129). Notably, the heart was the most commonly affected organ, with the lungs following in order (127). Despite the observed radiological changes in several organs from symptomatic and asymptomatic patients, the relationship between these changes and the development of PASC remains unclear.

Impairment of adaptive immune responses to SARS-CoV-2 is considered one of the susceptibility factors in PASC. Researchers reported that the detection of anti-N, -M, and -S T effector memory (TEM) cells were reduced in PASC patients compared to convalescent individuals. At the same time, anti-N T follicular helper cells and anti-N IgGs are elevated in the circulation (130). One of the leading hypotheses supporting these observations is the presence of viral antigens in PASC patients. Another potential mechanism of PASC development is autoimmunity. Elevated levels of autoantibodies have been reported in patients with PASC, including autoantibodies (aAB) against ACE2, beta-adrenergic receptor, muscarinic acetylcholine receptor M2, and several angiotensin receptors (104). Moreover, some other aABs were found in a cohort of acute COVID-19 patients, specifically aABs, targeting extracellular matrix components, vascular system proteins, coagulation factors, platelet surface proteins, and immunomodulatory proteins (85,86,101). To a certain extent, aAB titers correlate with disease severity and it has been suggested that COVID-19 patients demonstrate an increase in double negative 2 (DN2) B cells, which are negative for IgD, CD27, CXCR5 and CD21, similar to the ones observed in SLE(131).

However, there is currently a lack of studies demonstrating the role of autoantibodies in the pathophysiology of PASC.

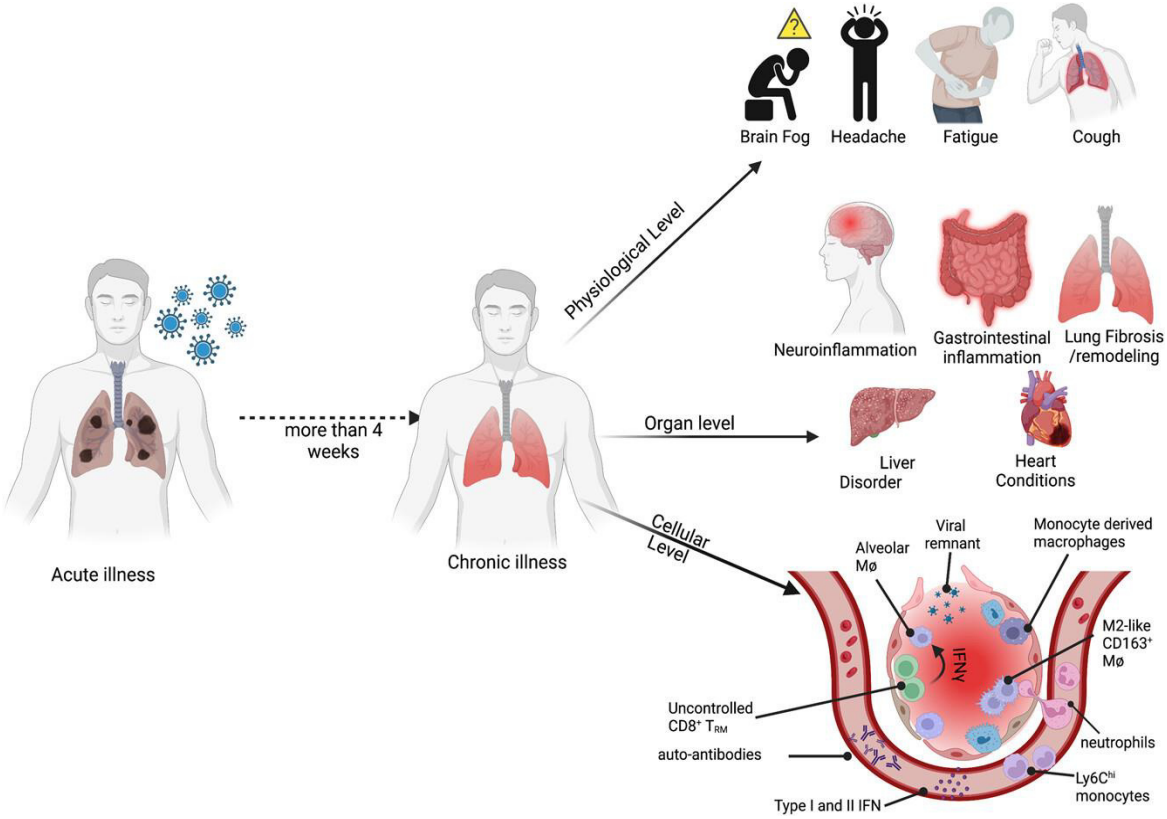

Figure 1.5: Immunopathology of long COVID. The immunopathology of post-acute sequelae of COVID-19 (PASC) manifests itself on several levels. PASC patients exhibit various persistent symptoms, such as brain fog, headache, fatigue, and cough. Long-term neuro- and gastro inflammation, as well as liver and heart conditions, are observed in PASC patients after the acute phase of SARS-CoV-2 infection. However, the underlying cellular processes and mechanisms that drive PASC remain unclear. Recent scientific reports suggest the persistence of virus particles, tissue damage, autoantibodies, and autoreactive T cells, which contribute to the disease's etiology. The figure is taken from (132), copyright permission is acquired from the publisher.

Main question

My work aimed to derive protein signatures obtained from proteome profiles of BALF and plasma unique to COVID-19 patients compared to influenza and bacterial pneumonia, with a primary focus on gaining a better understanding of the autoimmune aspects of severe COVID-19. The biomarkers undercovered in this analysis will assist in improving the diagnosis of pneumonia in uncertain cases and predicting the response to therapy in episodes of ventilator-acquired pneumonia.

Specific objectives for each chapter consist of:

1. Proteomic analysis of biofluids of patients with infectious lung diseases

Here I applied proteomics to profile bronchoalveolar lavage fluid (BALF) and plasma samples from a longitudinal cohort of intubated pneumonia patients to identify unique molecular signatures specific to COVID-19, influenza, and bacterial pneumonia. Moreover, I examined the persistence of the identified protein signatures throughout the hospitalization period and defined plasma- and lung-abundant proteins, yielding distinct proteomic profiles in the early stages of SARS-CoV-2 infection.

2. Single-cell multi-omic analysis of COVID-19-induced B cell populations

I used two single-cell multi-omic datasets to define the molecular characteristics of B cells that contribute to COVID-19-specific humoral immune responses in severe COVID-19. Additionally, I evaluated B cell responses across various disease severities and identified B cell subsets contributing to autoantibody production.

3. Study of autoantibody binding repertoire of acute COVID-19 patients

I aimed to identify putative autoantibody targets in acute COVID-19 patients from two independent cohorts using the DAC assay and to analyze the dynamic changes in autoantibody profiles over time. Furthermore, I explored the correlation relationship between autoantigens and clinical parameters, providing insights into the immunopathology of severe COVID-19 and its potential role in multi-organ damage and susceptibility to secondary infections.

2. Material and Methods

2.1. Human participants and sample availability: Chicago cohort

Samples from COVID-19, bacterial pneumonia, Influenza, and non-pneumonia control patients were collected from participants enrolled in The Successful Clinical Response in Pneumonia Therapy (SCRIPT) study, STU00204868 (133). The Northwestern University Institutional Review Board granted ethical approval for the study, and informed consent was secured from all participants or their legal representatives.

Participants in the SCRIPT study were at least 18 years old and had a clinical suspicion of pneumonia, as indicated by fever, radiographic infiltrate, and respiratory secretions. All patients experienced respiratory failure and required mechanical ventilation in the ICU. Intubation was performed based on the judgment of bedside clinicians to worsening hypoxemia, hypercapnia, or the work of breathing refractory to high-flow oxygen or non-invasive ventilation modes. Decisions regarding extubation were made by bedside clinicians following a protocol-guided assessment of spontaneous breathing, especially in patients demonstrating physiological improvement in cardiorespiratory status during the mechanical ventilation period.

Bronchoscopy coupled with blood draws for most of the samples was performed as a part of routine clinical operations to guide antimicrobial therapy. Bronchoalveolar lavage (BAL) and plasma samples from the SCRIPT study participants were collected between June 15th, 2018, and July 6th, 2020, in the ICU at Northwestern Memorial Hospital in Chicago. Clinical laboratory tests adhered to the local ICU protocols, including multiplex PCR (BioFire Film Array Respiratory 2 panel), automated cell count, and urinary antigen testing for *Streptococcus pneumoniae* and *Legionella pneumophilia* serogroup one on the day of admission. Additionally, clinicians followed ARDSNetwork protocols for all patients, including those with COVID-19. The protocols involved the implementation of a higher PEEP and lower fractional inspired Oxygen (FiO2) strategy for individuals experiencing severe hypoxemia (134). For 16 hours per day, prone positioning was employed in patients with PaO2/FiO2 <150 without contradictions (135). For patients showing improved oxygenation to prone positioning, the procedure was repeated. The care team used esophageal balloon catheters (Cooper Surgical, USA) to estimate transpulmonary pressure and optimize PEEP, particularly in patients with a higher-than-normal body mass index (BMI).

2.1.1. Definition of pneumonia subgroups

Critical care physicians at Northwestern Memorial Hospital (NMH) in Chicago retrospectively categorized patients into groups, including COVID-19 pneumonia, non-COVID-19 viral pneumonia,

pneumonia due to other pathogens, or non-pneumonia controls. This classification was performed according to a standardized adjudication procedure (133). Specifically, the non-pneumonia control group consisted of patients who underwent bronchoscopy to exclude pneumonia from the diagnosis but did not display any quantifiable cultures, as well as negative PCR for bacterial and viral pathogens. Besides that, all the patients had an alternative diagnosis and negative antigens for *S. pneumoniae* and *L. pneumoniae* serogroup 1 in the urine. However, some of the patients from this group acquired ventilator-associated pneumonia later in the course. Patients with a positive nasopharyngeal swab or BAL for respiratory viral pathogen were assigned to the viral pneumonia group. Patients with the detection of bacterial pathogens by PCR analysis, a positive urine antigen, or positive quantitative cultures with more than 100 colony-forming units per ml, were assigned to the bacterial pneumonia group. Additionally, during the study, BAL fluid was screened for methicillin-resistant *S.aureus* (MRSA) using the PCR method (MRSA/SA SSTI), as well as the BioFire FilmArray Respiratory 2 (RP2) panel and Pneumonia panels. Patients assigned to the COVID-19 subgroup had a positive SARS-CoV-2 antigen detected by one of the platforms: the Cepheid Gene Expert, Abbott ID NOW, Becton Dickinson, and a locally developed and validated PCR. Moreover, pneumonia was diagnosed in some patients without COVID-19 based on the clinical witness, radiographic findings, and positive response to the antimicrobial therapy. Lastly, patients with detected new respiratory pathogen with a quantitative culture or PCR more than 48 hours after intubation in serial BAL samples were assigned to the ventilator-assigned pneumonia subgroup. Northwestern Medicine Enterprise Data Warehouse provided the clinical laboratory data. Acute physiology score (APS) and SOFA, commonly used as severity assessment scores, were calculated from Electronic Health Record data with the help of previously validated scripts (133).

2.1.2. Sample collection

BAL was collected from intubated ICU patients with single-use aScope (Ambu, USA) devices under sedation and topical anesthetic. Based on the available chest imaging or observations acquired during the procedure, the bronchoscope was wedged in the area of interest. Aliquots of 30 ml of normal saline each were sequentially installed and received back, reaching a total volume ranging from 90 to 120 ml, the fluid returned after the initial aliquot was discarded. The obtained samples were divided between clinical testing and research. Similar collecting procedures were applied for non-bronchoscopic BAL (NBBAL) samples, except that NBBAL was performed with directional guidance by a respiratory therapist rather than a pulmonologist. In the case of COVID-19 patients, sampling was performed from the area with the highest radiographic abnormality by a critical care physician using a disposable device. Sedation and neuromuscular blockade were administered to prevent cough during bronchoscopy, with the earliest procedure being performed immediately after intubation to take advantage of the prior neuromuscular blockade administration.

Besides BAL, whole blood from the patients of the SCRIPT cohort was collected in lithium heparin tubes. The collection was performed on the same day as BAL or NBBAL procedures. After spinning down for 10 minutes at 1690 x g at 4˚C, a cellular component was removed, and the plasma fraction was stored at -80˚C before the following proteomic analysis.

Consent was obtained from patients or their legal representatives to collect all BAL and plasma samples.

Additionally, I received BAL and plasma samples from the SCRIPT cohort from healthy individuals enrolled in the studies Pro00088966 and Pro00100375 at Duke University. BAL was collected from the healthy volunteers under sedation and topical anesthesia in the bronchoscopy suite or the intensive care unit. Clinicians selected the bronchopulmonary segment of interest based on the chest CT scan, installed 90 to 120 ml of saline into the segment, and aspired back. The first 5 ml of the returned fluid was discarded.

2.1.3. Visualization of the clinical metadata

Clinical metadata and clinical blood chemistry from Chicago cohort patients were plotted using ggplot2 (v.3.4.4) in the R (v.4.3.0) environment. Statistical comparison of the groups was performed using base R (v.4.3.0) with tidyverse (v.1.3.0) and visualized the plots using ggpubr (v.0.6.0). For statistical testing, I assessed the distribution of the variables using a Shapiro-Wilk test. I applied non-parametric tests for parameters that did not fit the normal distribution. *P* values <0.05 were considered significant. Two-sided statistical tests were performed in all cases. Alluvial plots for categorical clinical parameters were generated using ggalluvial (v.0.12.5) and edited in Adobe Illustrator 2024. Graphical illustrations were generated with BioRender license, copyright permissions were acquired.

2.2. Human participants and sample availability: Munich cohort

Serum samples of SARS-CoV-2 positive patients, confirmed by PCR result, were collected from March to June 2020 from the patients admitted to the University Hospital of LMU (Ludwig Maximilian University) (136). The sampling was performed longitudinally, up to 54 days from the day of admission on the patients in regular wards and intensive care units (ICU). All serum samples were preserved as 250ul aliquots in 2D barcoded biobanking vials (Thermo Scientific, USA) at −80°C in the LMU LabMed Biobank.

Clinical and clinical chemistry data was obtained from electronic patient records and included sex, age, date of onset symptoms, immunosuppression, ARDS, and outcome, etc., as well as the Elecsys Anti-SARS-CoV-2 ECLIA (Roche Diagnostics International, Switzerland) for both spike (S) and nucleocapsid (N) antigens.

The Ethics Committee of LMU Munich (reference number 21-0047) approved the anonymized analysis. The experiments adhered to the principles outlined in the WMA Declaration of Helsinki and the Department of Health and Human Services Belmont Report.

2.2.1. Experimental design

To assess the heterogeneity within the Munich cohort and select samples and time points for longitudinal profiling, I applied the t-distributed Stochastic Neighbor Embedding (t-SNE) dimensionality reduction method using the Rtsne package (v.0.16). This method utilizes the combination of both numerical and categorical clinical data parameters for dimensional reduction and clustering of patients, allowing us to further subdivide subgroups within a cohort that share similar clinical phenotypes. This way, clinical metadata and blood chemistry data from 29 individuals at the time of admission to the hospital were used as an input matrix. I performed separation of the patients based on categorical variables, such as sex, immunosuppression, covid-stage, extracorporeal membrane oxygenation (ECMO), acute respiratory distress syndrome (ARDS), etc., and numerical values: C-reactive protein (CRP) [mg/dl], Anti-SARS-CoV-2 antibody titers, aspartate aminotransferase (GOT) [U/l], alanine aminotransferase (GPT)[U/l], etc. Only numerical values that did not require imputation on the day of admission were used. First, I computed the Gower distance matrix to find the most similar and dissimilar patients. Then, the optimal number of clusters was selected based on the maximal silhouette width, which led to the 2 clusters. Finally, I manually calculated the perplexity and visualized the findings in the t-SNE embedding. This way, I ended up with ‘severe’ and ‘mild’ clusters. The ‘severe’ cluster was formed exclusively by patients with ARDS and exhibited higher levels of CRP, Interleukin-6, and anti-SARS-CoV-2 antibodies. The baseline characteristics of both clusters are presented in Table A2.

To define the timeline of the study, I performed longitudinal profiling of clinical metadata: anti-SARS-CoV-2 N antibodies, anti-SARS-CoV-2 S antibodies, CRP [mg/dl], Creatinine Jaffe [mg/dl], Lymphocytes [g/l], and Leukocytes [g/l]. All the parameters were plotted longitudinally for both 'severe' and 'mild' groups of COVID-19 patients defined by t-SNE analysis. The time points demonstrating the closest resemblance in clinical values between the two groups were selected as boundaries for the time windows: specifically, day 11, day 25, and day 36. Additionally, among the initial 29 patients, only those with at least three-time points in at least two-time windows were retained, resulting in a final cohort of 23 COVID-19 patients.

For further analysis, individual serum aliquots from each patient were pooled in four defined time windows: 0-11 days, 12-25 days, 26-36 days, and 36-54 days. Within each window, three random samples were selected and combined in equal amounts, resulting in 59 serum samples. This way, each patient contributed from 2 to 4 time points.

The final cohort consisted of 23 COVID-19 patients, among whom 16 were classified as 'severe' (admitted to ICU), and the remaining seven were categorized as 'mild' according to the t-SNE analysis. Both patient groups were matched in age, proportions of female and male patients as well as length of hospitalization (Table A2). However, 18.8% of the patients in the 'severe' group required ECMO support, and the administration of immunosuppression was doubled compared to the mild group (56.2% vs. 28.6%). Finally, 75% of the patients in the severe group exhibited signs of acute kidney injury, in contrast to 28.6 % in the mild group.

2.2.2. Selection of the control samples: Munich cohort

In addition to COVID-19 samples, I included serum aliquots from 262 PCR-negative controls obtained from the same study cohort. These patients were admitted to the University Hospital of LMU Munich with possible symptoms of SARS-CoV-2 but with a negative PCR result.

To separate auto-reactivities within the COVID-19 cohort arising from inflammatory processes within the patient's body and those specific to the viral infection, I subdivided these patients into two cohorts based on high and low proinflammatory blood chemistry parameters. To achieve that, I applied a hierarchical clustering approach using clinical parameters that did not require imputation: specifically, CRP, Creatinine, and Leukocyte counts. The analysis was conducted in the R environment (v.4.3.0) using pheatmap package (v.1.0.12).

Patients falling within the third and fourth quantiles (50-75%) of the distribution for each of the clinical parameters mentioned above were assigned to the high inflammatory control group (n=23), while those within the first and second quantiles (0-50%) were defined as low inflammatory control group (n=24) (Fig. 3.2.2). This approach facilitated the establishment of two distinct control groups to complement the longitudinal COVID-19 cohort (Munich).

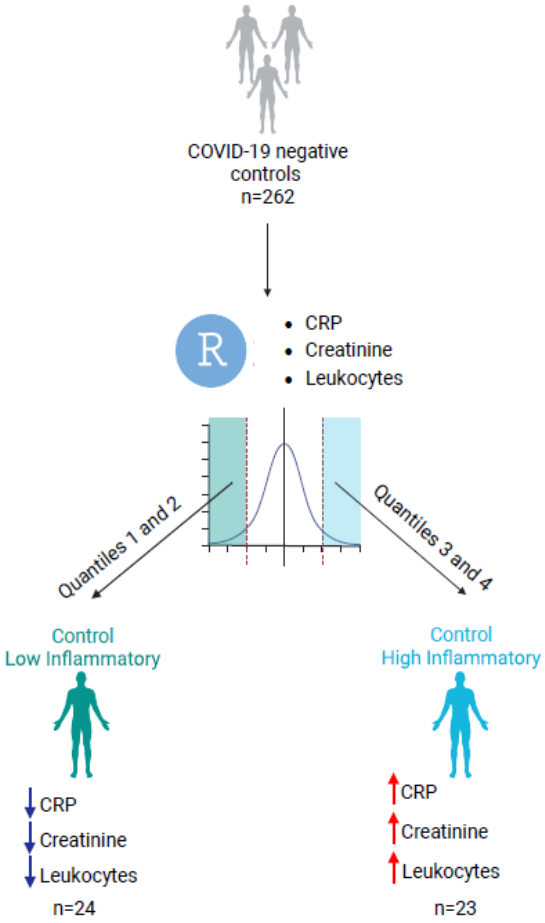

Figure 2.2.2: Schema of control cohort selection (the Munich cohort). The procedure of selection of control low inflammatory (n=24) and control high inflammatory (n=23) groups from SARS-CoV-2 negative patients (n=264) enrolled to the University Hospital of LMU based on the distribution of C-reactive protein (CRP), Creatinine and Leukocyte values.

2.3. Sample processing methods

2.3.1. Protein extraction from donor lung tissue

To obtain a protein lysate mixture further used for auto-antigen detection, proteins from the peritumoral lung tissue samples of donors undergoing lung transplantation due to lung carcinoma were extracted. Following the lung transplantation, the lung tissue was preserved by CPC (Comprehensive Pneumology Center) BioArchive using a standardized procedure. Lung tissue was cut into pieces of 0.5 cm^3, snap-frozen in liquid nitrogen, and stored at -80°C.

In total, 32 samples from 18 male and 14 female donors were processed. The donor cohort was age-matched with a mean age of 63±10 years.

Before protein extraction, lung tissue was homogenized using a dry pulverizer (CP02, Covaris, USA). The resulting powder was resuspended in RIPA buffer (50 mM Tris HCl pH 7.4, 150 mM NaCl, 1% Triton X100, 0.5% sodium deoxycholate, 1 mM EDTA, 0.1% SDS) containing protease inhibitors (cOmplete, Roche, Switzerland). Samples in the buffer were incubated on ice for 30 min, followed by sonication (10 cycles, 30-sec power, 30-sec pause) (Bioruptor, Diagenode, Germany). After sonication, unsolvable residues of the tissue were removed by centrifugation for 5 minutes at 18,000 x g. The protein concentration of the samples was determined using Bicinchonic acid Assay (BCA) (Pierce, Thermo Fisher Scientific, Germany).

2.3.2. Differential antigen capture assay (DAC)

Auto-antibody-antigen complexes in the serum/plasma of pneumonia patients were detected with a DAC assay for both Munich and Chicago cohorts (137). The assay is based on immunoprecipitation and utilizes Protein L agarose-coupled beads (Pierce, Thermo Fisher Scientific, Germany) to capture antibodies of IgG, IgA, IgM, and IgD isotypes from serum. After purification, antibodies on the beads are incubated with a protein extract of ‘healthy’ lung tissue to initiate capture self-antigens followed by mass spectrometric identification of the assembled protein complexes.

Serum/plasma aliquots were thawed on ice and centrifuged at 2,500 x g for 5 min to remove a precipitate. As previously described, a 1.5 g protein lysate mixture from the peritumoral lung tissue of 32 age-matched patients was aliquoted and each aliquot was thawed on ice before the experiment. As a first step, 20 ul of Protein L agarose beads (Pierce, Thermo Fisher Scientific, Germany) were distributed in 96 well-filter plates (MultiScreenHTS-BV, 1.2 um, Millipore, Germany) and washed with 200 ul wash buffer (WB) (0.1% IGEPAL, 5% Glycerol, 50 mM Tris-HCl pH 7.4, 150 mM NaCl, EDTA-free protease inhibitor cocktail (cOmplete, Roche, Switzerland)) followed by centrifugation at 100 x g for 1 min.

Later, beads were resuspended in 195 ul of WB and supplemented with 5 ul of serum/plasma sample per well. Plates were incubated for 1 h at 700 rpm at room temperature (RT). As a next

step, plates were spun down at 100 x g for 1 min and washed 3x with WB. Beads with bound antibodies were later incubated with 150 mg of lung protein lysate mixture diluted with WB (200 ul per well) and incubated for 1 h at RT and 700 rpm. Finally, plates were washed 3x with WB and 3 times with PBS (Gibco, Thermo Fisher Scientific, Germany) followed by protease digestion for bottom-up proteomic analysis.

Firstly, beads were supplemented with 50 µl 8 M Urea Hepes pH8, 0.5 µg LysC,10 mM DTT (Pierce, Thermo Fisher Scientific, Germany) and incubated at 600 rpm for 1h at RT. Secondly, I added 200 µl 50 mM ammonium bicarbonate (= 50mM NH_4HCO_3), and 55 mM chloroacetamide with 0.5 µg trypsin (Pierce, Thermo Fisher Scientific, Germany) followed by incubation at 600 rpm for 1h at RT.

As a next step, plates were centrifuged at 100 x g for 1 min and digested peptides were collected in the clean 96-well plate. Finally, beads were washed with 50µl quenching buffer (2M Urea, 50 mM Thiourea, 2 mM HEPES in 50 mM ammonium bicarbonate). All three fractions were combined and digested overnight at 37°C, 600 rpm. The next day, digestion was stopped by adding 1% trifluoroacetic acid (TFA) to the samples.

2.3.3. Fluid sample preparation

Serum and plasma samples of Munich and Chicago cohorts were preprocessed for mass spectrometry analysis using automated workflow (138). Serum/plasma proteins in a 96-well format were denatured, alkylated, and digested with Trypsin and LysC, and peptides were purified using an automated liquid handling platform (Agilent Bravo, USA). Besides that, 20 serum samples were pooled and fractioned into 24 fractions using high pH-reversed phase liquid chromatography for spectral library generation, which is later used as a reference to identify proteins in the other samples.

BALF samples of the Chicago cohort were denatured with 4% SDS in Tris-HCL solution at 99 °C and further processed using the Protein Aggregation Capture (PAC) protocol (139). In brief, samples were precipitated on the magnetic beads (Sera-Mag, Cytiva, USA), and washed with multiple rounds of acetonitrile (ACN) and ethanol to denature and isolate protein aggregates bound to the beads. In the end, precipitated proteins were reduced and alkylated on the beads using tris(2-carboxyethyl) phosphine (TCEP) and chloroacetaldehyde (CAA), followed by Trypsin and LysC digestion overnight at 37°C and 700rpm. For purification of peptides, stage tipping was performed with 3 layers of Octadecyl-bonded silica (C18). First, stage tips were activated with 100 ul MeOH, then equilibrated with buffer B++ (0.1% formic, 80% ACN) and A++(0.1 % formic acid). Samples with 1% TFA were loaded on the tips followed by elution with 60 ul buffer B++. Finally, samples were evaporated at 30°C (Eppendorf Evaporator Plus, Germany) and dissolved in 20 ul buffer A*(0.1% TFA, 2% ACN). Peptides were stored in the -20°C freezer until mass spectrometry was analyzed.

2.3.4. LC-MS/MS analysis

Following digestion, peptides underwent online separation through nanoflow reversed-phase chromatography using an Evosep One liquid chromatography (LC) system (Evosep). The separation occurred on an 8 cm × 150 um column packed with 1.9 um ReproSil-Pur C18-AQ particles (Dr. Maisch) using the 60 SPD method with a 21-minute gradient. The Evosep One was connected online to a timsTOF Pro mass spectrometer (Bruker Daltonics) operating in the DDA PASEF mode (ref). Each acquisition cycle included 3 PASEF scans, and accumulation and ramp times were set to 100 ms each. Singly charged precursors were excluded, the “target value” was set to 15,000, and dynamic exclusion was activated with a duration of 0.4 min. The quadrupole isolation width was adjusted to 2 Th for m/z < 700 and 3 Th for m/z > 800.

Digested peptides were separated by nanoflow reversed-phase chromatography for the DAC samples using an Evosep One liquid chromatography (LC) system (Evosep). The separation occurred on an 8 cm × 150 um column packed with 1.9 um ReproSil-Pur C18-AQ particles (Dr. Maisch) applying the 60 SPD method with a 44-minute gradient. The mass spectrometer was operated in diaPASEF mode with a full scan range of 100–1,700 *m/z* with a ramp time of 100ms, ion mobility was set between 0.7 to 1.45 1/K0. 27 diaPASEF windows followed one full scan in 9 acquisition frames. The DIA window ranged from 300 m/z to 1110 m/z with an isolation window of 30 Da. The collision energy was set dynamically.

2.3.5. Proteomics raw data processing

The standard pipeline for raw mass-spectrometry data processing in bottom-up proteomics consists of several steps. First, individual peptide ions are recognized from the background signals by determining m/z values and intensities of the individual ions in the peak-picking process. This process is followed by a database search aiming to match experimental peptide masses with theoretical masses derived from protein sequences using software such as MaxQuant, Proteome Discoverer, or Mascot (140). Identified peptides are then aligned to MS/MS spectra and confirmed based on peptide sequence, mass accuracy, and fragmentation pattern similarity. As a next step, the software groups unique peptides together and assigns them to a certain protein. The last step is the quantitation of the proteins, which is performed by accessing the intensity or abundance of peptide ions in the MS data using quantification methods such as label-free quantification (LFQ) or intensity-based Absolute Quantification (IBAQ) (141).

The MaxQuant software (version 1.6.17.0, (142)) was employed to analyze the mass spectrometry raw files of BALF and plasma from the Chicago cohort. MS spectra were matched against the UniProt reference proteome FASTA file downloaded in January 2022. A contaminant database, generated by the Andromeda search engine, and the human database were configured

with cysteine carbamidomethylation as a fixed modification and N-terminal acetylation and methionine oxidation as variable modifications. The false discovery rate (FDR) was set at 0.01 for both protein and peptide levels, with a minimum peptide length of seven amino acids. FDR determination involved searching a reversed sequence database. Enzyme specificity, expected to be C-terminal to arginine and lysine, was configured to trypsin and LysC proteases. Up to two missed cleavages were allowed, and proteins and peptides matching the reversed database were excluded. The mass tolerance for the main precursor search was set to 20 ppm, and a minimum of one peptide was required for protein quantification.

The DAC raw mass spectrometry files were processed with DIA-NN (v.1.8.1), an open-source software designed for the processing of data-independent acquisition (DIA) proteomics data (143). This software employs a two-step spectral library refinement procedure (144). During processing, filtering was applied at multiple levels, including precursor level q-value (1%), library q-value (0.5%), and gene group q-value (1%). Enzymatic cleavage was defined by Trypsin/P and LysC proteases with match-between-runs (MBR) mode enabled for the library-free searches. Methionine oxidation and N-terminal acetylation were selected as variable modifications. All other processing parameters were kept by standard settings of the DIA-NN version utilized in the analysis.

Output protein group matrixes from MaxQuant and DIA-NN were filtered (at least 3 proteins detected per group), normalized, and imputed from the normal distribution using the standard pipeline of the DEP package (v.1.24.0). Visualization and additional statistical analysis of longitudinal samples were completed within the R environment (v.4.3.0).

2.4. Proteomics data analysis

2.4.1. Principal component analysis (PCA)

Principal component analysis (PCA) is a linear dimensionality reduction technique that was applied to perform exploratory analysis of the Chicago cohort plasma and BALF proteomics data. To achieve the separation between the groups, I used the 10% most variable proteins across the conditions as input values for the analysis using the factoextra package (v.1.0.7).

2.4.2. Co-expression network analysis

Gene co-expression network analysis (GCNA) is an analytical tool aiming to identify groups of genes/proteins with similar expression patterns across different conditions. The identification is achieved by pair-wise comparison of genes/proteins with similar patterns across all samples and creating a co-expression network for each gene. This method is applied to explore gene/protein

expression groups (modules) that are correlated with specific disease conditions and can be controlled by the same transcription regulators or have similar molecular functions (145).

The GCNA was applied to the Chicago cohort plasma and BALF proteomics data for the identification of protein clusters, that exhibit similar behavior within each pneumonia group and the in-depth characterization of their functional properties. This analysis was conducted in the R environment (v.4.3.0) using the CoCena2 package (https://github.com/MarieOestreich/hCoCena). Log_2-transformed, normalized, and imputed protein intensity matrixes for plasma and BALF were used as input for the analysis (section 3.3.5).

The correlation cut-off calculated through the weighted sum of the Multicriteria Decision Aiding (MCDA) output was applied to maximize the correlation coefficient (R2) and the number of edges/nodes while minimizing the number of independent networks resulting from the selected cut-off (146). The cut-off of 0.81 was applied to the BALF dataset and 0.74 to the plasma dataset.

The network results were clustered using the Louvain algorithm (147) with a minimum cluster size of 10 nodes. The results were presented as a mean fold change for each module and condition in a heatmap with the module/condition setting.

2.4.3. Over-representation analysis (ORA)

Over-representation analysis (ORA) is a statistical method determining whether genes associated with specific molecular pathways are represented more than expected in the selected dataset. I employed ORA for each $CoCena^2$ module of BALF (B1-B12) and plasma (S1-S7) independently to detect biological terms associated with these modules and thus with different disease conditions. The analysis was performed using the clusterProfiler package (v.4.10.0) (148). As a reference for biological processes, I used the Reactome, an open-source pathway database of human pathways and processes (149). For each module, the top 5 overrepresented molecular terms with n >5 detected proteins per term and adjusted P-value <0.05 were presented as a grouped dot plot.

2.4.4. Gene set variation analysis (GSVA)

To access the variation in biological processes between patient groups in a longitudinal setting, I applied the GSVA approach to the imputed, log2-transformed protein intensity matrix of BALF samples (150). In summary, GSVA compares the expression levels of genes from a predefined gene set to the expression levels of all genes in each sample and calculates an individual enrichment score. As gene sets, I used enriched Reactome terms from the ORA analysis of BALF samples and custom gene lists. To determine pathway activity scores for individual samples, I utilized the GSVA package (v.1.5.0) with a minimum pathway size corresponding to 3 genes. To visualize differential activities of molecular pathways between patient groups, I employed box plot charts using the ggplot2 (v.3.4.4) package.

2.4.5. Analysis of protein circulation between plasma and BALF in pneumonia patients

To study the overlap of proteins in plasma and BALF fluids from the Chicago cohort, I created a custom plot by merging non-imputed, normalized plasma and BALF protein log2-transformed intensity matrices using base R functions. Each matrix was scaled column-wise and then transformed to the long format using group-specific annotation as a guide. Later, I calculated the mean value for each protein and each condition for both BALF and plasma tables separately. As a next step, I merged two tables based on proteins detected in both fluids and for all other proteins that were detected in one of the fluids, the missing value was assigned to 0. The distribution of the proteins was displayed as a dot plot in the 'Scaled protein intensity BALF' vs 'Scaled protein intensity plasma' axes. For each type of pneumonia, the plot was created separately. Proteins with 'Scaled protein intensity BALF' value >0 and 'Scaled protein intensity plasma' <0.5 were considered locally produced in BALF. Conversely, proteins that followed the rule: 'Scaled protein intensity BALF' value >0 and 'Scaled protein intensity plasma' >0.5 were considered circulating between both fluids.

Overlap between 'locally produced' and 'circulating' immunoglobulin categories for all four patient groups in the Chicago cohort was visualized using the ComplexUpset package (v.1.3.5) in the R environment.

2.4.6. Analysis of the autoreactivity data

I evaluated the DAC assay's reliability by conducting receiver operator characteristic (ROC) analysis using the R package plotROC (v.2.3.1). Our objective was to compare the number of patients from the Chicago cohort with anti-IL6R antibodies detected and the clinical evidence of drug administration (anti-IL6R monoclonal antibody) in severe COVID-19 cases.

I compared COVID–19–specific autoreactivities (DAC data) of the Munich and Chicago cohorts separately and assessed the putative autoantigen overlap between them. For this purpose, protein intensity matrices were log2-transformed and selectively imputed following the rule that imputation takes place only if there are less than three values for control conditions. Log2-transformed protein intensity values for COVID-19 groups were not imputed. This procedure was implemented to ensure that only proteins appearing in at least three patients in the COVID-19 group and significantly enriched over at least one of the controls were interpreted as autoantigens (137). For further statistical testing, I defined the compared groups with four time windows for COVID-19 patients of the Munich cohort, described earlier, and 4-time points for the COVID-19 patients of the Chicago cohort; each time point was composed by a selection of the consequent time point for each patient starting from the day of intubation. Only two time points were available for bacterial pneumonia and influenza groups. Control high inflammatory(n=23) and low inflammatory

(n=24) from the Munich cohort and non-pneumonia control (n=7) from the Chicago cohort contained a single sample per patient and were used as reference groups for each cohort in the following analysis.

To reveal COVID-19-specific autoreactivities in the Chicago cohort, I performed a Welch non-parametric test for the COVID-19 (n=13) samples against bacterial pneumonia (n=6), Influenza (n=7) and non-pneumonia control groups (n=7) separately for each time point. The protein was considered significantly enriched as an output if the FC >1.5 and the p-value <0.05.

For the Munich cohort, I repeated the same procedures with the COVID-19 group against control high inflammatory (n=24) and control low inflammatory (n=23) separately for each time window. Additionally, the Munich COVID-19 patients were split on ARDS (n=16) and mild (n=7) to achieve compatibility of the results with the Chicago cohort.

The lists of putative autoantigens from both cohorts, composed of significantly enriched proteins in the severe COVID-19 group in at least one condition and one time point, were compared to identify common autoreactivities in both cohorts. The output was visualized using a Euler diagram with the Eulerr (v.7.0.0) package.

All the statistical and bioinformatics operations listed above were run with the Perseus software package (version 1.6.14.0) (151), and the results were visualized in the R (v.4.3.0) using the ggplot2 (v.3.4.4) packages.

2.4.7. Modeling of time and severity effects on the autoreactivities in the Munich cohort

Log2 transformed protein matrixes of 23 patients in a longitudinal setting of Munich cohort containing 1,210 identified proteins were divided based on t-SNE analysis into two groups representing COVID-19 patients with different severity stages: ‘mild’ and ‘severe’. The linear mixed-effects model was used to identify differential protein expression profiles in each of these groups at four time points:

$$Protein_{ij} = \beta_{0i} + \beta_{1i} * Time\ window_{ij} + \beta_2 * Severity\ group_{ij} + \varepsilon_{ij}$$

$Protein_{ij}$ is the log2 transformed fold change between COVID-19 and averaged Control low inflammatory group of expression value for sample *i* in patient *j* for a single protein. B_{0i} is a random intercept for the *i*th patient, β_{1i} is a random slope for the *i*th patient and β_2 is a fixed coefficient for the severity group. $Time\ window_{ij}$ and $Severity\ group_{ij}$ represent the fixed effect for the time in the *j*th observation. The model was built in n the R environment (v.4.3.0) using lme4 (v.1.1-35.1), lmerTest (v.3.1-3), and psych (v.2.3.9) packages. The evaluation of the model was addressed using the performance package (v.0.10.8) with a focus on Akaike Information Criterion (AIC), Bayesian Information Criterion (BIC), Bayes Factor (BF) characteristics, and normality of distribution of the residuals, as quality factors. The false discovery rate (FDR) adjusted P-value <0.05

was considered significant. The significance of each fixed effect on the protein levels was evaluated using the ANOVA F-test.

1.1.1 Calculation of the autoantigen score

I calculated the autoantigen score to study the cumulative autoreactivity for each patient. It comprises a sum of all fold changes of all autoreactivities above the custom threshold. To start with, log2-transformed protein intensity matrixes for the Chicago and Munich cohorts were transformed into the fold change matrixes for each protein in the COVID-19 group by subtraction of the mean protein intensity of the non-pneumonia control group (n=7) in the case of the Chicago cohort, and control low inflammatory (n=23) in case of the Munich cohort. For the Munich cohort, the analysis was focused only on the severe COVID-19 patients (n=16).

The threshold was defined manually based on the experimentally observed threshold for true positive control, IL6R, and comprised of fold changes above 3. This way, all the autoantigens with a fold change above 3, excluding immunoglobulins, were summarized for individual patients and time points in the Chicago and Munich cohorts.

1.1.2 Analysis of the associations between autoantigens and clinical parameters

To obtain associations between cumulative autoreactive background in COVID-19 patients and clinical manifestations, I performed Pearson correlation tests between available clinical values and autoantigen scores for the Chicago and Munich cohorts, selecting only first-time points for each patient. This analysis was conducted in R-environment (v.4.3.2) using ggpubr (v.0.6.0) and corrplot (v.0.92) packages. The results were visualized on the bar plot with an x-axis corresponding to the clinical parameters and a y-axis correlation coefficient between each parameter with an autoantigen score. The bars were ordered from the strongest positive to the strongest negative correlation; the significant results ($p<0.05$) were highlighted with a star sign.

2.5. Single-cell RNA sequencing data analysis

2.5.1. Pre-processing

Data from the multi-omics single-cell atlas of peripheral blood immune cells from hospitalized COVID-19 patients and healthy control donors was downloaded from the ArrayExpress repository (E-MTAB-10026) in the h5ad format. This dataset contained transcriptomic raw gene expression counts, cellular indexing of transcriptomes, epitopes (CITE-seq) data, and lymphocyte immune receptors (152).

CITE-seq is a sequencing-based method that enables the quantification of cell surface proteins alongside transcriptomic data within a single experiment. It uses antibodies tagged with unique oligonucleotides to identify surface proteins, with sequencing as a readout. Studying both transcriptomic and surface protein modalities simultaneously enhances understanding of molecular mechanisms underlying certain disease conditions and provides insights into new cell types.

The atlas contained several severity categories of COVID-19 patients: asymptomatic (n=12), mild (n=26), moderate (n=32), severe (n=15), critical (n=17), and three control types: healthy (n=24), hospitalized non-COVID-19 patients (n=5), lipopolysaccharide (LPS)-stimulated patients (n=12). The samples were collected in 3 different cities: Newcastle, London, and Cambridge, and each patient contributed one sample. The downloaded dataset contained 647,366 cells and 24929 genes, and in the original publication, it was classified into 18 cell types.

From the original object using scanpy (v.1.9.1) package, I removed LPS-stimulated and hospitalized non-COVID-19 patients to understand better the COVID-19 severity stages (n =102). The downstream preprocessing and analysis for the dataset were performed in the Seurat (v.4.2.1) I preprocessed combined raw data from the three centers to remove cells with >10% mitochondrial reads and <1000 unique feature counts using subset() function of the package. Data was normalized using NormalizeData() function applying “LogNormalize” normalization method and scale factor 10000 and scaled afterward with the ScaleData().

2.5.2. Downstream analysis of single-cell data

As a next step, genes with the highest variation across all cells, and highly variable genes (HVGs) must be calculated. HVGs were calculated using scvi-tools (v.0.6.8) function scib.preprocessing.hvg_batch() with patient ID as a batch factor. The target genes were set to reach 15% of the total number of genes in the object, excluding genes with an expression level equal to 0. In this case, 4000 HVGs were selected. I used an outside function to encompass the batch factor from processing patients in different centers.

As a next step, I integrated the dataset, using a computational approach to compare cellular entities across various datasets or patients. HVGs were imported into the Seurat object, and data was scaled and normalized. I used Harmony (v.0.1.1) to adjust Principal components (PCs) by the patient ID and used it to generate the neighborhood graph and embeddings using Uniform Manifold Approximation and Projection (UMAP). Clustering was performed using the Louvain algorithm with an initial resolution of 0.5 and 30 PCs. Differentially expressed genes were calculated for initial clustering using the Model-based Analysis of Single-cell Transcriptomics (MAST) algorithm (153), a statistical test for characterizing transcriptional heterogeneity in single-cell data. As a next step, I manually annotated the clusters using marker genes for the PBMCs (154) and subsetted cells that expressed B and plasma marker genes (*CD79A, MS4A1, CD19, CD22, JCHAIN, IGKC, IGHG1, IGHA1, IGHG4, IGHG3, IGHG2*) for further analysis.

HVGs for the B and Plasma cells subset were calculated analogously as previously described. After scaling the data and assigning PCs, I ran Harmony to align the data of the different patients better and avoid the batch effect.

2.5.3. Annotation of B and plasma cells

To annotate B and plasma cell subsets, I calculated new UMAP embeddings to separate cluster identities. For the final visualization of the B and Plasma cell dataset, the UMAP was generated using 20 PCs, resolution equal to 0.5, and harmony as a reduction component.

This allowed us to identify cell states by exploring the differentially expressed genes (DEGs) per cluster via FindAllMarkers() Seurat function utilizing the MAST algorithm. Genes with > 0.25 log-fold changes, at least 25% expressed in tested groups, and Bonferroni-corrected p values < 0.05 were considered significant. The top 20 significant DEG per cluster were further used to manually annotate each cluster based on available in the literature B and plasma cell marker genes (155).

To address the identity of each cluster, I utilized both transcriptomic and surface protein markers (CITE-seq) available in the dataset. The CITE-seq is based on antibodies against surface proteins of interest tagged with oligonucleotides, allowing their sequencing alongside single-cell transcriptomics data. This method provides additional information for each cell, including the level of surface protein expression besides sequenced transcripts.

The normalization of CITE-seq data was carried out using NormalizeData() function with a centered log ratio (CLR) normalization method, which aids in better separation of cell populations. Still, it does not directly estimate and correct specific sources of technical noise, including the apparent background noise, as in the case of transcriptomics data (156). To compute protein markers, I applied FindAllMarkers() using the MAST algorithm and the surface protein layer as input. For more detailed annotation, I utilized surface protein markers reported by Woodruff and colleagues (131) and B1 cell-specific markers: CD5, CD19 high, CD23 low, CD43 high, IgM high,

IgD low (157). The dataset was split into subsets for B1 cells, IgA high plasma cells, dividing Plasma blasts, Immature B cells, Naive B cells, and Memory B cells (Table 2.5.3).

Table 2.5.3: Transcriptomic markers of B and plasma cell subsets. The top 20 significantly differentially expressed genes per cluster are displayed.

Cluster	**Maker Genes**
Immature B cells	*TCL1A, CXCR4, FCER2, CD69, BTG1, DUSP1, IL4R, LINC00926, FOS, TSC22D3, BACH2, LAPTM5, TUBA1A, HVCN1, CD37, ZFP36L1, FOXP1, TXNIP, HLA-DRA, CALHM6*
Memory B cells	*CD82, LINC01781, CRIP1, AIM2, COTL1, GPR183, CAPG, TNFRSF13B, ACP5, S100A4, MS4A1, S100A6, PLEK, BLK, CIB1, SCIMP, BANK1, LTB, SPIB, CLECL1*
Naive B cells	*TCL1A, IL4R, FCER2, BACH2, IGHD, CD69, CXCR4, FOS, FCRL1, CD83, HVCN1, COL19A1, AFF3, LINC00926, TSPAN13, TUBA1A, PLPP5, DUSP1, FOXP1, BTG1*
IgA high plasma cells	*JCHAIN, MZB1, FKBP11, TXNDC5, SEC11C, IGHG1, MYDGF, XBP1, SDF2L1, CD38, ITM2C, DERL3, HSP90B1, SSR3, TNFRSF17, LMAN1, IGHA1, PDIA4, SPCS3, HM13*
B1 cells	*LINC01857, FCRL2, ARHGAP24, GPR183, TTN, CD82, PARP15, RALGPS2, FCRLA, BANK1, MS4A1, NR4A2, KLF6, BLK, SYK, NAPSA, FCRL3, IL10RA, SLC2A3, COTL1*
Dividing plasmablasts	*RRM2, IGHG1, SDF2L1, JCHAIN, TXNDC5, MZB1, TYMS, STMN1, MYDGF, MANF, FKBP11, TUBA1B, FABP5, CCND2, TXN, MKI67, SSR3, SEC11C, HMGB2, HSP90B1*

2.5.4. BCR-seq analysis

The single-cell V(D)J data derived from multi-omics single-cell atlas of peripheral blood immune cells from hospitalized COVID-19 patients and healthy controls was initially processed with Cell Ranger vdj pipeline (4.0.0) (152). This processing involved filtering out reads with noisy barcodes and unique molecular identifiers (UMIs) while generating full-length transcripts (contigs) for each chain in all observed cells.

For preprocessing and subsequent analysis, I utilized the 'filtered_contig_annotations.csv' file downloaded from the ArrayExpress repository (E-MTAB-10026), adhering to guidelines from the Single-cell best practices book (158).

Subsequently, the contigs table was filtered within a python (v) environment using the Scirpy package (v.0.11.2). Specifically, I followed the selection criteria of only a single complete immune receptor (IR) per cell, thereby removing all the contigs for incomplete IR or ones containing extra chains. This process ensured the selection of cells containing a singular BCR per cell and a full set of VDJ chains required for receptor assembly.

In the next step, I integrated the filtered contigs with the single-cell multi-omics B and plasma cell object described above using scirpy: ir.pp.merge_with_ir() and removed all the cells in the object, which did not have IR, resulting in 38 000 cells.

2.5.5. B cell clone/clonotype definition

The B cell receptor (BCR) consists of heavy and light chains (κ and λ), with the light chains formed by Vand J—genes and the heavy chain containing V-, D—and J—genes. This genetic construct confers high variability to the final receptor, providing flexibility to capture various antigens.

The IR encompasses three regions of high variability known as the Complementary Determining Regions (CDRs) 1-3, which are detected per chain where the IR binds to its target antigen. The V-gene encodes CDR1 and CDR2, while CDR3 is at the intersection of V-, (D-), and J-genes, making it the most diverse element. Thus, it is considered that the specificity of the IR is determined by its CDR3 region (159).

This way, the data obtained from VDJ-sequencing enables the study of cell functionality, which is directly connected to receptor specificity. Identifying cells with the same or similar IR allows the association with the same receptor specificity and molecular phenotype. Defining these groups facilitates the tracking of how infection induces transcriptomic changes in the immature B cell subsets and how the diversity of the immune cell repertoire changes after the immune response.

The theoretical part behind the computational clonotype assignment relies on the following principles: usage of identical V and J genes, matching CDR3 amino acid length, and 85% and higher

similarity of amino acid sequence of the CDR3 junction (based on hamming distance). To assign a clonotype for each receptor, I used the Python-based package Dandelion (v.0.3.0), which provides a BCR distance-based clonotype definition method that searches for the similarity between CDR3 regions of the cells taking into consideration the possibility of the point mutations (160). The method considers all possible 5-mer combinations for the analogous mutation case, where the amino acid represented by the codon stays unmodified, making it especially helpful in dealing with somatic hypermutation of the B cells (160). For clonotype definition based on distance, I defined the separation threshold for close-related receptor sequences using ddl.pp.calculate_threshold() to be able to assign which cells could be considered clones. As the distribution of the distances is expected to be binomial, the threshold is selected as a middle point between both modes (161). All clones/clonotypes were called across the entire dataset. All downstream visualization and gene segment usage analysis were performed using scirpy() and Seurat (v.4.2.1) plotting functions.

3. Results

3.1. Proteomic analysis of biofluids of patients with infectious lung diseases

Infectious respiratory diseases comprise the 4th most fatal group of diseases worldwide, following ischemic heart disease, stroke, and chronic obstructive pulmonary disease (COPD), according to a recent World Health Organization (WHO) report (WHO, 2020).

COVID-19 is an infectious respiratory disease affecting the lower respiratory tract caused by the SARS-CoV-2 virus (8). Compared to pneumonia cases caused by other respiratory pathogens, such as the Influenza virus, severe COVID-19 patients are characterized by profound systemic inflammation and distinct pathophysiology findings, including increased hypercoagulation and multi-organ damage (133). In the lung microenvironment, SARS-CoV-2 induces a gradual, localized alveolitis where alveolar macrophages containing the virus and T cells create a feedback loop leading to persistent inflammation.

COVID-19 patients exhibit unique pathophysiology, which is not observed in pneumonia caused by other respiratory viruses or bacterial pathogens with similar severity. The clinical picture of COVID-19 includes a prolonged incubation period, high mortality within the severe COVID-19 patients (20-40%), the prevalence of extrapulmonary manifestations, which include deep vein thrombosis, AKI, and myocardial tissue damage (44,60,73). All of these features were specific for COVID-19 pneumonia, which creates an increasing need to comprehend the specific immune mechanisms associated with COVID-19 compared to other types of pneumonia with similar severity. This can be accomplished by evaluating the SOFA score and Acute Physiology Score (APS) scores, considering the respiratory parameters of intubated patients, and examining the demographics of the cohort.

To sum up, it is hypothesized that SARS-CoV-2 pneumonia has a distinctive pathobiology. In the following chapter, I compared the proteomic profiles of COVID-19 to other types of pneumonia with similar severity to elucidate unique molecular signatures observed in BALF and plasma of severe COVID-19 patients.

3.1.1. Demographics of the SCRIPT cohort

To address this question, I joined forces with colleagues from Northwestern Memorial Hospital in Chicago (NMH), who collected 73 longitudinal samples of bronchoalveolar lavage fluid (BALF) and matched plasma samples (n=73) from patients with respiratory failure secondary to the infection. This cohort was assembled as a part of the Successful Clinical Response in Pneumonia Therapy (SCRIPT) study, which aims to improve treatment strategies for patients with severe pneumonia.

Subsequent categorization of patients was based on the specific type of molecular pathogen detected, employing various diagnostic tools for each type. The final cohort included the non-pneumonia control group (n=7), patients with severe non-COVID-19 viral pneumonia (influenza, n=7), patients with severe pneumonia caused by bacterial or fungal pathogens (bacterial pneumonia, n=6), and patients with severe SARS-CoV-2 pneumonia (COVID-19, n=13).

According to the standard clinical protocols, BALF and plasma are routinely collected fluids in ICU-admitted patients, which can be screened for biomarkers predicting patient outcomes alongside conventional blood chemistry parameters. One of the modern approaches allowing reproductive and reliable discovery of such clinical biomarkers is mass–spectrometry–based proteomics (162). Considering this, I acquired BALF and plasma proteomes using high-resolution mass spectrometry to investigate the early pathogenesis in the pulmonary environment and the trajectory of disease progression to reveal potential soluble biomarkers (Fig.3.1.1a).

To elucidate pneumonia-specific responses in the bronchoalveolar space of the patients, I initially selected samples based on the following criteria: the earliest time of intubation, as well as the absence of secondary bacterial infection resulting from the mechanical lung ventilation at that specific time point (Fig.3.1.1b). Most viral pneumonia patients (COVID-19, influenza) acquired bacterial superinfection at later points in the ICU due to lung ventilation and were therefore excluded from further analysis. This selection procedure yielded ten COVID-19 patients, seven influenza patients, six bacterial pneumonia patients, and seven non-pneumonia control patients (Fig.3.1.1b).

I ensured that all the pneumonia subgroups had compatible age, race, and sex profiles and diverse clinical outcomes (Fig.3.1.1c, Table A1). Notably, the percentage of deceased patients among the COVID-19 subgroup was the lowest (15%) in comparison with other types of pneumonia, while the bacterial pneumonia subgroup comprised the highest (67%) (Table A1, Fig.3.1.1e). The severity assessment of the disease was estimated using the SOFA score, revealing a similarity between COVID-19 patients and patients with other types of pneumonia (Fig.3.1.1e, Table A1). At the same time, COVID-19 patients exhibited prolonged lengths of stay in the ICU with significantly higher applied PEEP compared to other groups (Fig.3.1.1e), which indicates excessive lung damage. Besides that, significant differences were observed in the macrophage and neutrophil counts in BALF. An elevated macrophage proportion was detected in the BALF of non-pneumonia control patients, while the highest neutrophil counts were present in the bacterial pneumonia group (Fig.3.1.1e).

Taken together, I introduced a cohort of patients with infectious lung diseases, including COVID-19, influenza, and bacterial pneumonia patients, as well as non-pneumonia controls. All the patients were admitted to the ICU and were comparable concerning disease severity.

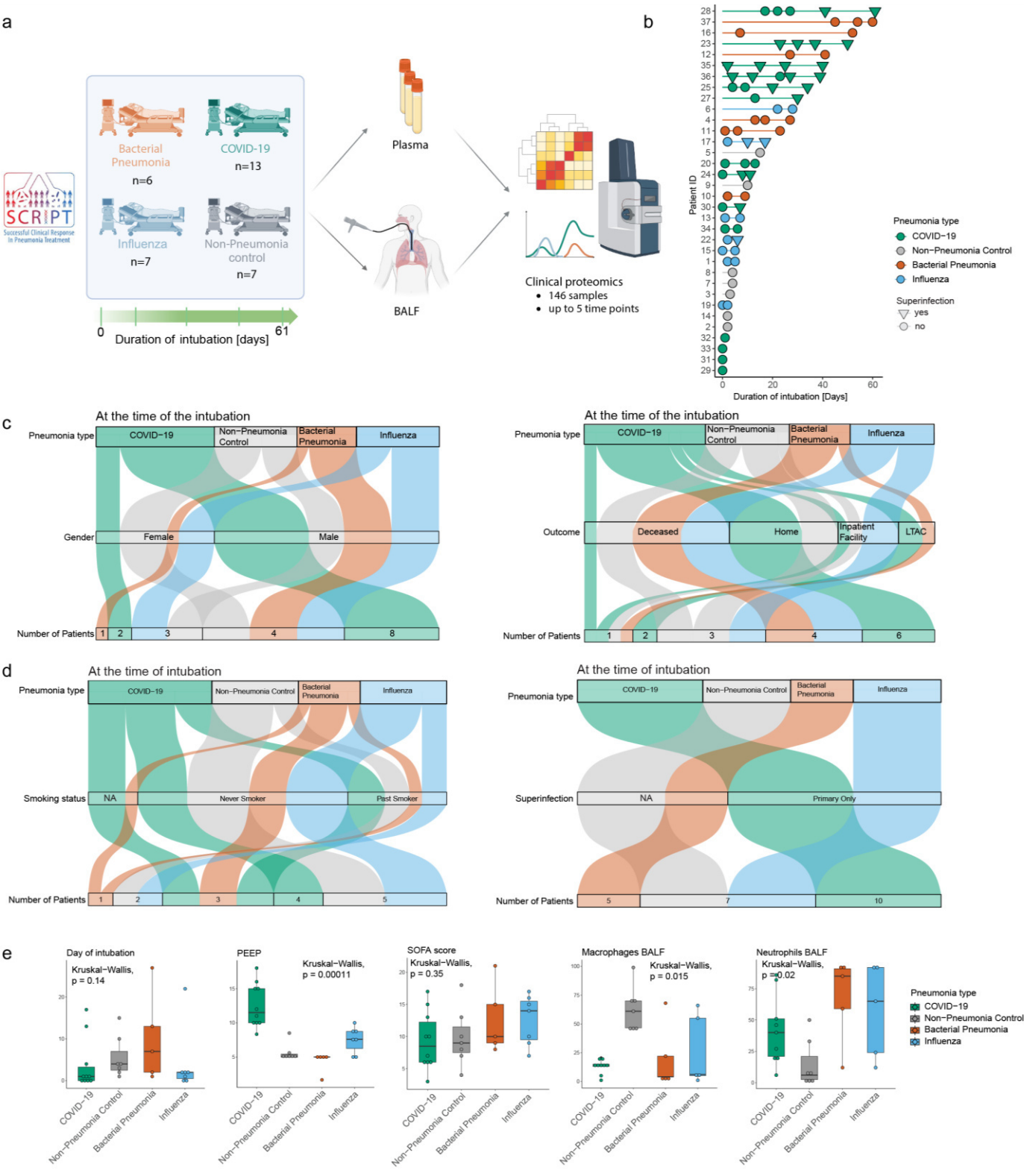

Figure 3.1.1: The SCRIPT cohort demographics. a, Overview of study design. **b**, Overview of the samples of the Chicago cohort. Each point represents a BALF/plasma sample, the color corresponds to the pneumonia type, and the point shape refers to the presence of superinfection. **c**, Gender, and outcome composition of the samples selected for the analysis of the fluids on day 0 of intubation. **d,** Smoking status and superinfection status of the samples selected for the analysis

of the fluids on day 0 of intubation. **e,** Clinical parameters for all four pneumonia groups (Kruskal-Walli's test applied to detect the differences).

3.1.2. Identification of pneumonia-specific molecular signatures upon the intubation

BALF and plasma proteome profiles were first analyzed with principal component analysis (PCA) across all four patient subgroups to assess the systemic differences in proteomes of both biofluids (Fig. 3.1.2a). Notably, the proteome profiles of the COVID-19 patients, influenza, and bacterial pneumonia groups were well separated in the bronchoalveolar environment and the circulation. PC1 was defined by SDC1, PTGDS, SPARCL1, PA2G4, and S100A12, indicative of tissue damage, while separation on the PC2 axes was due to variability of CA1, CA2, BLVRB, HBA2, IGFALS proteins between pneumonia subgroups. This suggests that diversity between pneumonia groups can be observed in both fluids upon intubation and is driven by soluble factors and immune effector proteins.

I next identified BALF and plasma proteins that could reliably distinguish the specifics of the immune response triggered by each type of pathogen. For this reason, I constructed a co-expression network analysis using the BALF and plasma proteomes from COVID-19 (n=10), bacterial pneumonia (n=5), and influenza (n=7) patients, as described in Fig.3.1.1 at the time of intubation to assess their proteome profiles before therapy administration. Proteins were organized into modules based on their relative expression levels, grouping ones with similar expression patterns among patients within each subgroup. I identified twelve protein modules in the BALF and seven in the plasma, each containing a minimum of 10 to a maximum of 60 proteins (Fig. 3.1.2 b, f).

The analysis of the BALF modules' contents revealed that the B1-B6 protein modules were upregulated in bacterial pneumonia patients. They included members of the Rho GTPase effectors (MYH11, ACTR3, SPTBN1, RAC2, ARHGAP30, RHOA, MAPK14, ARPC4, LMNB1, ARPC2, RCC2, ARPC1B, ARPC5, S100A8, VIM, S100A9) (Fig.3.1.2c), neutrophil degranulation (S100A12, CTSG, RNASE2, ELANE, PGLYRP1, FCN1, CEACAM8, PRTN3, ITGAM, ARG1, OLFM4, ITGB2, RHOA, MAPK14, PGM1, BIN2, LAMTOR3, ARPC5, S100A8, ALDOA, S100P, PKM, S100A9), and proteins involved in glucose metabolism (GPI, PGAM1, PGK1, ALDOC, TPI1) (Fig.3.1.2d). These findings were validated by correlating the levels of neutrophil degranulation proteins in the BALF of bacterial pneumonia patients with the corresponding neutrophil cell counts from the same individuals. The data showed a significant positive correlation with a correlation coefficient (R2) of 0.75 and a p-value of 0.01, demonstrating my proteomic results a reflection of the neutrophilic inflammation in the lung microenvironment in bacterial pneumonia (Fig. 3.1.2h).

On the contrary, modules B8 and B9 were elevated in the BALF of COVID-19 patients and consisted of proteins related to the regulation of the complement cascade (F2, CFI, C1S, VTN, C9, CFB, SERPING1, C4B), platelet activation, signaling, and aggregation (HRG, CLEC3B, F2, AHSG, ITIH4, SERPINF2, PLG, APOA1, ORM2, FN1, A1BG, ORM1, SERPING1, APOH, ECM1, ALB, A2M), and T53 regulation of metabolic genes (PRDX5, YWHAG, YWHAQ, TXN, PRDX1)

(Fig.3.1.2e). Module B11 exclusively comprised immunoglobulin variable heavy and light chains (IGHV1-69, IGKV1-39, IGHV3-15, IGLV3-10, IGLV1-47, IGLV1-40, IGLV3-16, IGLC7, IGKV2-30, IGJ, IGLL5, IGLV1-51, IGHM, IGHA1, IGHG3-1). Lastly, influenza-specific modules B7 and B12 contained proteasome components (PSMD4, PSMC2) and extracellular space proteins (GLG1, TIMP2, GPC1, BAX, UBE2N, ATP6V1H, ATP1B1, FABP3, FBP2, YWHAZ, RPS8, TSTA3, ENO2, IGKV1D-33, PPT1) (Fig. 3.1.2c).

Similar to the analysis conducted on BALF, examining plasma proteomes through co-expression network analysis also uncovered diverse patterns across different pneumonia subgroups. Specifically, proteins associated with the complement cascade (CPN1, CFHR4, C9, CPN2, CFB, FCN3, C2, C4A, C4BPB, C4BPA, PROS1, CPB2, C3, CFI, C4B, SERPING1, C8A) and platelet degranulation (FLNA, TAGLN2, PPIA, TMSB4X, VCL, ACTN1, CALM1, FERMT3, PPBP, CAP1) were upregulated in influenza patients (S5, S6, S7), whereas COVID-19-specific modules featured signal transduction proteins (FLNA, S100A8, TPM4, VCL, ACTN1, TPM3, RAP1B, CALM1, PPBP, ACTC1, ACTG1, ACTB; module S1) and immunoglobulins (P06889, IGKV2-24, IGLV1-36, SDC1, IGKV1-17, IGLV3-10, IGLV2-11, IGLV1-40, P01780, P01612, IGLV3-25, IGKV3-7, IGHV2-26, P04431, FAM153A, IGKV4-1, IGHV3-15, P04206, IGKV1-16, P01708, IGKV6D-21, IGKV1-5, IGHG4, IGKV2-40, IGKC-2, P01620, LYZ, P01619, IGKV1D-33, IGLV3-19, IGLV6-57, COPS3, IGKC-1, IGHV3OR16-9, IGLV1-47, P01596, P01717, P04430, IGKV2D-29, IGKV2D-28, P01598, IGHG1-2, IGHG3, P01594, P01611, IGHV3OR16-12, IGHV3-49, IGHV5-51, P01622, IGHV1-46, GP1BA, P01609, IGLL5; module S2). In contrast, plasma modules specific to bacterial pneumonia consisted of proteins involved in the regulation of insulin-like growth factor (IGF) transport and uptake (IGFALS, ITIH2, APOA2, APOA1, SERPIND1, PLG, SERPINC1, F2; module S3) (Fig.3.1.2f).

In conclusion, assessment of the proteomic profiles in BALF and plasma samples collected from patients suffering from COVID-19 revealed the upregulation of the complement cascade, platelet degranulation proteins, and immunoglobulins in the COVID-19 subgroup. Conversely, individuals with bacterial pneumonia exhibited elevated levels of proteins implicated in neutrophil degranulation, glucose metabolism, and Rho GTPase effectors. In the case of Influenza infection, specific proteomic signatures were enriched in complement cascade and platelet degranulation proteins in the plasma, as well as proteasome components and extracellular space proteins in BALF. These findings highlight the initial distinctions between the bronchoalveolar environment and circulation in the pneumonia-relevant molecular processes.

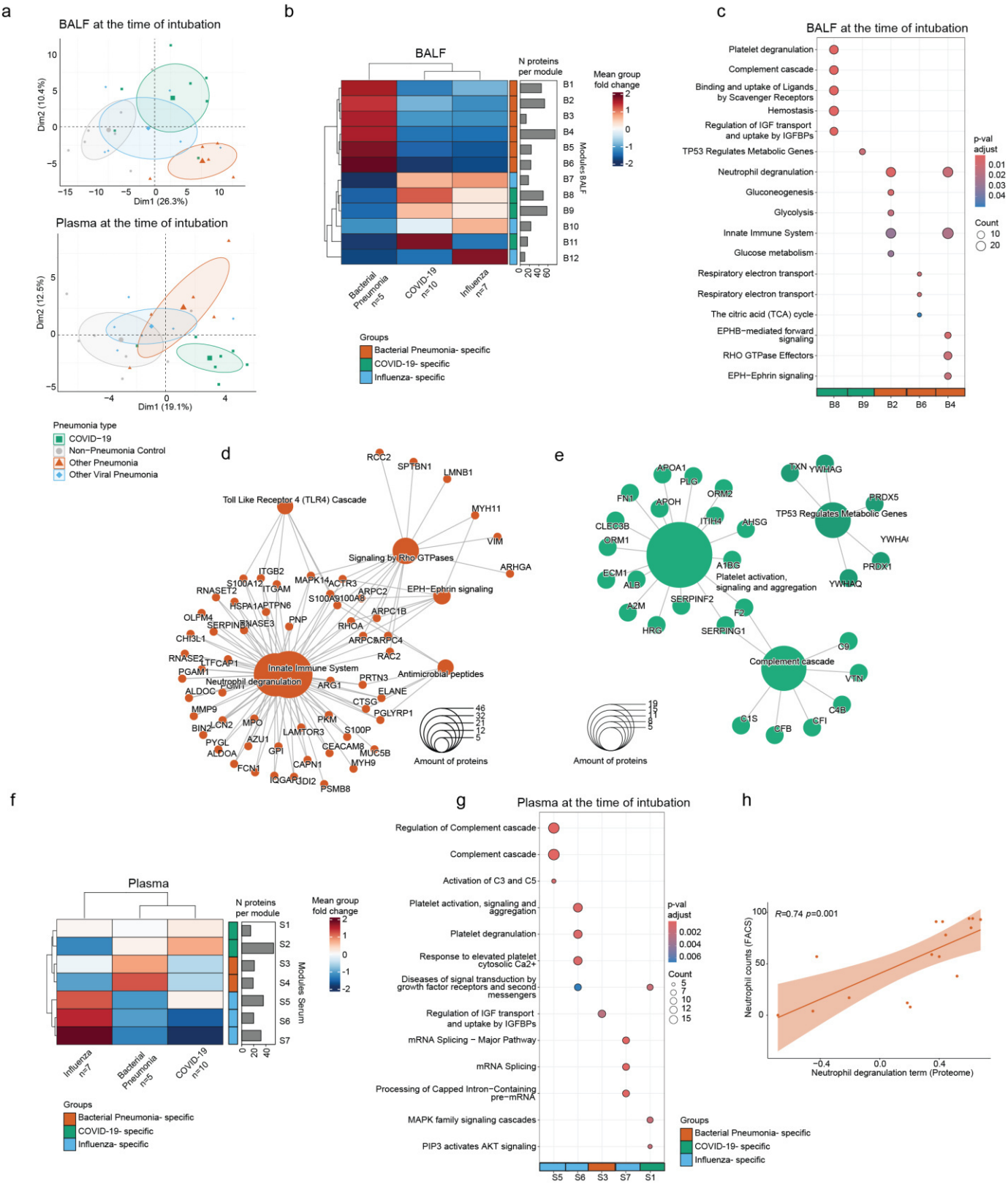

Figure 3.1.2: Pneumonia-specific protein signatures can be detected in BALF and plasma on the day of intubation. a, PCA of BALF, and plasma samples at the time of intubation. **b,** Hierarchical clustering of 12 BALF modules for the subset of pneumonia patients at day 0 of

intubation. The bar plot represents the number of proteins in each module, and the row annotation highlights the group specificity of the module. The color scale reflects the mean fold change of the proteins in the module. **c,** Reactome terms of over-representation analysis (ORA) enriched in BALF modules at day 0 of intubation. The top 5 enriched terms for each module are displayed (p. adj<0.05), color codes for adjusted p-value, and point size refers to the number of proteins detected per term. Modules were assigned specific colors according to their specificity to the pneumonia group in BALF heatmaps on panel b. **d,** Reactome terms with proteins enriched in the bacterial pneumonia BALF modules from Fig.1e. The point size of the terms corresponds to the number of included proteins. **e,** Reactome terms with proteins enriched in the COVID-19 BALF modules from Fig.2b. The point size of the terms corresponds to the number of included proteins. **f,** Hierarchical clustering of 7 serum modules for the subset of pneumonia patients at day 0 of intubation. The bar plot represents the number of proteins in each module, and the row annotation highlights the group specificity of the module. The color scale reflects the mean fold change of the proteins in the module. **g,** Reactome terms of ORA enriched in serum and modules at day 0 of intubation. The top 5 enriched terms for each module are displayed (p. adj<0.05), color codes for adjusted p-value, and point size refers to the number of proteins detected per term. Modules are assigned specific colors according to their specificity to the pneumonia group in serum heatmaps on panel f. **h,** Pearson correlation of enrichment score of 'neutrophil degranulation' term proteins and neutrophil cell counts in the BALF of bacterial pneumonia patients.

3.1.3. Dynamics of pneumonia-specific molecular signatures in BALF

Subsequently, I followed up the significantly upregulated Reactome terms in BALF of pneumonia patients upon intubation longitudinally to investigate how pneumonia-specific immune responses develop over time. For this purpose, I applied the gene set variation analysis (GSVA) algorithm, enabling the exploration of variability within the biological processes across different conditions. GSVA generates an enrichment coefficient for a protein group at each time point and for each patient. This allowed me to group enrichment coefficients for pneumonia subgroups within selected time frames, providing insights into the dynamics of specific biological processes during disease progression.

First, I focused on the longitudinal behavior of bacterial pneumonia-specific molecular terms, specifically neutrophil degranulation and signaling by Rho GTPases. Both terms were elevated in the BALF of bacterial pneumonia patients on the day of intubation, persisting during the initial 0–15-day period compared to influenza, COVID-19, and non-pneumonia control patients (Fig. 3.1.3a, b). However, over time, these protein sets exhibited downregulation in bacterial pneumonia patients while demonstrating an increase in the COVID-19 subgroup. This behavior may be attributed to the resolution of bacterial pathogens in the bacterial pneumonia cohort and the development of bacterial superinfection in the COVID-19 patients during later time points of the ICU stay.

Secondly, platelet activation signaling and aggregation term was initially detected to be significantly upregulated in the BALF of COVID-19 patients at the time of intubation and maintained an upward trajectory, reaching the peak levels during the 45-55 days period (Fig.3.1.3c) compared to other cases of pneumonia. Besides that, proteins involved in the regulation of complement cascade, initially upregulated during intubation, remained elevated in COVID-19 patients throughout the 0-55 day of ICU stay (Fig. 3.1.3e). Furthermore, as part of the co-expression network analysis described earlier, one of the COVID-19-specific modules (B11) consisted of immunoglobulins, which were elevated in BALF of COVID-19 patients. Following this, my data show that immunoglobulins peaked during the initial (0-15 day) period, with a resolving trajectory over time in the ICU among COVID-19 patients (Fig. 3.1.3d). Additionally, observations regarding the persisting upregulation of complement, platelet degranulation proteins, as well as immunoglobulins in a bronchoalveolar environment of severe COVID-19 patients, were supported by existing scientific evidence that highlighted them as a hallmark of the pathobiology of severe COVID-19 patients, often associated with hypercoagulopathy and multi-organ damage (14,35,46,59,70).

Several reports have highlighted the increased deposition of extracellular matrix proteins in the lungs of severe COVID-19 patients, contributing to fibrosis (163). Leveraging my enrichment findings of protein groups in my pneumonia proteomics dataset with GSVA, I further investigated the early signs of pulmonary fibrosis in COVID-19 patients by utilizing a biomarker panel derived from the BALF proteomic dataset of interventional lung fibrosis patients (IPF) (164). These biomarkers

are significantly associated with IPF patients' lung function decline and increased mortality and include FN1, ITIH4, POSTN, APOE, KLKB1, FTL, and BASP1. Calculation of the enrichment score for each subgroup of pneumonia patients using those fibrotic markers revealed the increased scores in the BALF of COVID-19 patients compared to influenza, bacterial pneumonia, and non-pneumonia control patients persisting longitudinally (Fig. 3.1.3f). Remarkably, only the bacterial pneumonia subgroup reached similar levels of fibrotic markers as COVID-19 during the latest time window (45-55 days). This observation suggests that early signs of pulmonary fibrosis can manifest in the lung microenvironment of COVID-19 patients shortly after intubation, contrasting with other types of pneumonia of similar severity.

To conclude, proteins involved in regulating complement cascade and platelet activation signaling and aggregation displayed an unresolved trajectory in the BALF of COVID-19 patients during the first two months in the ICU, distinguishing this pneumonia type from influenza and bacterial pneumonia patients. Lastly, I observed an accumulation of immunoglobulins in the bronchoalveolar space of COVID-19 patients on the day of intubation, progressively decreasing over time in the ICU. This phenomenon can be supported by existing scientific reports revealing that hyperactivation of the immune system facilitates the early production of neutralizing antibodies against SARS-CoV-2 with low specificity (165).

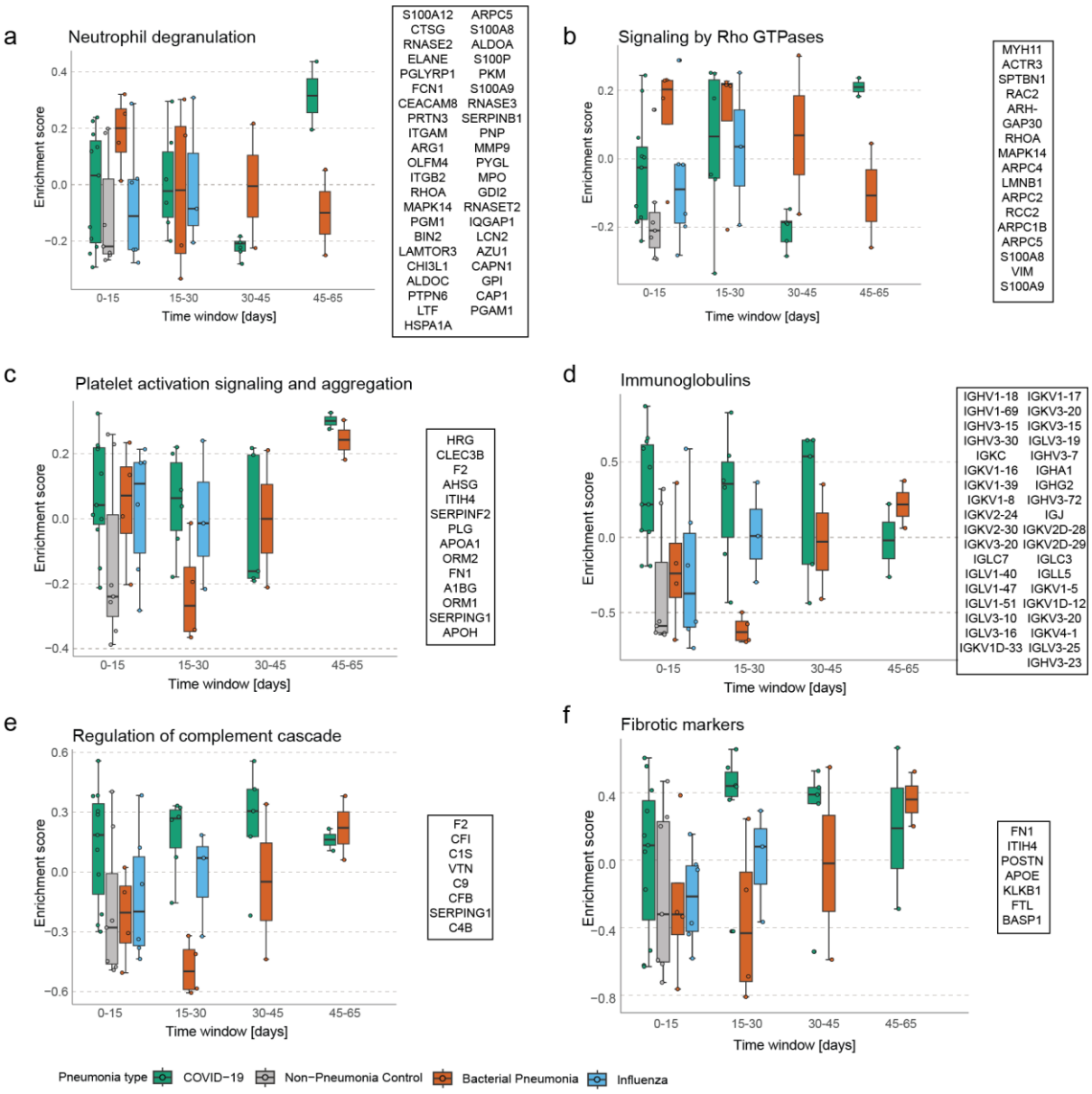

Figure 3.1.3: Pneumonia-specific signatures detected in BALF during intubation persist longitudinally. a, Box plot graph displaying longitudinal behavior for platelet activation signaling and aggregation Reactome term enriched in BALF of four pneumonia groups. Each dot represents the enrichment score for an individual patient, and the box color corresponds to the patient subgroup. Proteins for the term are displayed on the left side of the graph. **b,** Box plot graph displaying longitudinal behavior for immunoglobulins enriched in BALF of four different pneumonia groups. **c,** Box plot graph displaying longitudinal behavior for regulation of complement cascade Reactome term enriched in BALF of four pneumonia groups. **d,** Box plot graph displaying longitudinal behavior for fibrotic markers from (164) enriched in BALF of four different pneumonia groups. **e,** Box plot graph displaying longitudinal behavior for neutrophil degranulation Reactome term enriched in BALF of four pneumonia groups. **f,** Box plot graph displaying longitudinal behavior for signaling by Rho GTPases Reactome term enriched in BALF of four pneumonia groups.

3.1.4. Presence of plasma proteins in the lung environment in COVID-19 patients is associated with a decreased P/F ratio

Upon observing an increased proportion of immunoglobulins and platelet-associated proteins in the BALF of COVID-19 patients at the time of intubation, I hypothesized that a breach in the endothelial integrity might lead to the leakage of plasma proteins and cells into the lung environment, thereby promoting inflammation and obstructing the recovery (166).

To assess pulmonary damage severity in pneumonia patients, I focused on the longitudinal profiles of the partial pressure of oxygen in arterial blood (PaO2) to the fraction of inspiratory oxygen concentration (FiO2) ratio (P/F), commonly used to classify ARDS severity. Interestingly, the P/F ratio remained consistently lower in COVID-19 patients throughout the intubation period than in influenza and bacterial pneumonia patients (Fig. 3.1.4a), implying an expanded lung damage in this subgroup. Next, I followed up on the presence of plasma proteins in BALF across pneumonia types. I calculated enrichment scores for the hundred most abundant plasma proteins derived from the healthy controls for each sample, revealing that the plasma proteins in BALF peak during the 0-15 days period for the COVID-19 patients compared to bacterial pneumonia and influenza, and persist elevated throughout the stay in the ICU (Fig.3.1.4b).

Lastly, to explore the association between these parameters, I performed pairwise Pearson correlation tests between molecular terms specific to BALF of COVID-19 and bacterial pneumonia subgroups (as described in Fig.3.1.2 and Fig. 3.1.3) and clinical metadata, including respiratory parameters, BALF cell counts, severity parameters, and blood chemistry values (Fig.3.1.4c). My analysis revealed significant positive correlations ($p<0.05$) between plasma proteins in BALF of COVID-19 patients and Positive End Expiratory Pressure (PEEP), along with a significant negative correlation with the P/F ratio. Moreover, the presence of IPF fibrotic markers and upregulated complement cascade proteins in the BALF of COVID-19 were negatively associated with the P/F ratio. These findings suggest that the accumulation of the plasma proteins and proteins related to the regulation of complement cascade in the bronchoalveolar environment of COVID-19 patients is indicative of profound lung damage, possibly arising from endothelial dysfunction followed by plasma leakage, which distinctly affects the lung state in COVID-19 patients compared to other pneumonia groups with similar severity.

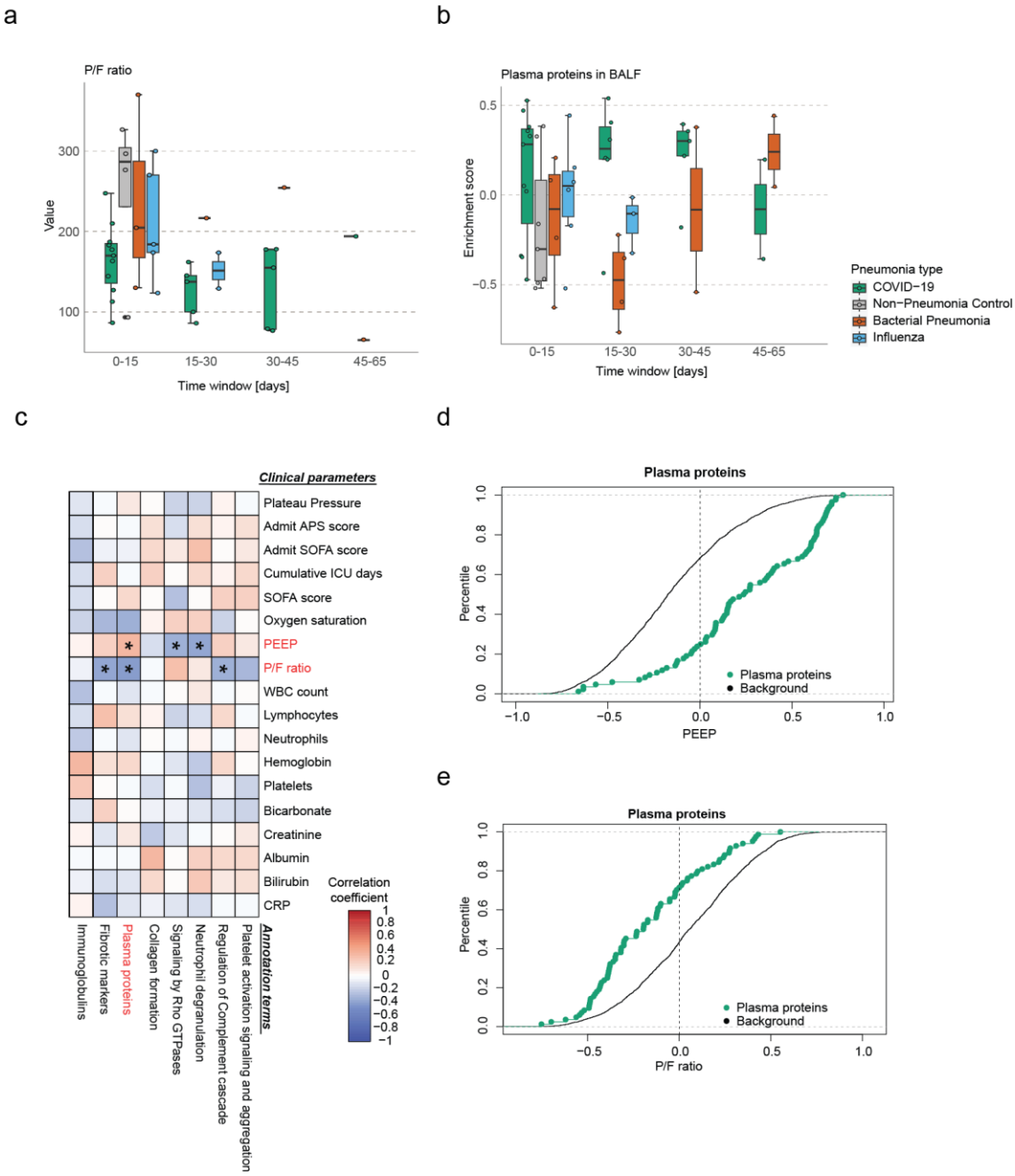

Figure 3.1.4: Elevated levels of plasma proteins in the bronchoalveolar environment of COVID-19 patients are associated with a decreased P/F ratio. a, Longitudinal box plot of P/F ratio in four groups of pneumonia patients. Each dot represents an enrichment score for an individual patient and the box color corresponds to the patient subgroup. **b,** Box plot graph displaying longitudinal behavior for plasma proteins enriched in BALF of four pneumonia groups. Each dot represents an enrichment score for an individual patient, and the box color corresponds to the patient subgroup. **c,** The heatmap demonstrates Pearson correlation coefficients of molecular terms enriched in BALF samples and indicated clinical parameters. The color code represents the correlation coefficient, highlighting significant associations ($p<0.05$). **d-e,** Cumulative density

plots depict the distribution of correlation coefficients for plasma proteins enrichment scores with Positive end-expiratory pressure (PEEP) and partial pressure of oxygen in arterial blood (PaO2) to the fraction of inspiratory oxygen concentration (FiO2) (P/F) ratio in BAL compared to all background proteins (black line).

3.1.5. The COVID-19-specific signature consists of lung-abundant and plasma-abundant proteins

Prompted by the co-existence of plasma proteins in the bronchoalveolar space of COVID-19 patients, I next investigated the relative abundance of COVID-specific proteins (described in chapter 3.1.2) in BALF and plasma to subdivide the ones responsible for systemic effects and the ones providing the local immune response.

To achieve this, I visualized the scaled mean intensity of proteins in BALF of COVID-19 patients upon the intubation on the x-axis and in plasma on the y-axis of a scatter plot. The proteins with a mean-scaled intensity in BALF above 0 and mean-scaled intensity in plasma above 0.5 were selected as 'plasma-abundant' proteins (Fig. 3.1.5 a). Among these proteins, I detected complement factors (C4B, C9, CFB, CFI), acute phase proteins (CRP, SERPINF2, SAA2, SAA4, ITIH4, A2M, F2, AHSG, ORM1, ORM2), apolipoproteins (APOA2, APOA1, APOC3), as well as a subset of immunoglobulins (IGHA1, IGHG2, IGHV3-72, IGJ, IGKV2D-28, IGKV2D-29, IGLC3, IGLL5), which are shared between both fluids and are considered to be a hallmark of the severe COVID-19 infection (73).

In contrast, 'lung-abundant' proteins in COVID-19 patients were involved in protection against oxidative stress (PRDX1, PRDX5, TXN), vitamin and hormone binding (GC, TTR), and signal transduction (PEBP1, YWHAG). Moreover, a distinct set of immunoglobulins dominated the bronchoalveolar space of the COVID-19 patients (IGHV1-18, IGHV1-69, IGHV3-15, IGHV3-30, IGHV3-7, IGKC, IGKV1-16, IGKV1-17, IGKV1-39, IGKV1-8, IGKV1D-33, IGKV2-24, IGKV2-30, IGKV3-15, IGKV3-20, IGLC7, IGLV1-51, IGLV3-10, IGLV3-16, IGLV3-19). Adaptive immune response was formed by the production of immunoglobulins, part of which can be found in circulation already at the early stages of the disease (upon intubation), and another part, 'lung-abundant,' is produced as a local immune response to the virus evasion.

Subsequently, I aimed to determine whether the detected immunoglobulin fragments were exclusive for COVID-19 or could also be detected in other types of pneumonia, particularly of viral origin. To stratify lung and plasma-abundant immunoglobulins in COVID-19 and influenza subgroups, I compiled all the immunoglobulins detected in BALF and plasma proteomes. As described, I visualized them on the scatter plots (Fig.3.1.5c, d) and observed that COVID-19 patients exhibited higher levels of locally produced immunoglobulins than the influenza subgroup.

I compared immunoglobulins for COVID-19, bacterial, pneumonia, influenza, and non-pneumonia control groups. The results were visualized on upset plots (Fig. 3.1.5 e, f). COVID-19 patients contained the largest unique pool of lung-abundant immunoglobulins (n=15) compared to other types of pneumonia, specifically influenza (n=9), non-pneumonia control (n=10), and bacterial pneumonia (n=6) (Fig. 3.1.5 e). Additionally, all the groups shared 11 fragments detected in the

lung environment of each type of pneumonia. In contrast, among plasma-abundant immunoglobulins, the biggest group of proteins was commonly detected in each patient category, with four unique fragments for the COVID-19 subgroup, three - for influenza patients, and one for bacterial pneumonia (Fig. 3.1.5 f).

In COVID-19, I observed a specific group of immunoglobulin variable fragments detected upon intubation at the primary site of viral evasion. In contrast, plasma-abundant immunoglobulins for COVID-19 and other pneumonia types exhibited similarity to a certain extent (11 shared fragments). That leads to the conclusion that the immune response in COVID-19 patients is characterized by the production of lung-abundant antibodies, which are not observed in other pneumonia types. The presence of these immunoglobulins in the lung upon intubation can be explained by the early production of SARS-CoV2 neutralizing antibodies, which in several cases were described as cross-reactive to the host antigens (167).

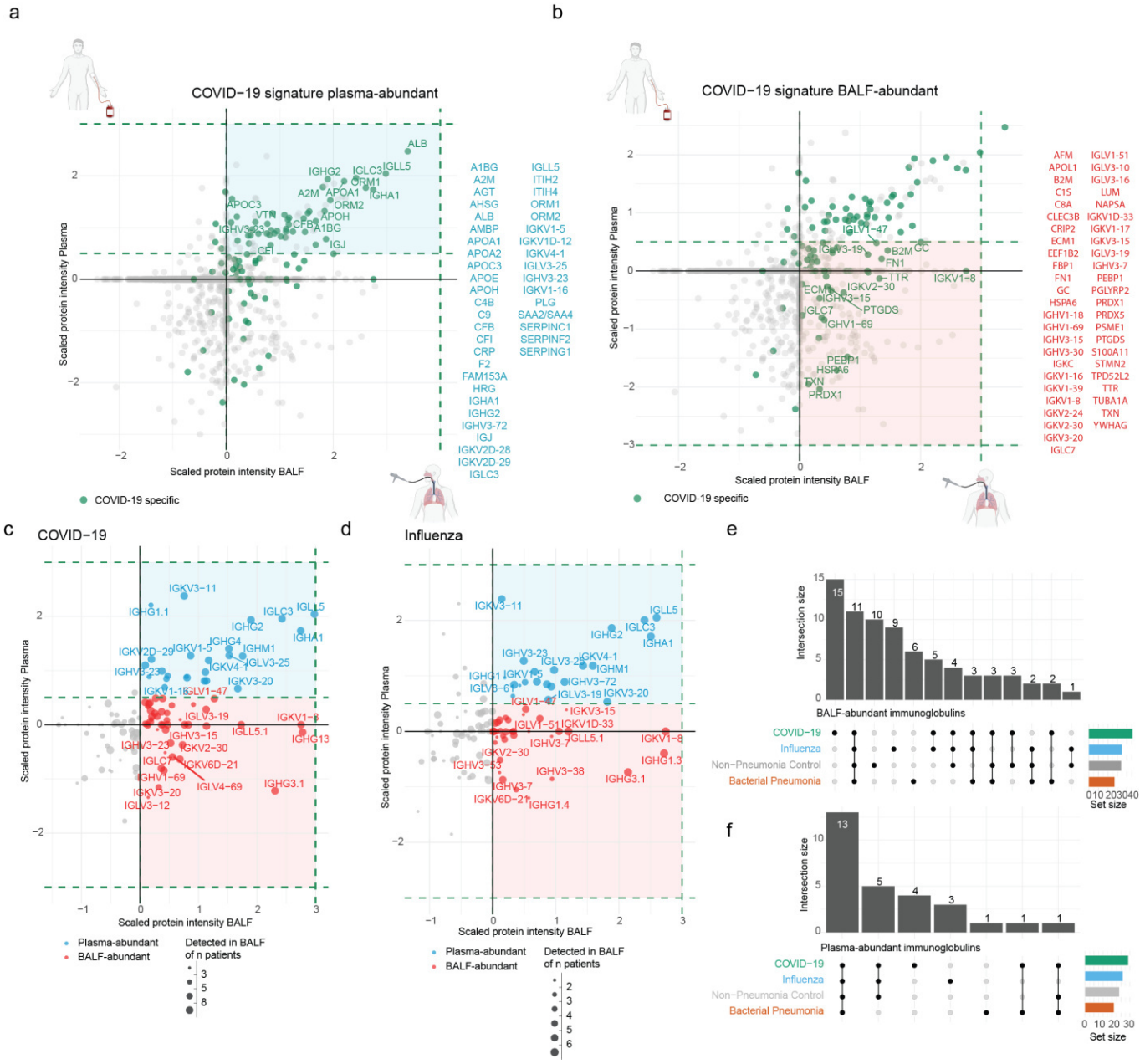

Figure 3.1.5: COVID-19 patients contain both plasma-abundant and lung-abundant immunoglobulins, distinguishing them from patients with other types of pneumonia. a, Scatter plot displaying the distribution of proteins between BALF on the x-axis and plasma on the y-axis. COVID-19-specific modules detected in BALF upon intubation are highlighted in green. A light blue box frames proteins shared between both fluids. A list of COVID-19-specific proteins shared between fluids is displayed in light blue on the right side of the plot. **b,** Scatter plot displaying the distribution of proteins between BALF on the x-axis and plasma on the y-axis. COVID-19-specific modules detected in BALF upon intubation are highlighted in green. A pink box frames proteins that are more abundant in the lung. A list of COVID-19-specific proteins more abundant in the lung is displayed in red on the right side of the plot. **c,** Scatter plot displaying the distribution of

immunoglobulins between BALF on the x-axis and plasma on the y-axis of the COVID-19 subgroup. The point size corresponds to the number of patients for which this protein was detected. The color of the point highlights if the immunoglobulin is lung-abundant or plasma-abundant. **d,** Scatter plot displaying the distribution of immunoglobulins between BALF on the x-axis and plasma on the y-axis of the influenza subgroup. **e,** Upset plot depicting the intersection between lung-abundant immunoglobulins of COVID-19, influenza, bacterial pneumonia, and non-pneumonia control subgroups. **f,** Upset plot depicting the intersection between plasma-abundant immunoglobulins of COVID-19, influenza, bacterial pneumonia, and non-pneumonia control subgroups.

3.2. Single-cell multi-omic analysis of COVID-19-induced B cell populations

3.2.1. Molecular mechanisms of self-tolerance in B cells

B cell-mediated immunity relies on the highly diverse repertoire of B cell receptors (BCR) expressed by naive B cells in the bone marrow. The BCR consists of a heavy and a light chain which define the structure and specificity of the receptor. BCRs are assembled via the process of V(D)J rearrangement, which provides diversity to the repertoire by pairing heavy (H) and light (L) chains in B cell precursors. As a result, the final receptor is composed of randomly selected H and L chains and possesses the ability to bind foreign antigens.

During the maturation phase, hematopoietic stem cells (HSC) commit to the lymphoid lineage, divide, and eventually develop into naive B cells through a process tightly controlled by cytokines, independent from the foreign antigen. Originating in the bone marrow, HSCs undergo several transitional developmental stages, specifically the pro-B cell (progenitor B cell), the pre-B cell (precursor B cell), the immature naïve B cell, the transitional B cell, and the mature naïve B cell (168). Early pro-B cells, which are characterized by the expression of CD34 and CD45, give rise to late pro-B cells which undergo immunoglobulin heavy chain gene rearrangement, expressing CD19, CD79a, and CD79b (169). Upon successful rearrangement of the heavy chain, the pro-B cell transits into the pre-B cell, characterized by the expression of a functional pre-B receptor complex composed of surrogate light chains and the mu heavy chain. Pre-B cell rearranges the immunoglobulin light chain genes, forming the complete BCR and expressing the pre-B cell upregulate surface CD10 and CD20 alongside IgM (169). Immature B cells with functional BCRs migrate to the secondary lymphoid organs, such as the spleen and lymph nodes where they recognize antigens and undergo processes of positive and negative selection. Positive selection relies on the recognition of specific foreign antigens by the immature B cells, while negative selection removes B cells that recognize self-antigens. The subsequent differentiation phase can be subdivided into the activation of mature naive B cells by their specific antigen and their transformation into antigen-specific plasma cells and memory B cells, capable of producing antibodies.

Approximately 50% of primary BCRs carry certain degrees of autoreactivity, in other words, are specific against host antigens (170–172). This would be catastrophic for the host due to the uncontrolled presence of antibodies binding self-antigens which can lead to the development of autoimmune conditions and long-lasting tissue damage. Thankfully, with the help of self-tolerance mechanisms, only a small proportion of these B cells will reach the GC, where they will further differentiate and secrete ABs. Multiple mechanisms exist to eliminate auto-reactive B cells from the repertoire or limit their ability to produce auto-antibodies. the mechanisms that prevent the

spread of auto-reactive B cell clones could be further subdivided into central and peripheral tolerance (169). Central tolerance mechanisms remove self-reactive lymphocytes during their initial development in the bone marrow. In contrast, peripheral tolerance acts in the peripheral tissues and secondary lymphoid organs, suppressing escaped self-reactive B cells (169).

Tolerance mechanisms include receptor editing, clonal deletion, clonal anergy, and clonal ignorance (173),(174). The first mechanism of central self-tolerance is clonal deletion. It removes B cells that strongly interact with self-antigens via induced apoptosis, preventing their migration to the secondary lymphoid organs (175). Secondly, self-reactive B cell clones may undergo receptor editing, which alters receptor specificity through further VJ rearrangements. This way, cells with a potentially autoreactive BCR may migrate into the periphery. However, clones that exhausted all the V segment rearrangement possibilities will be deleted (176). Moreover, auto-reactive B cells can develop in a functionally inactive clonal anergy state. A defined molecular feature of anergy is the non-responsiveness of the BCR to its antigen (177); alternative features may also include the down-regulation of IgM secretion, resistance to the activation with LPS, and resemblance of immature-like molecular phenotype (178,179). Finally, the last mechanism of self-tolerance is clonal ignorance. Auto-reactive B cell clones, which failed to encounter their antigen due to its availability in the primary lymphoid organs or are weakly crosslinked to the antigen, will still migrate to the periphery as non-self-reactive B cells (as their ligand stays unavailable) (180). The decision if self-reactive B cells undergo receptor editing, are removed, or become anergic relies on receptor avidity, with stronger signaling resulting in editing or deletion and weaker interaction permitting anergy (181). In summary, several central and peripheral tolerance mechanisms exist, from completely removing the clone from the repertoire to functional inactivation, shaping the B cell repertoire.

Recent advancements in multi-omic techniques have proven highly effective in dissecting complex biological processes that underlie adaptive immune responses. These techniques serve as a valuable tool for studying immune cell functions and communication circuits and can aid in biomarker implementation for translational research. One of the most noticeable aspects of COVID-19 was an autoimmune background in patients with acute disease after virus elimination. To elucidate the nature of such manifestations, researchers turned to single-cell transcriptomics, immune receptor profiling techniques, and proteomics for potential answers. However, they faced certain difficulties as the concept of auto-reactivity holds a degree of complexity due to the absence of the affinity cutoff, which can separate autoreactive BCRs (182). Autoreactivity is usually screened by *in-vitro* binding assays in the clinics, specifically enzyme-linked immunosorbent assay (ELISA), with a custom definition of ‘positive’ or *in vitro* via interaction of B cell clones with a self-target in the molecular biology field (183). Unfortunately, neither of these techniques gives an unbiased and comprehensive view of potential auto-antibody targets and their association with a patient’s prognosis.

One of the tools particularly useful in this context is single-cell B-cell receptor sequencing (scBCR-seq), which allows interpreting immune responses to the infection by collecting information about BCR repertoire and gauging its diversity and clonal evolution. This method is based on isolating B cells from the sample of interest using microfluidic devices or fluorescence-activated cell sorting (FACS). As a next step, the BCR of each isolated cell, consisting of the V, D, and J segments of heavy and light chains, is amplified and sequenced using next-generation sequencing (NGS) technologies, resulting in millions of short reads. The high variability of each BCR, particularly in the complementarity-determining regions (CDRs) 1-3, makes this technique particularly useful for examining receptor specificity. The CDR3 region, formed at the intersection of V-, (D-), and J-genes, is exceptionally diverse and crucial for receptor specificity. As a final step, several bioinformatics pipelines are applied to assemble the sequenced fragments into the full-length BCRs, which are then assigned to unique B cell clones, allowing the further exploration of the clonal diversity and B cell lineage development trajectories. In summary, scBCR-seq is particularly useful at dissecting humoral immune responses at the single-cell resolution, allowing insights into antigen-specific responses during infectious disease (184).

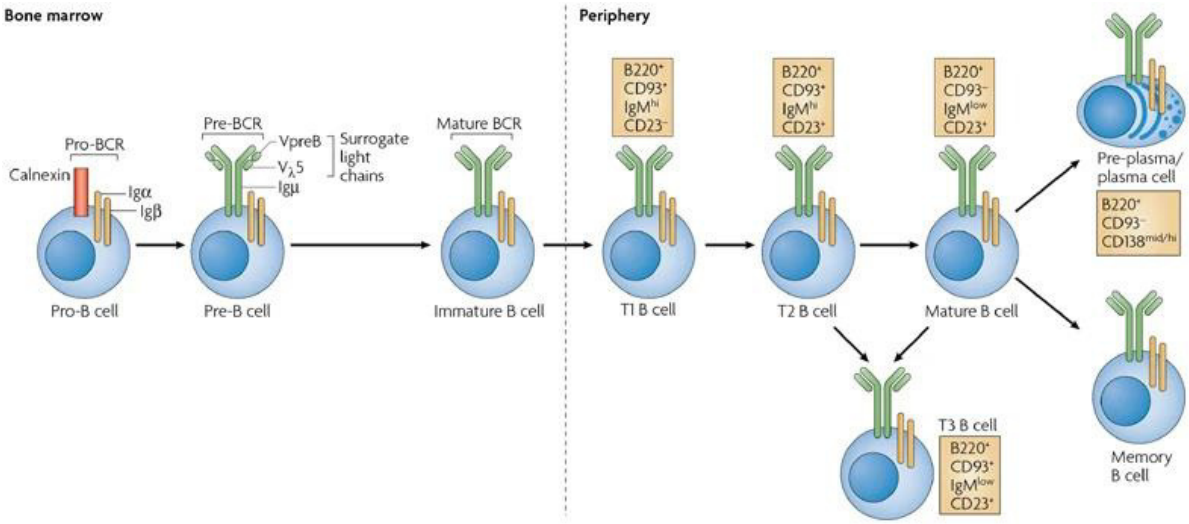

Figure 3.2.1: B cell development. B cell development starts in the bone marrow and continues in the peripheral lymphoid tissues. The process begins with hematopoietic stem cells (HSCs) in the bone marrow, which differentiate into naive B cells through several stages, including pro-B and pre-B cells. The pre-B-cell receptor (pre-BCR) is generated during this differentiation, composed of an Igμ heavy chain and surrogate light chains (VpreB or Vλ5). Subsequently, B-cells express mature BCR, organized with rearranged heavy- and light-chain genes and capable of recognizing foreign antigens. Simultaneously, immature B cells undergo a selection process to remove self-reactive B cells through central tolerance, including clonal deletion, anergy, and receptor editing. Cells that complete all checkpoints leave the bone marrow as transitional B cells. Later, upon recognizing the foreign antigen, they differentiate into plasma or memory B cells. The figure is taken from (185), copyright permission is acquired from the publisher.

3.2.2. COVID-19-specific antibody variable domains are associated with disease severity

Upon performing longitudinal profiling of severe patients with infectious lung diseases biofluids, I revealed that antibody generation is essential to the immune response in severe COVID-19 patients. Antibodies are dominant in the bronchoalveolar environment and can be detected in the BALF and plasma of COVID-19 patients at the time of intubation. I was able to identify 15 unique COVID-19-specific antibody fragments, which were abundant in the lungs of severe COVID-19 patients, specifically, IGHV1-24, IGHV1-69-2, IGHV3-15, IGHV3-23, IGHV3-30, IGKC, IGKV2-24, IGKV3-15, IGLV10-54, IGLV1-44, IGLV3-1, IGLV3-10, IGLV3-12, IGLV3-19, IGLV3-25.

Considering the abundance of immunoglobulins in the primary infection site of SARS-CoV-2, I hypothesized that a unique B cell population could produce these proteins. Several studies have suggested that dysregulated B-cell immunity plays a significant role in the pathogenesis of severe COVID-19 (167,185), therefore focusing on particular B-cell populations and clonotypes can provide more insight into the origin of antibody-mediated immunity and autoantibodies in particular.

To address this question I retrieved B cells, which utilize any of the 15 lung-specific antibody fragments from severe COVID-19 patients of the Chicago cohort (Figure 3.2.2 a). As a reference dataset, I selected open-access peripheral blood mononuclear cells (PBMCs) single-cell multi-omic atlas, consisting of different severity categories of COVID-19 patients (152). The dataset contained several modalities, such as single-cell transcriptomics, single-cell BCR, or cellular indexing of transcriptomes and epitopes (CITE-Seq). The samples were obtained from three medical facilities in Newcastle, London, and Cambridge. The initial dataset was re-integrated and re-processed, selecting only B and plasma cells. The final object consisted of 38,063 B cells divided into six clusters based on the transcriptomic and surface protein markers (Table 2.5.3): memory B cells (*CD82, LINC01781, CRIP1, AIM2, COTL1*), immature B cells (*TCL1A, CXCR4, FCER2, CD69, BTG1*), naive B cells (*TCL1A, IL4R, FCER2, BACH2, IGHD*), B1 cells (*LINC01857, FCRL2, ARHGAP24, GPR183, TTN*), dividing plasmablasts (*RRM2, IGHG1, SDF2L1, JCHAIN, TXNDC5*) and IgA high plasma cells(*JCHAIN, MZB1, FKBP11, TXNDC5, SEC11C*) (Fig 3.2.2b). Additionally, the strength of this atlas is a representation of the patients with different COVID-19 severity stages, specifically asymptomatic (n=9), mild (n=23), moderate (n=30), severe (n=13), critical (n=15), and healthy control samples (n=23), as B-cell mediated immune responses were demonstrated to vary according to the severity of the disease (81). Besides the single-cell transcriptomics information, each cell contained information about a single BCR, which allowed me to detect and study particular clonotypes.

I identified 12,302 cells that carried at least one of the selected fragments in their receptors and selected clonotypes that contained at least three cells, ending up with 41 clones (Fig. 3.2.2 c).

Detected clones mainly came from IgA high plasma cells and dividing plasmablast populations. Thus, I focused on these two clusters and continued the analysis in a separate object.

As can be noticed, selected clones were detected only in the COVID-19 samples and not in the healthy controls. This supports my observations from the biofluid proteomics data and indicates that detected immunoglobulin fragments are indeed COVID-19-specific. Further analysis revealed that these cells mainly originated from severe study population patients (Fig. 3.2.2d). Furthermore, cells and clonotypes containing selected immunoglobulin fragments derived predominantly from severe patients, have a steadily increasing proportion with a COVID-19 severity from asymptomatic to severe, followed by a reduction in the critical patient subgroup. This observation can be supported by various articles reporting that critical COVID-19 patients develop lymphopenia, a condition characterized by a reduced number of lymphocytes (71).

Additionally, selected BCRs of the severe patients belonged to IgA and IgG isotypes, while those from mild and moderate patients also included IgD and IgM (Fig. 3.2.2 d). This gives us insight into the fact that B cells from severe patients already have a more differentiated B cell phenotype at the early stages of the infection. At the same time, mild and moderate patients also contain less-differentiated B cells secreting IgM.

To sum up, I have demonstrated that immunoglobulin fragments detected in the bronchoalveolar space of the COVID-19 patients of the Chicago cohort are COVID-19-specific. Moreover, there is evidence that immunoglobulin variable fragments are biased towards disease severity. B cell clones containing selected immunoglobulin chains as a part of their BCRs originate from plasma cell and plasmablast groups, expressing mostly IgA and IgG isotypes as their receptor.

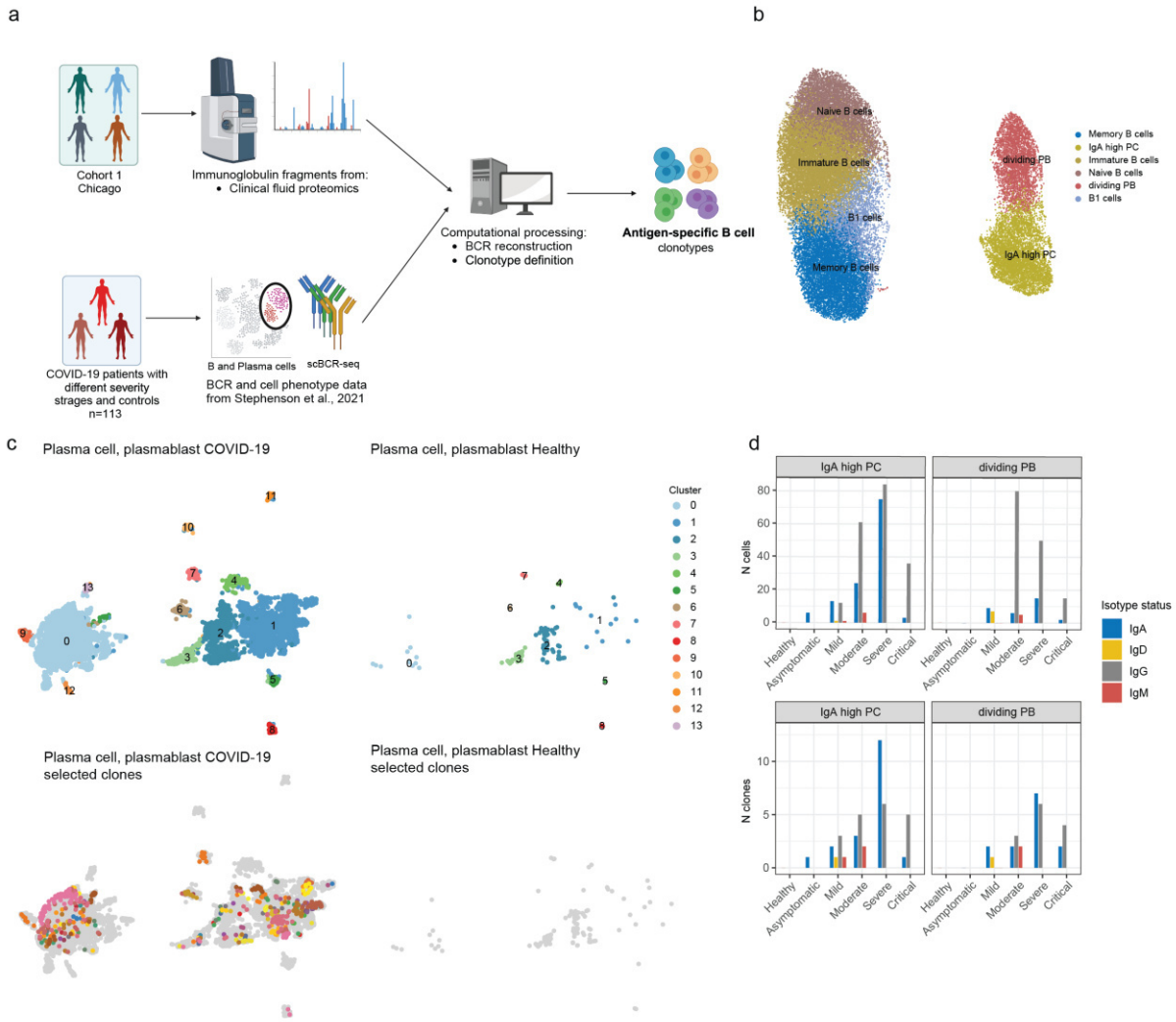

Figure 3.2.2: Variable fragments of BCR are predictive of the COVID-19 severity. a, Schema representing experimental workflow. **b,** UMAP visualization of B cell clusters from 38,063 B cells from PBMCs of 102 COVID-19 patients and healthy controls. **c,** UMAP visualization of plasma cell and plasmablasts 14 clusters from 8,599 cells from PBMCs of 90 COVID-19 patients and 23 healthy controls. Cells from healthy donors and COVID-19 patients are separated. 41 clones containing chains of interest as a part of their BCR are highlighted with color. **d,** Bar plot representing counts of cells and clones, which contain immunoglobulin fragments detected in BALF of the Chicago cohort of COVID-19 patients as a part of their BCR. Counts are displayed per severity category, and isotype status is defined by color.

3.2.3. Revealing cellular identities of COVID-19-specific B cell clones

After discovering a bias in the repertoire of immunoglobulin variable domains and its correlation to COVID-19 severity, I decided to delve further into the molecular phenotypes of the identified B-cell clones. For this purpose, I calculated the top differentially expressed genes (DEGs) for cell clusters 0 to 13 of plasmablast/plasma cell origin. The top unique marker genes were displayed on the heatmap (Fig. 3.2.3a) and in table 3.2.3. Paying particular attention to the clusters containing higher proportions of the clones expressing immunoglobulins as a part of their BCR, I further focused on clusters 0, 1, 2, 3, 6, 7, 8, and 9 (Fig. 3.2.3b). More particularly, clusters 0,1,2,3 consisted of a variety of smaller-sized clones, while clusters 6,7,9 were dominated by a few but more expanded clonal populations.

Notably, cluster 3 had the most outstanding molecular phenotype. Alongside typical markers involved in B cell activation, such as *KLF6, MS4A1 (CD20)*, cluster 3 also expressed elevated levels of *NR4A2, LTB, AFF3, CD69, CD83,* and *HLA-DMB (MHC II)*. Orphan nuclear receptor *NR4A2* and lymphotoxin β (*LTB*) were reported to be markers for RA-specific B cell population, responsible for the formation of ectopic lymphoid structures and pathological B cell responses (186). Additionally, researchers demonstrated that *NR4a1-3* acts in conditions with the absence of co-stimulation (187). Besides that, *AFF3* is a facilitator of class switch recombination and one of the susceptibility factors for RA and type I diabetes (188). *CD69* and *CD83* are B cell activation markers, while *HLA-DMB* is upregulated on the B cells upon antigen presentation. *SCIB* is a transcriptional factor that induces an anti-apoptotic program and promotes B cell survival. It controls the expression of proteins involved in the BCR signaling pathway, such as BAFFR and TLRs (189). Additionally, to the transcriptomic marks, differentially expressed surface proteins for cluster 3 supported autoimmune-like phenotype derived from the gene expression data. In this case, I observed elevated expression of the BAFF receptor, and pro-survival factor, which led to the development of autoreactive B cells (190), CD52, and CR-1, which are known to be expressed in the B cell subsets of RA and SLE patients and associated with the production of autoantibodies (Fig. 3.2.3c) (191,192). Cluster 3 expresses transcriptomic and surface protein markers related to molecular B cell phenotype observed in classical autoimmune diseases. Moreover, it possesses several activation and survival markers, which generally support the hypothesis of the existence of autoimmune-like B cells in COVID-19 patients. In comparison to cluster 3, clusters 6, 7, and 9 contained the largest proportions of cells with fragments of severe COVID-19 patients as a part of their BCR and mainly comprised one enlarged clone. Transcriptomic markers for these clusters consisted mainly of variable domains: *IGKV3D-15, IGKV3-15, IGKV3D-11* - cluster 6, *IGHV4-31, IGHV4-28, IGHV4-55, IGHV4-61, IGHV4-4* - for cluster 7, and *IGHV4-55, IGHV4-28, IGHV4-31, IGHV4-61* - for cluster 9, that participated in the formation of BCR and antibody secretion.

In conclusion, following my previous findings, the humoral immune response dominates from the day of intubation in the lung environment of severe COVID-19 patients compared to bacterial pneumonia and influenza subgroups. By identifying 15 unique COVID-19-specific antibody fragments abundant in severe patients' lungs, I followed up on the molecular phenotypes of B cells producing these antibodies using single-cell multi-omic datasets from COVID-19 patients of varying severity. Subsequently, I characterized distinct plasma cell clusters, revealing bias in the BCR repertoire among severe patients. Notably, I described B cells exhibiting a molecular phenotype close to canonical autoimmune diseases, suggesting the presence of autoreactive B cells in severe COVID-19 patient repertoire. Besides that, most clusters containing enlarged clones carrying fragments of severe COVID-19 patients' BALF immunoglobulins displayed transcriptomic markers associated with antibody secretion. Overall, this targeted analysis highlights the range of B cell reactivities and molecular phenotypes observed in severe COVID-19 patients, giving insights into potential B cell types participating in autoantibody production.

Table 3.2.3: Transcriptomic markers of dividing plasmablast and IgA high plasma cell clusters. The top 20 significantly differentially expressed genes per cluster are displayed.

Cluster	Marker genes
0	*UBE2C, PLK1, TOP2A, CKAP2L, CDCA8, HJURP, KIF20A, KIF23, CCNA2, KIF2C, AURKB, CDK1, CDCA2, SPC25, PBK, CDCA3, KIFC1, PKMYT1, CDC20, GTSE1*
1	*IGLC2, IGLC3, IGHGP, CALCOCO1, P2RX1, IGHV6-1, IGHA1, BTG2, SDC1, IGHG4, PDK1, LINC02362, CPEB4, AC012236.1, FNDC3B, MBNL2, PECAM1, KLHL14, CD27, CNKSR1*
2	*RGS1, FOSB, FOS, DUSP1, RGS2, MTRNR2L8, MTRNR2L12, PTP4A1, CD69, KLF6, JUN, CITED2, SPINT2, AC007952.4, IGHA2, ATP2B1-AS1, PPP1R15A, KLF2, TSC22D3, BCL2*
3	*CD24, AFF3, SPIB, LTB, NR4A2, MS4A1, CD83, HLA-DMB, CD22, ALOX5, CCR7, ARHGAP24, LY86, HVCN1, MTSS1, VPREB3, DEK, BANK1, BCAS4, TUBA1A*
4	*IGKV1-39, IGKV1D-39, IGKC, MXD4, GSTM2, LINC02362, SGK1, DLG1, BTG2, TRAPPC6A, SNX29, SLC12A6, RNASE6, FCHSD2, TP53INP1, GRINA, PCED1B, NMRK1, ARSA, TUT7*
5	*IGHV3-43, IGHV3-20, AC233755.2, LINC01480, KLHL14, CCDC88A*
6	*IGKV3D-15, IGKV3-15, IGKV3D-11, IGKC, APOO, SSR4*
7	*IGHV4-31, IGHV4-28, IGHV4-55, IGHV4-61, AC233755.1, IGHV4-4, DERL3, BTG2, HERPUD1, NUCB2, SSR4, PSAP, JCHAIN, PRDX4, ERLEC1, HM13, MZB1, ITM2C, TMBIM6, FKBP11*
8	*IGKV2-28, IGKV2D-28, IGHV2-5, IGKC, PECAM1, CCDC107, LHPP, POU2F1, FAM3A, UBR2, CCR10, NFX1, CHD9, KCNK6, BTG2, JARID2, TBL2, MSI2, PIP5K1B, OPTN*
9	*IGHV4-55, IGHV4-28, IGHV4-31, IGHV4-61, COPRS, PAQR4, HPDL, PSMC3IP, UHRF1, MCM10, SUV39H1, TIMELESS, SLC43A3, ESCO2, GINS4, DONSON, CENPV, GINS2, AURKB, ACOT7*
10	*IGKV2D-30, IGKV2-30, IGHV3-7, EPSTI1, S100A6, IGKC, HERPUD1, DERL3, CD27, HSH2D, JCHAIN, SSR4, UBE2J1*

11	*IGHV3-66, IGHV3-53, JCHAIN, MZB1*
12	*IGKV2-30, IGKV2D-30, RAD54L, ORC1, CDK1, SPC25, HMMR, MIS18A, MCM10, RAD51, OIP5, UBE2T, CDCA3, RRM2, CCNB1, CENPP, AURKB, RAD51AP1, UBE2C, SKA3*
13	*IGHV3-53, IGHV3-66, SKA3, POLD3, ASF1B, PXMP2, PKMYT1, NDC80, DHFR, CDCA5, DIAPH3, HPRT1, CENPN, CDC6, CHAF1A, TYMS, RRM2, AURKB, TACC3, GINS2*

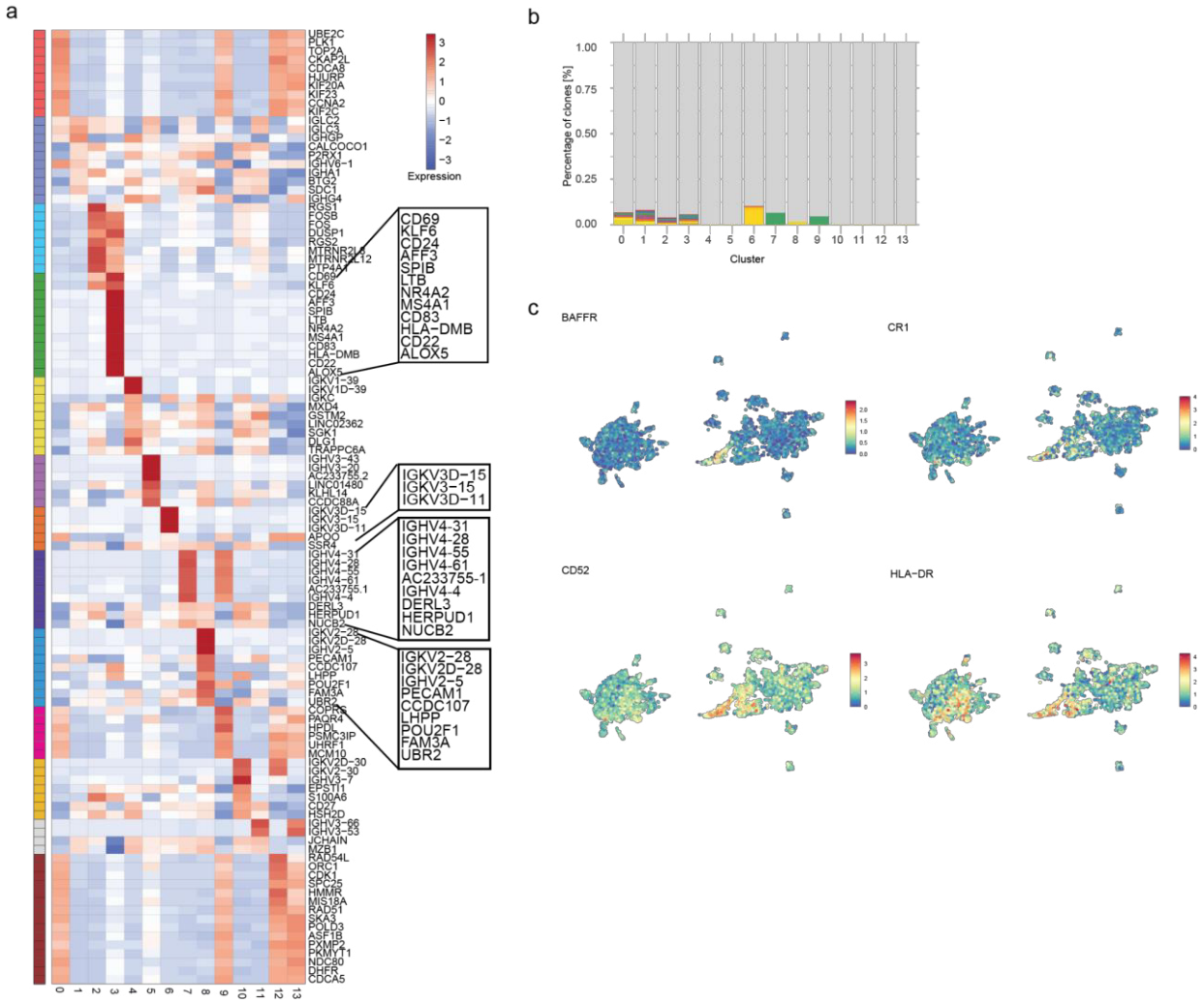

Figure 3.2.3: COVID-19-specific B cells display antibody-producing and autoimmune-like phenotypes. a, Heatmap displays each cell cluster's top differentially expressed genes (DEGs). The top unique DEGs of clusters 3, 6, 7, and 8 are magnified. **b,** Bar plot displays proportions of selected clones per cluster. **c,** Selected differentially expressed surface proteins for cluster 3. Color corresponds to the expression levels of each surface molecule.

3.3. Study of autoantibody binding repertoire of acute COVID-19 patients

3.3.1. COVID-19 and autoimmunity

Upon SARS-CoV2 entry in the host cell, several immune cell subsets become activated and produce effector molecules, such as cytokines and antibodies which lead to the amplification of signaling cascades and overall activation of the immune system. Therefore, the characterization of the immune cells, their communication, and effector functions is crucial for understanding mechanisms of molecular pathogenesis and regulatory processes of the immune system. Multi-omics techniques have proved to be particularly useful while dealing with complex biological processes. They serve as a powerful tool to unravel functions and communication circuits of immune cells and have great potential for implementation in translational medicine.

During the recent COVID-19 pandemic, many multi-omic studies allowed the research community to get a comprehensive view of the pathogenic mechanisms associated with the severe and lethal cases of the novel virus. Utilizing single-cell RNA transcriptomics approaches, researchers have followed the dynamic changes in the composition of activated subsets of PBMCs throughout the severity stages of COVID-19. One of the crucial discoveries was the accumulation of $CD8^+$ T cells in the repertoire of severe COVID-19 patients and an overall higher ratio of $CD8^+$ to $CD4^+$ T cells. In contrast, Tfh cells were detected in the circulation in mild disease cases while absent in severe patients (152). Additionally, several research groups reported enlarged proportions of plasma cells and plasmablasts in severe COVID-19 cases, which could contribute to the autoimmune-like phenotype observed in some critical patients (152,193). The knowledge generated during the early stages of the COVID-19 pandemic and clinical observations provided valuable information for diagnostics and prognostic evaluation of COVID-19 patients (73,74).

The hypothesis that autoimmune and inflammatory conditions can be caused by viral infection has been previously described; in the case of COVID-19, most of the autoimmune symptoms have an increased frequency in individuals during and after the acute phase of COVID-19 (90). One of the main concepts is immune system dysregulation, induced by COVID-19, which includes bystander activation of the immune cells, molecular mimicry by viral proteins, and systemic manifestations caused by ubiquitous expression of ACE2 (SARS-CoV-2 receptor), as well as the release of autoantigens from damaged by virus tissues (194). Although the rates of COVID-19 infection have been decreasing over recent years, I have witnessed the accumulation of patients with new-onset autoimmune and pro-inflammatory conditions acquired after the initial virus infection. However, up to date, there are no defined predictors of the risk of developing autoimmune disease post-COVID-19.

While scBCR-seq provides information about particular receptors, it doesn't consider their specificity. An approach to discovering putative auto-antibody targets was described by Leuschner et al. in the context of fibrotic lung diseases (137). The authors introduced the Differential Antigen Capture (DAC) assay, which is based on the immunoprecipitation of human proteins obtained by the homogenization of lung tissue specimens by antibodies captured from the plasma. The assembled complexes are washed and evaluated using quantitative shotgun proteomics. The assay has proven its sensitivity and specificity by predicting the enrichment of Scl-70 antigen in the Scl-70-positive patients previously profiled with ELISA in the clinics. The main advantages of such a method over conventional assays are the reduced amount of plasma needed for the experiment and the possibility of exploration of autoantibody targets in a non-targeted fashion. Finally, the usage of the lysed tissue material allows the preservation of proteins in their native state with potential disease-associated post-translational protein modifications (PTMs), which cannot be addressed with assays using recombinant protein panels.

3.3.2. Demographics of the Munich cohort

To get insights into the antibody binding profiles of the patients, I utilized an additional longitudinal cohort from the University Hospital of Ludwig Maximilian University (LMU) in Munich. The latter consisted of patients admitted to the facility from March to June 2020 with a positive SARS-CoV-2 PCR test. This way, the Munich cohort encompassed patients with varying severity stages of COVID-19, including those admitted to the regular wards. Upon admission to the hospital, the serum of the patients was collected longitudinally with the latest time point of 54 days.

I performed a t-distributed Stochastic Neighbor Embedding (t-SNE) analysis of all patient metadata upon admission to the hospital to obtain a more detailed characterization of the cohort and stratify the initial heterogeneity within the patient pool. This analysis involved clustering the patients in two distinct clusters (Fig. 3.3.2 a). Cluster 2 included patients with ARDS requiring mechanical ventilation support, and cluster 1 consisted of the less severe patients with lower COVID-19 severity stages. Additionally, cluster 2 exhibited significantly higher levels of inflammatory parameters, such as CRP and Interleukin-6 (Fig. 3.3.2 b), and was labeled as ‘severe’, while cluster 1 received a ‘mild’ label.

I next established a timeline of the experiment and created comparative time windows for all patients. This was achieved by longitudinal profiling of the clinical parameters, specifically SARS-CoV-2 anti-N antibodies, SARS-CoV-2 anti-S antibodies, CRP [mg/dl], Creatinine Jaffe [mg/dl], Lymphocytes [g/l], and Leukocytes [g/l] for severe and mild clusters (Fig. 3.3.2 c). The time points at which both clusters displayed similar values for each clinical parameter were selected as boundaries of the time windows. Finally, I stratified four time windows: 0-11 days, 12-25 days, 26-36 days, and 36-54 days from the hospital admission so that each patient in the cohort would have from two to four time points in these defined intervals.

Finally, the Munich cohort consisted of 23 COVID-19 patients, with 16 classified as severe (admitted to ICU) and 7 as mild. Both patient groups were composed of patients with a similar average age component of 66.3±19 for mild and 66.4±11.1 for severe, as well as sex composition of 86% male and 14% female for the mild group and 81% male and 19% female for the severe patients (Table A2). The differences between the groups were caused by the immunosuppression component, which was doubled in the severe group (56.2% vs. 28.6%), and acute kidney injury, which reached 75% among severe patients compared to 28.5% in the mild group. Besides that, 18.8% of the severe patients required ECMO support. Besides COVID-19 patients, the Munich cohort included two COVID-19 negative control groups: control low inflammatory (n=24), defined by low levels of CRP, Creatinine, and Leukocytes, and control high inflammatory (n=23), characterized by high levels of mentioned blood parameters. These two controls were introduced to account for potential autoreactivities arising from the overall proinflammatory background of the patients.

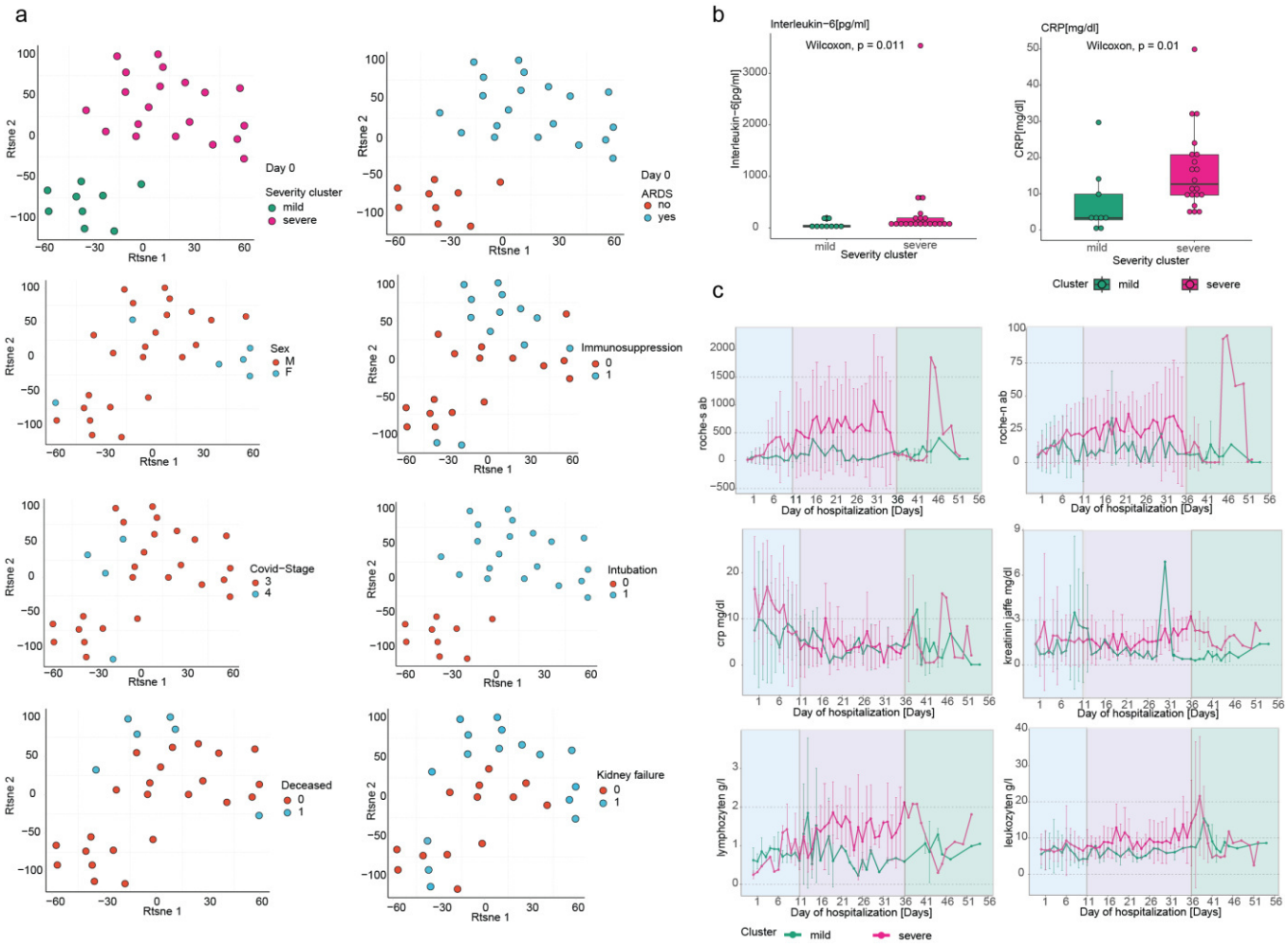

Figure 3.3.2: Demographics of the Munich cohort. a, t-SNE plot of the Munich cohort patients on the day of hospital admission. Each dot represents a patient, and the color corresponds to the clinical parameter. **b,** Interleukin-6 and CRP box plots of the Munich cohort's mild and severe COVID-19 patient groups (Wilcoxon test). **c,** Longitudinal profiles of anti-COVID antibody titers, CRP, Creatinine, lymphocytes, and leukocytes. The X-axis is assigned to the day of hospitalization, and the line's color corresponds to the COVID-19 cluster, described at a. The color of the boxes highlights selected time windows for further analysis.

3.3.3. Comparative analysis of autoantibody repertoire of two independent COVID-19 cohorts

To study potential autoantibody binding profiles, I leveraged two independent longitudinal cohorts of COVID-19 patients (Fig. 3.3.3 a). Cohort 1 (Chicago cohort) was introduced in chapter 3.1.1 and consisted of COVID-19 (n=13), bacterial pneumonia (n=6), influenza (n=7), and non-pneumonia control (n=7) patients undergoing intubation procedures in the ICU. Cohort 2 (the Munich cohort), introduced in chapter 3.3.2, consisted of severe COVID-19 patients admitted to the ICU (n=16) and mild patients in the regular wards (n=7).

I performed a DAC assay for both cohorts to obtain autoantibody binding profiles. In the case of the COVID-19 experiment, I selected the lung as a target tissue due to the high involvement in the pathology of this infection. The lung tissue pool was obtained by homogenizing peritumoral lung tissue from 32 donors (methods 2.3.1). After precipitation of the lung antigens, antibody-antigen complexes were washed and processed for mass spectrometry detection (Fig. 3.3.3 b).

Furthermore, to validate the assay's specificity I addressed a target of the monoclonal antibody Tocilizumab, administered to several COVID-19 patients in hospital care longitudinally. IL6R was detected via DAC assay in several patients of both cohorts. I compared the detection rates of the DAC assay and clinical records. Applying receiver operating characteristic (ROC) analysis, I confirmed the assay's accuracy with an area under the curve (AUC) characteristic equal to 0.89, corresponding to the high specificity. This way I can validate the reliability of the applied method and the observed results.

In my analysis, I focused on screening for putative autoantigens in severe COVID-19 patients of the Chicago cohort (n=13) and severe COVID-19 cases from the Munich cohort (n=16) to have a compatible severity of the patients. I began this analysis by defining significantly enriched antigens for severe COVID-19 patients of each cohort. For this purpose, I utilized the Welsch test on all the proteins detected in each cohort separately between COVID-19 patients and bacterial pneumonia (n=6), influenza (n=7), and non-pneumonia control (n=7) groups for the Chicago cohort, control low inflammatory (n=24) and control high inflammatory (n=23) groups for the Munich cohort at the earliest time point available. Considering that autoreactivities can exhibit non-linear temporal behavior, I also performed the same statistical test using reference groups specified earlier for the later time points: time points 2 and 3 for the Chicago cohort and time points 2, 3, and 4 for the Munich cohort. Together, I focused only on the antigens detected in at least 3 COVID-19 patients at least one-time point.

At the time of hospitalization, I could identify putative autoantibodies enriched exclusively in COVID-19 patients in the Chicago or Munich cohort (Fig. 3.3.3 c, d). In the Chicago cohort, putative autoantigens enriched in COVID-19 patients compared to influenza and bacterial pneumonia were against ABCC3 (n patients=8), ALAD (n patients=6), CCDC178 (n patients=4), CCT6B (n

patients=3), CFHR5 (n patients=7), HLA-G (n patients=3), HMBS (n patients=5), HSPA2 (n patients=3), IFIT1 (n patients=3), IGF1R (n patients=5), IL6R (n patients=5), KMT2C (n patients=3), KRT84 (n patients=3), KRT86 (n patients=4), KRT31 (n patients=3), TEP1 (n patients=3), TSKU (n patients=5). My mass spectrometry data also detected the presence of certain antibody variable domains, specifically IGHV7-4-1 (n patients=6), IGKV1D-17 (n patients=5), IGKV1D-43 (n patients=5), IGKV2-29 (n patients=6), IGLV3-1 (n patients=7), which could compose potential autoantibodies. Secondly, putative autoantibodies significantly enriched in COVID-19 patients of the Munich cohort upon hospitalization compared to control low and high inflammatory were against IL-6R (n patients=3), STAT6 (n patients=3), and TENM2 (n patients=4), KRT6B (n patients=7) and IGLV3-1 (n patients=8), IGHV3-30-3 (n patients=15).

Upon assembling significant findings from all the time points, I developed comparative lists of putative antigens for both cohorts (Fig. 3.3.3 e). The results are displayed on the Venn diagram and highlighted as overlapping fractions (n=19) or as putative antigens specific for each cohort (n=95 for the Chicago cohort, n=63 for the Munich cohort). All the antigens were grouped according to their origin or molecular function, with the most prominent groups being extracellular matrix proteins, proteins associated with or involved in the regulation of complement, nuclear antigens, receptors, and proteins related to signal transduction in the immune cells. Notably, among 19 shared antigens, HAMP and SAA2 were involved in the acute phase response, CFHR2, MASP2, COLEC10 were associated with complement activation, FGL1, IFIT1, IL6R - with immune regulation, IGHA2, IGHV1-58, IGHV3-30-3, IGLV3-1 - immunoglobulin domains, and CPS1, GSTO1, SERPINA10, ST3GAL6, SVEP1, TEP1, TSKU were associated with various other functions. Previous reports described the existence of autoantibodies against acute-phase proteins in systemic autoimmune diseases (195). Additionally, anti-glutathione S-transferase omega-1 (GSTO1) autoantibodies have been reported in patients with chronic inflammatory conditions, including RA and COVID-19, and signal extended tissue damage (196). Moreover, anti-complement antibodies were reported in complement-mediated autoimmune diseases such as SLE and RA, and autoantibodies towards complement regulatory proteins were associated with increased kidney damage (197). Among other proteins, SVEP1 is an extracellular matrix protein that is associated with platelet reactivity in humans and known to promote atherosclerosis (198); TEP1 catalyzes the addition of new telomeres on the chromosome ends, CPS1 is an essential enzyme for the urea cycle ubiquitously expressed in the liver. Following the proteins associated with immune regulation, FGL1 is secreted by the liver and is responsible for proliferation- and metabolism, FGL1 is a ligand for LAG3, and several studies consider targeting FGL1/LAG3 as the next generation of immune checkpoint therapies (199). Finally, IFIT1 is a signaling protein in the IFN I response, protecting from viral and bacterial infection, and autoantibodies interfering with IFN signaling have been described in severe COVID-19 patients (86,200).

Among the putative autoantibodies detected only in one cohort, I discovered receptors and accessory proteins, such as human leukocyte antigen G (HLA-G) (201), insulin-like growth factor 1

receptor (IGF1R) (202), Insulin-like Growth Factor Binding Protein 6 (IGFBP6), IL-1 receptor accessory protein (IL1RAP), Lymphocyte antigen 96 (LY96), Protein kinase C and casein kinase substrate in neurons protein 2 (PACSIN2) (Chicago cohort). Furthermore, established antigens, specifically HSPA2, and LGALS7B are classical DAMPs, which are present in the blood of patients with excessive tissue damage. PPL autoantibodies were described in the context of pulmonary fibrosis (203). Anti-U1 snRNP (SNRPC) are often linked to mixed connective tissue disease (MCTD) and SLE (204). Anti-SP100 are associated with primary biliary cholangitis (PBC), a chronic liver disease characterized by scarring of the liver tissue (205).

To conclude, a comparative analysis of putative autoantibodies in two independent severe COVID-19 cohorts revealed 19 common antigens, including acute phase proteins, regulators of complement signaling, and regulators of the immune response, alongside other proteins with varying molecular functions. Overall, observed putative antigens for two cohorts had majorly overlapping molecular origins, for example, ECM proteins, keratins, and actin-associated proteins, which support one of the autoimmunity hypotheses associated with the promotion of the autoantibody production due to the chronic inflammation and extensive lung tissue damage, which are considered hallmarks for the severe COVID-19. Additionally, autoantibodies against complement and complement-regulating proteins can play a dual role in the pathogenesis of the disease, being as protective as pathogenic. The repertoire of the autoantigens of two severe COVID-19 cohorts exhibits overall high diversity, which the limited sizes of both cohorts can explain in the context of high variability of autoimmune phenotypes. However, I was able to identify novel and already known autoantibodies, which can have protective or harmful properties, interfering with the infection outcome.

Figure 3.3.3: Comparative analysis of the putative auto-antigen repertoire of two independent COVID-19 cohorts. a, Schema with a composition of the Chicago and Munich cohorts. **b,** Overview of the Differential Antibody Capture assay (DAC) and benchmarking processes with anti-

IL6R antibody (tocilizumab administration). **c,** Scatterplot displaying fold changes of individual antigens in COVID-19 patients (n=13) of the Chicago cohort versus bacterial pneumonia patients (n=6) on the x-axis and influenza patients (n=7) on the y-axis upon intubation. The size of the dot and the color are responsible for the number of COVID-19 patients with a particular autoantigen. The enriched autoantigens enriched in the COVID-19 subgroup over bacterial pneumonia and influenza are placed in the red rectangular. **d,** Scatterplot displaying fold changes of individual antigens in severe COVID-19 patients (n=16) of the Munich cohort versus control high inflammatory patients (n=23) on the x-axis and control low inflammatory patients (n=24) on the y-axis upon hospitalization. The size of the dot and the color are responsible for the number of COVID-19 patients with a particular autoantigen. The enriched autoantigens in the COVID-19 subgroup over both controls are placed in the red rectangular. **e,** Venn diagram demonstrating putative autoantigen repertoires of the Chicago and the Munich cohorts grouped by the protein origin or molecular function. Autoantigens displayed are significantly enriched at least at a one-time point over at least one control group and in at least 3 COVID-19 patients.

3.3.4. Dynamics of the autoimmune response in COVID-19 patients

After defining the pool of the putative antigens for two independent COVID-19 cohorts, I followed up on the longitudinal trajectories of the autoantibodies. Assuming that different autoantibodies may have varying expression dynamics in individual patients, I aimed to infer groups of autoantigens with similar temporal trajectories in the patients of the Munich cohort. This cohort was selected as primary for the analysis due to the better longitudinal resolution, more significant number of patients, and different severity categories within the cohort. To define antibodies against self-antigens associated with the time course or severity of the disease, I performed a mixed-effect linear model with fixed effects for time and severity and a random effect for the patient. As a result, I constructed a list of 52 autoantigens with significant associations ($p<0.05$) with one or both fixed effects of the model (Fig. 3.3.4 a).

First, five autoantigens were significantly associated with both time and severity, SPTB, APOH, SELENOP, APOC3, and RBP4. SPTB was elevated at the initial time point in mild COVID-19 patients. In contrast, APOH, SELENOP, APOC3, and RBP4 autoantibodies were prevalent in more severe patients and increased over hospitalization duration. Notably, SPTB is an intracellular red blood cell protein, and this autoreactivity was observed to a larger extent in mild COVID-19 patients. Anti-APOH (phospholipid-binding protein β2 glycoprotein I) antibodies are an essential hallmark for APS and were broadly described in severe COVID-19 cases, where they potentially interfere with the blood clotting pathways and contribute to deep vein thrombosis (206,207). Additionally, anti-SELENOP antibodies were elevated in severe COVID-19 patients and increased over time during hospitalization. Strikingly, anti-SELENOP antibodies have been observed in patients with chronic fatigue syndrome, where they impaired selenium transport (208).

Regarding differences between mild and severe COVID-19 cases, I observed similar autoreactivity levels against different protein targets. Severe COVID-19 patients had higher levels of anti-F13 b (213), anti-CFHR1/CFHR2, and anti-GPX3 antibodies, while mild patients had higher levels of anti-TUBB1, anti-SAMM50, and anti-HSPA12 B (Hsp70 member) antibodies. Overall, I can conclude that despite the similar levels of autoreactivity in mild and severe patients, the targets of autoantibodies in mild and severe patients vary.

Finally, among the autoantibodies associated with time course, the most prominent ones were against structural lung proteins, specifically MFAP5, LYVE1, RELN, and LTBP1, which were upregulated in both severe and mild patients and had an overall uprising trajectory with the disease course. Also, multiple putative autoantigens described earlier exhibited a linear behavior in both the Munich and Chicago cohorts, for example, FGL1, SAA2, and CFHR2, which were elevated at the initial timepoint and decreased over time (Fig. 3.3.4 b, c). Additionally, RELN - ECM protein, MMRN1 - platelet protein, and ALDOB - glucose metabolism enzyme, initially detected in the Chicago cohort, were associated with time or severity in the Munich cohort, and all three had a persisting trajectory.

To sum up, longitudinal analysis of autoreactivities in Munich and Chicago cohorts revealed autoantibody targets varied for both groups. Among the targets specific for severe patients were APOH, SELENOP, CFHR1/CFHR2, F13B, GPX3, and for mild patients TUBB1, SAMM50, CRYZ, SPTB. Notably, several detected antigens were reported to be associated with diseases with autoimmune backgrounds besides COVID-19. Additionally, both mild and severe groups had increased levels of autoantibodies reactive to structural lung proteins, which can be explained by the increased release of these proteins from the lung due to the extended tissue damage. As a following step, it will be essential to classify the autoantibodies by their role in the pathogenesis of COVID-19, elucidating their potential protective or harmful properties.

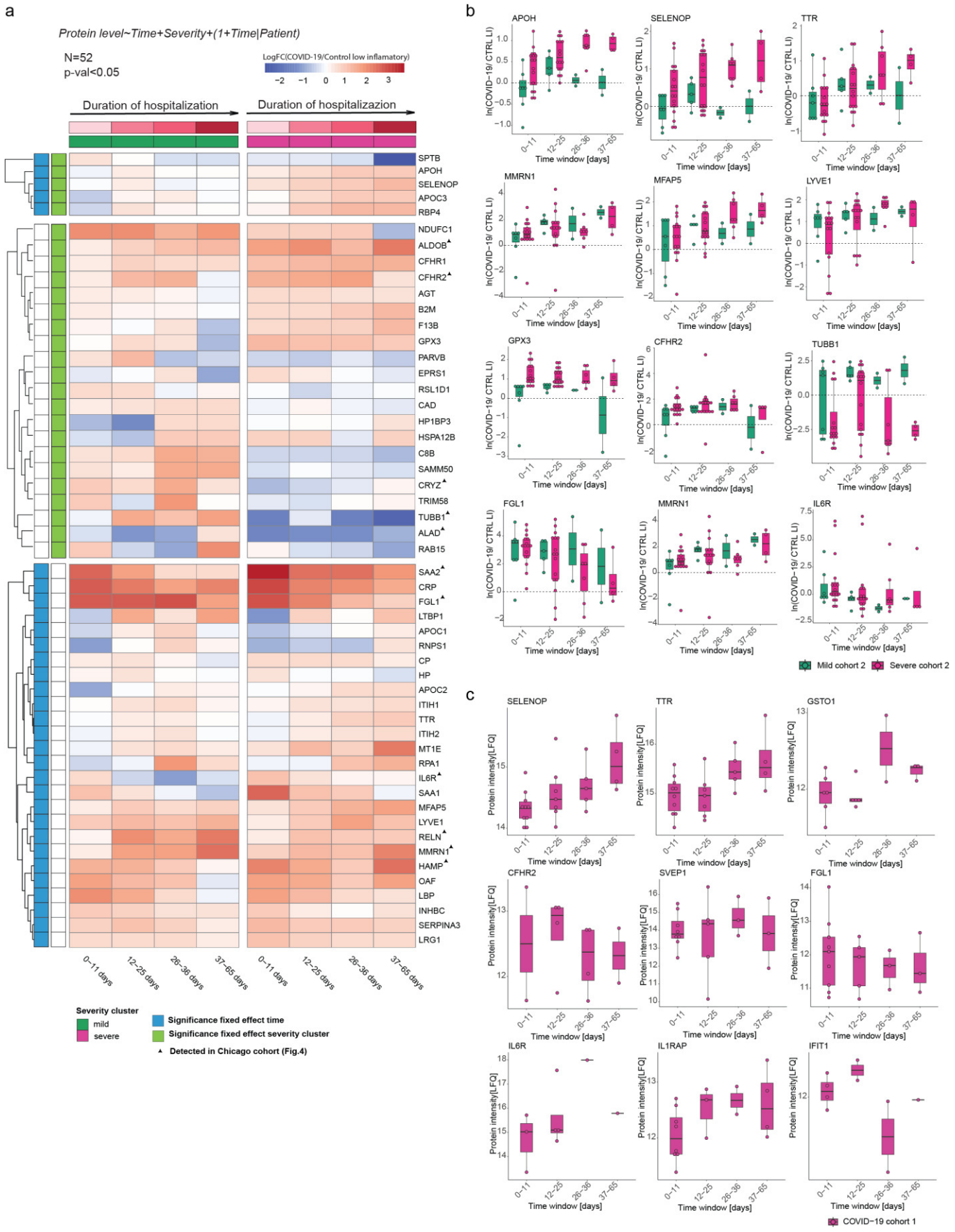
a
Protein level~Time+Severity+(1+Time|Patient)
N=52
p-val<0.05
LogFC(COVID-19/Control low inflamatory)
−2 −1 0 1 2 3
Duration of hospitalization
Duration of hospitalizazion
SPTB
APOH
SELENOP
APOC3
RBP4
NDUFC1
ALDOB▲
CFHR1
CFHR2▲
AGT
B2M
F13B
GPX3
PARVB
EPRS1
RSL1D1
CAD
HP1BP3
HSPA12B
C8B
SAMM50
CRYZ▲
TRIM58
TUBB1▲
ALAD▲
RAB15
SAA2▲
CRP
FGL1▲
LTBP1
APOC1
RNPS1
CP
HP
APOC2
ITIH1
TTR
ITIH2
MT1E
RPA1
IL6R▲
SAA1
MFAP5
LYVE1
RELN▲
MMRN1▲
HAMP▲
OAF
LBP
INHBC
SERPINA3
LRG1
0–11 days
12–25 days
26–36 days
37–65 days
Severity cluster
mild
severe
Significance fixed effect time
Significance fixed effect severity cluster
▲ Detected in Chicago cohort (Fig.4)
b
APOH
SELENOP
TTR
MMRN1
MFAP5
LYVE1
GPX3
CFHR2
TUBB1
FGL1
MMRN1
IL6R
ln(COVID−19/ CTRL LI)
Time window [days]
Mild cohort 2
Severe cohort 2
c
SELENOP
TTR
GSTO1
CFHR2
SVEP1
FGL1
IL6R
IL1RAP
IFIT1
Protein intensity[LFQ]
Time window [days]
COVID−19 cohort 1

Figure 3.3.4: Longitudinal profiling of autoreactivities in mild and severe COVID-19 patients. **a,** Heatmap with results of mixed effect model for time and severity. Only significant results are displayed. Column names represent time intervals from 0 to 65 days, rows show autoantigens. Row annotation highlights if the antigen is significantly changing with time or if it differs between mild and severe COVID-19 groups. Column annotation displays severity groups and synchronized time frames of hospitalization. **b,** Individual box plots for the antigens of the Munich cohort. The x-axis represents the time of hospitalization in a time frame, the y-axis is a fold change of COVID-19 patients to the average protein expression of the control low inflammatory. Severe and mild COVID-19 patient groups are defined with color. **c,** Individual box plots for the antigens of the Chicago cohort. The x-axis represents the time of intubation in a time frame, the y-axis is a fold change of COVID-19 patients to the average protein expression of the non-pneumonia controls.

3.3.5. Associations between putative autoantigens and clinical parameters

Lastly, I followed the individual and cumulative effects of the autoantibodies on the clinical manifestations in severe COVID-19 patients. To achieve this, I performed statistical testing using the Wilcoxon signed-rank test to stratify the differences caused by the detection of each autoantibody from the list described earlier (Fig. 3.3.3e) on blood chemistry values, respiratory parameters, cell counts, cumulative length of stay in the ICU, as well as the SOFA score and patient-specific parameters, such as age and BMI for the Chicago cohort and blood chemistry values, cell counts, COVID-19 stage, length of stay in the hospital, as well as anti-SARS-CoV2 antibody titers and patient age for the Munich cohort. The analysis was inspired by the notion that detecting autoantibodies upon hospitalization can be prognostic of the patient status and overall disease course. I anticipated discovering two groups of autoantibodies, one with protective qualities and the other correlating with a worsened patient prognosis (104).

Firstly, the results of the statistical testing for the Munich and Chicago cohorts were depicted as heatmaps, where putative autoantigens were grouped according to their specificity to the cohort, and p-values of the test were highlighted by color with red tones corresponding to the significant findings (p-value <0.05) (Fig 3.3.5 a, b). In both cohorts of severe COVID-19 patients, I identified a broad spectrum of associations between putative autoantigens and clinical parameters upon admission to the hospital. My previous analysis identified 19 putative autoantigens, which were significantly upregulated in both cohorts in at least 3 COVID-19 patients at least one time point over selected controls for each cohort. Among these 19 autoantigens, several were associated with various clinical manifestations in COVID-19 patients in both cohorts (Fig.3.3.5 c, d). For example, IL-6R used as a true positive before, is a binding target of therapeutic monoclonal antibodies administered to several severe COVID-19 patients. IL-6R-positive patients of the Chicago cohort had increased cumulative ICU days (p=0.016) and plateau pressure (p=0.04). This supports the hypothesis that COVID-19 patients who are administered tocilizumab have more severe respiratory conditions and, thus, prolonged hospital stays. Besides that, I observed reduced levels of D-dimer, a clinical marker for blood clotting, in patients positive for anti-FGL1 antibodies (p=0.028) (Fig. 3.3.5 c). Notably, recent studies revealed that FGL1 performs a modulator function for the D-dimer levels, as mutations in the *FGL1* led to increased D-dimer in the circulation (209). This way detected autoantibodies can interfere with the soluble FGL1 form, resulting in decreased D-dimer in FGL1-positive patients. Additionally, FGL1 is considered the next molecular target for the immune checkpoint blockade in cancer patients, and elevated FGL1 plasma levels are associated with a poor treatment prognosis (199). Furthermore, I discovered that patients positive for GSTO1 had a significantly lower P/F ratio in the Chicago cohort, underscoring expended lung damage. Previous reports described anti-GSTO1 autoantibodies that were detectable in multiple autoimmune and inflammatory conditions, including COVID-19, as indicative of extended tissue

damage and, reduction of respiratory function. GSTO1 is expressed by hepatocytes in the liver and later released in the circulation upon tissue damage. It is also detected in alveolar macrophage populations in the lung (210). Finally, SVEP1-positive patients in the Chicago cohort had an increased proportion of lymphocytes compared to those without this autoantibody. SVEP1 is an ECM protein that plays an important role in lymphatic vessel development (211). Studies of coronary artery disease shed light on how the deficiency in SVEP1 promotes leukocyte recruitment in vitro via the upregulation of CXCL1 (212). Autoantibodies could trigger a similar mechanism via functional inhibition of SVEP1.

Furthermore, I noted different associations between clinical parameters and shared autoantibodies regarding the Munich cohort. For instance, IL-6R-positive patients had decreased levels of CRP ($p=0.022$). Unfortunately, there was no longitudinal metadata covering drug administration in the Munich cohort so the therapeutic after-effect of the IL6R blockade can create the observed effect. Moreover, elevated amounts of aspartate aminotransferase (AST), a marker of liver damage, were detected in patients with anti-COLEC10 antibodies (Fig. 3.3.5 d). COLEC10 is a protein mainly expressed in the liver and is reported to be associated with liver fibrosis (213). Furthermore, anti-COLEC10 antibodies in severe COVID-19 patients were also linked to increased leukocytes. Here, I hypothesize that the COLEC10-autoantibodies can play a potential role in liver damage in severe COVID-19 patients. Notably, among putative autoantigens described earlier, I observed a similar tendency with IL1RAP, the downstream target of the IL-1 signaling pathway. Patients with anti-ILRAP autoantibodies exhibited elevated levels of alanine transaminase (ALT), another liver enzyme prognostic for liver dysfunction. Hepatocytes ubiquitously express IL1RAP, and autoantibodies binding to it could lead to liver damage. Besides that, anti-ST3GAL6-positive patients had increased creatinine levels, which are indicative of kidney failure. Taking a precise look at the tissue expression of ST3GAL6, it can be observed that the liver and kidney predominantly express the enzyme. Finally, SERPINA10 is a serine protease inhibitor that inhibits the activity of factor Xa and prevents thrombosis. Notably, anti-SERPINA10 autoantibodies were detected in patients with elevated fibrinogen levels, which are commonly used in clinics as an indicator of thrombotic activity. The presence of anti-SERPINA10 antibodies can interfere with the functionality of the proteins, leading to an increased risk of blood clot formation.

Finally, I investigated the connections between the cumulative degree of autoreactivity in severe COVID-19 patients and its effect on their clinical picture. To achieve this, I calculated the autoantigen coefficient, a custom metric representing the sum of fold changes over the control for each potential autoantigen identified in the patients. Thus, a higher coefficient indicated a more significant number of autoreactivities present in an individual patient. In the Chicago cohort, the autoantigen coefficient ranged from 14 to 94, while in the Munich cohort, it ranged from 27 to 164. Notably, although the Chicago cohort exhibited more unique putative autoantigens (Fig. 3.3.5 e), the overall range of autoreactivities was higher among the severe COVID-19 patients in the Munich cohort.

To investigate the associations between the autoantigen score for individual patients and clinical parameters across both cohorts, I performed a pairwise Pearson correlation analysis between these values at the time of admission to the hospital. The study revealed significant positive correlations of autoantigen coefficient with procalcitonin (R=0.86, p=0.00019), cumulative intubation days (R=0.67, pl=0.013), cumulative ICU days (R=0.63, p=0.02), amylase (R=0.64, p=0.018) and troponin I (R=0.58, p=0.039) in the Chicago cohort (Fig. 3.3.5 e). Considering the biological functions of autoantibodies, it is plausible to hypothesize that increased autoreactivity may lead to a higher possibility of secondary bacterial infection, as indicated by the strong correlation between the autoantigen coefficient and procalcitonin. Procalcitonin is a blood marker for systemic bacterial or fungal infection, suggesting a link between autoantibody presence and susceptibility to secondary infections. Additionally, clinical evidence suggests that individuals with pre-existing autoimmune conditions are more susceptible to bacterial lung infections due to impaired local host defenses caused by the disease (214). Furthermore, a positive association between increased autoreactivity and extended ICU stays underscores the potential pathological impact of autoantibodies in the persistence of severe disease, whereas a robust positive relationship between the autoantigen score and Troponin I level in severe COVID-19 patients from the Chicago cohort suggests that myocardial injury may be induced in individuals with elevated autoantibody levels. Lastly, the coefficient exhibited positive correlations with SOFA score and LDH, indicating that heightened autoantibody levels in COVID-19 patients may correlate with increased disease severity and tissue damage.

In the Munich cohort, the autoantigen score was significantly positively correlated with liver enzymes AST and ALT and anti-N protein SARS-CoV2 antibody titers (Fig. 3.3.5 f). These findings shed light on the potential involvement of autoantibodies in the hepatic injury predominantly observed in severe COVID-19 cases compared to mild conditions (215).

Collectively, I hypothesized that autoantibodies targeting shared putative autoantigens in both the Munich and Chicago cohorts might disrupt molecular processes and contribute to the pathologies observed in severe COVID-19 patients. This was achieved by examining the association between autoantibody presence and various clinical parameters in autoantibody-positive and -negative patients. Notably, autoantigens discussed in this chapter are not restricted to the lung environment; many are liver or kidney enzymes or secreted proteins. However, scientific evidence regarding the functionalities and tissue localization of these proteins suggests that detected autoantibodies can interfere with several molecular functions, leading to multi-organ damage and blood clotting pathologies commonly observed in severe COVID-19 cases. Moreover, the analysis revealed significant associations between the overall level of autoantibodies and several clinical parameters, including cumulative intubation days, cumulative ICU days, procalcitonin, amylase, troponin I, AST, ALT, and anti-N ABs. These observations suggest that elevated autoantibody levels contribute to prolonged intubation periods, susceptibility to secondary bacterial infections,

and multi-organ damage, aligning with existing scientific knowledge for severe COVID-19 and common autoimmune diseases.

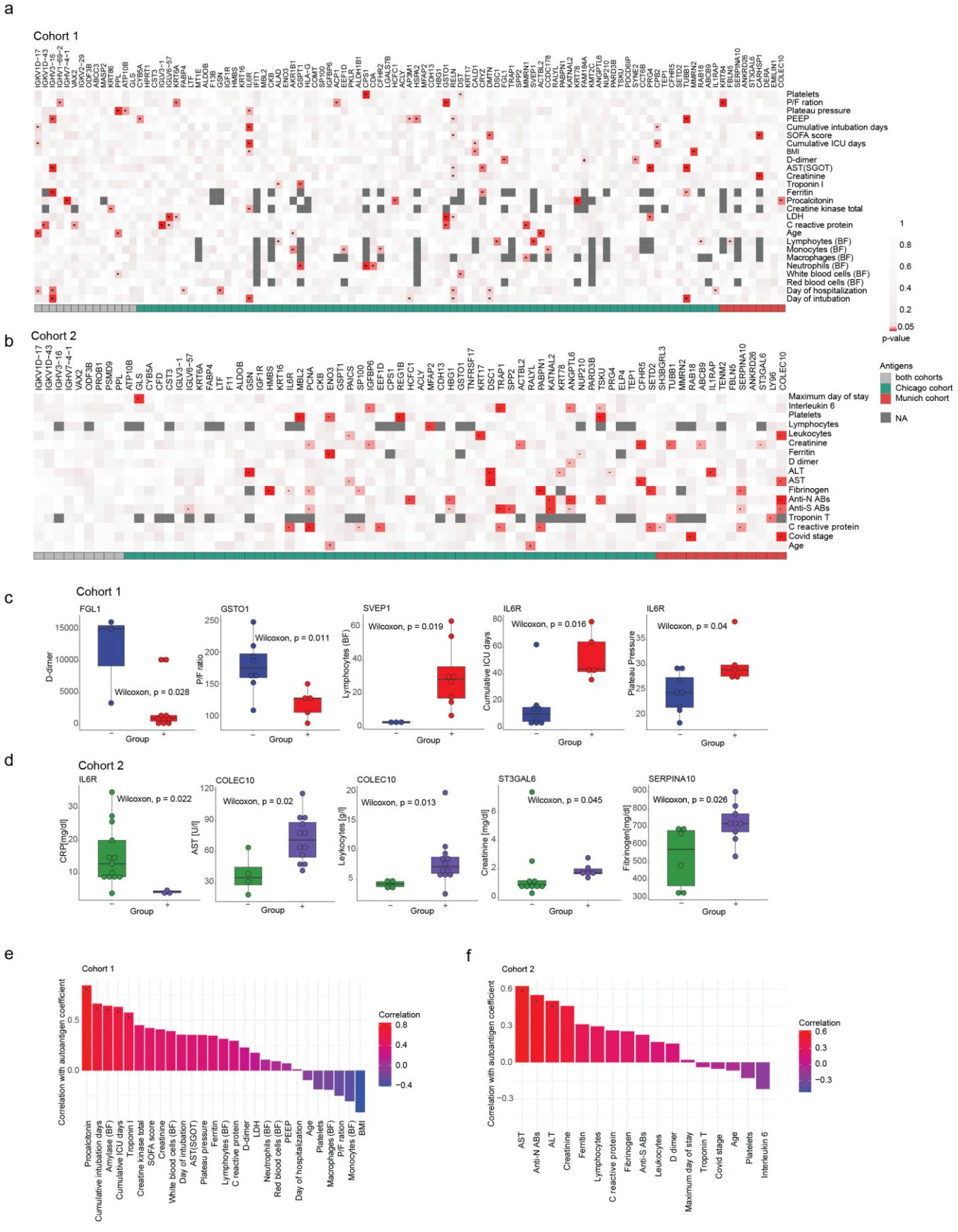
a
Cohort 1
Platelets
P/F ration
Plateau pressure
PEEP
Cumulative intubation days
SOFA score
Cumulative ICU days
BMI
D-dimer
AST(SGOT)
Creatinine
Troponin I
Ferritin
Procalcitonin
Creatine kinase total
LDH
C reactive protein
Age
Lymphoytes (BF)
Monocytes (BF)
Macrophages (BF)
Neutrophils (BF)
White blood cells (BF)
Red blood cells (BF)
Day of hospitalization
Day of intubation
p-value
b
Cohort 2
Maximum day of stay
Interleukin 6
Platelets
Lymphocytes
Leukocytes
Creatinine
Ferritin
D dimer
ALT
AST
Fibrinogen
Anti-N ABs
Anti-S ABs
Troponin T
C reactive protein
Covid stage
Age
Antigens
both cohorts
Chicago cohort
Munich cohort
NA
c
Cohort 1
FGL1
D-dimer
Wilcoxon, p = 0.028
GSTO1
P/F ratio
Wilcoxon, p = 0.011
SVEP1
Lymphocytes (BF)
Wilcoxon, p = 0.019
IL6R
Cumulative ICU days
Wilcoxon, p = 0.016
IL6R
Plateau Pressure
Wilcoxon, p = 0.04
Group
d
Cohort 2
IL6R
CRP[mg/dl]
Wilcoxon, p = 0.022
COLEC10
AST [U/l]
Wilcoxon, p = 0.02
COLEC10
Leykocytes [g/l]
Wilcoxon, p = 0.013
ST3GAL6
Creatinine [mg/dl]
Wilcoxon, p = 0.045
SERPINA10
Fibrinogen[mg/dl]
Wilcoxon, p = 0.026
Group
e
Cohort 1
Correlation with autoantigen coefficient
Correlation
Procalcitonin
Cumulative intubation days
Amylase (BF)
Cumulative ICU days
Troponin I
Creatine kinase total
SOFA score
Creatinine
White blood cells (BF)
Day of intubation
AST(SGOT)
Plateau pressure
Ferritin
Lymphoytes (BF)
C reactive protein
D-dimer
LDH
Neutrophils (BF)
Red blood cells (BF)
PEEP
Day of hospitalization
Age
Platelets
Macrophages (BF)
P/F ration
Monocytes (BF)
BMI
f
Cohort 2
Correlation with autoantigen coefficient
Correlation
AST
Anti-N ABs
ALT
Creatinine
Ferritin
Lymphocytes
C reactive protein
Fibrinogen
Anti-S ABs
Leukocytes
D dimer
Maximum day of stay
Troponin T
Covid stage
Age
Platelets
Interleukin 6

Figure 3.3.5: Associations between the presence of putative autoantigens and clinical parameters of two independent severe COVID-19 cohorts. a, Heatmap presenting the associations between clinical parameters on the y-axis of the Chicago cohort and detection of the putative autoantigens in COVID-19 patients (n=13) on the x-axis upon the intubation. The color decodes the output of the Wilcoxon test (p-value), demonstrating the difference between groups of COVID-19 patients with (+) and without (-) autoantigen. Values below the 0.05 threshold are depicted in red. The dark grey color corresponds to the absence of the test results due to the missing values. The column annotation highlights in which cohort the autoantigen was detected. **b,** Heatmap presenting the associations between clinical parameters on the y-axis of the Munich cohort and detection of the putative autoantigens in COVID-19 patients (n=16) on the x-axis upon the intubation. The color decodes the output of the Wilcoxon test (p-value), demonstrating the difference between groups of COVID-19 patients with (+) and without (-) autoantigen. Values below the 0.05 threshold are depicted in red. The dark grey color corresponds to the absence of the test results due to the missing values. The column annotation highlights in which cohort the autoantigen was detected. **c,** Box plots representing the significant associations between putative autoantigens shared between cohort 1 and cohort 2 and clinical parameters in the Chicago cohort. The x-axis displays groups of COVID-19 patients (n=13) with (+) detected autoantigen and without (-) upon the intubation. **d,** Box plots representing significant associations between putative autoantigens shared between cohort 1 and cohort 2 and clinical parameters in the Munich cohort. The x-axis displays groups of COVID-19 patients (n=16) with (+) detected autoantigen and without (-) upon the intubation. **e,** The bar plot shows the pairwise Pearson correlation analysis results between the Autoantigen coefficient of the Chicago cohort and clinical parameters. The y-axis shows the correlation coefficient (R), and a significant correlation is depicted with a star sign. The bar's color indicates a positive (red) or negative (blue) correlation. **f,** The bar plot shows the results of the pairwise Pearson correlation analysis between the autoantigen coefficient of the Munich cohort and clinical parameters. The y-axis shows the correlation coefficient (R), and a significant correlation is depicted with a star sign. The bar's color indicates a positive (red) or negative (blue) correlation.

Limitations of the study

This thesis has several limitations, which will be discussed hereby. First, the two COVID-19 cohorts described in the study are heterogeneous regarding the received treatments and other clinical care procedures. As both cohorts were assembled during the initial phase of the COVID-19 pandemic, it gave us an advantage due to the absence of previous infections with SARS-CoV-2; however, the novelty of the pathogen also contributed to the variability in the treatment strategies and hospital admission guidelines. One way to avoid it would be to utilize COVID-19 cohorts acquired at the later stages of the pandemic when the treatment guidelines were established and uniform. However, this approach would include patients with a history of SARS-COV-2 infections, which is also essential in studying newly emerged autoreactivities.

Secondly, in the Chicago cohort, my collaborators from NWMH attempted to standardize the BALF volumes, but the number of alveoli sampled and the return volumes varied. Also, the Chicago cohort was biased toward more severe patients; as part of clinical care, the sick patients were sampled more frequently. Unfortunately, according to standard critical care guidelines, BALF and plasma samples are collected from patients with indefinite or rapidly worsening clinical conditions to adjust the treatment strategy and prevent fast decay. This way, recovering patients stay under-sampled, and proteomic observations described in this thesis are biased toward patients with obstructed recovery trajectories.

A few considerations must be made concerning the DAC method employed in this thesis to identify putative autoantigens. First of all, the detection of the antigens can be affected by several factors: titers of the specific antibody in the plasma of the patient, affinity of the antibody, and abundance of the autoantigen in the tissue lysate. By adhering to particular conditions of the DAC protocol, specifically the selection of the target tissue, I expect to miss some possible autoantibody targets. In the case of COVID-19, the clinical manifestations spread outside the primary infection site and affect multiple other organs. This way, using the ‘healthy’ lung bait in the assay limited our findings toward the autoantigens available in lung tissue. Besides that, getting lung tissue from individuals not infected with SARS-CoV-2 may also restrict our conclusions by missing the targets carrying post-translational modification imposed by the virus on the host proteome. To overcome these limitations, the experiment's design should consider a lung tissue pool from individuals infected with SARS-CoV-2; ideally, the lung samples should be paired with the plasma/serum samples. Regrettably, this can only be accomplished in deceased COVID-19 patients, which restricts our findings to a specific severity group.

Furthermore, I noticed numerous proteins specific to the kidneys and liver among the putative autoantigens. This could be due to the assay's ability to enrich molecular complexes of the autoantibody-autoantigen present in the bloodstream.

Finally, I observed heterogeneity in DAC results between the Munich and the Chicago cohorts. This could be partially affected by the type of samples used. In the case of the Munich cohort, the received samples were serum, and in the Chicago cohort, they were plasma. Additionally, the sizes of both cohorts limited our findings regarding the putative autoantigens: 23 COVID-19 patients in the Munich cohort and 13 in Chicago. Several studies claimed that the high heterogeneity of the autoantibody targets among COVID-19 patients and a low detection rate of the specific autoantibodies in severe COVID-19 patients makes this research particularly challenging (216),(200). To ensure a comprehensive follow-up of the findings, it is recommended that the validation cohort be composed of a minimum of 100 COVID-19 patients with varying severity levels and longitudinal samples obtained after the acute phase of infection. This will enable a better understanding of common autoantibody targets in a larger group of patients and the role played by specific autoreactivities in the development of PASC.

Discussion

The humoral immune response is an essential aspect of the adaptive immune system. It is involved in recognizing and neutralizing pathogens, activating the accessory cells via antibody-coated pathogens, enabling their effector functions, and activating complement (217). Nevertheless, antibodies can contribute to autoimmunity, commonly reported in many infectious diseases, including COVID-19(88). SARS-CoV-2-induced pneumonia, as well as other highly inflammatory diseases, have been associated with the presence of autoantibodies (85,218). Notably, the role of the autoantibodies during the infection and their contribution to the outcome of the disease are emerging topics of interest. For example, the study of anti-phospholipid antibodies isolated from COVID-19 patients applied in a mouse model revealed that these antibodies can promote pathological coagulation events highly relevant to severe COVID-19 infection (102). Moreover, autoantibodies against cytokines and other immune signaling molecules have become a hallmark of severe COVID-19 (200).

Secondly, severe infection leads to hyperactivated immune responses, which, due to the circulation of pro-inflammatory mediators, yield a loss of tolerance mechanisms and a reduction of T-cell help requirement (219). Several studies revealed the expansion of autoimmune and atypical B cells in COVID-19 patients, which was explained by the enhancement of the extrafollicular B cell activation pathway (131), characterized by expanded populations of B cells and plasmablasts and loss of germinal centers. Besides that, antibody repertoires of hospitalized COVID-19 patients consisted of expanded clones with elongated CDR3 sequences and low levels of somatic hypermutation (81,220), which can be polyreactive (221) and resemble phenotype observed in other infections like acute Ebola (222) and salmonella infection (223). Strikingly, the latest evidence suggests that these responses in COVID-19 overlap with autoreactive B cells in SLE, which are also activated via an extrafollicular pathway through TLR-7 (224). Besides that, SARS-CoV-2 genomic RNA can costimulate TLR7, and many of the autoantigens identified in COVID-19 patients are capable of binding structural RNA, specifically U1-snRNA (found in Sm/RNP complexes), 7S RNA (a component of SRP), and tRNAs (Jo-1, PL-7, and PL-12) (223,225). Additionally, such ‘relaxation’ of B cell tolerance was suggested as one of the mechanisms promoting autoreactivity and autoantibody secretion in COVID-19 patients(219). These findings indicate the connection between immune responses during infection and autoimmune disorders, shedding light on common molecular mechanisms (224,226).

As part of my PhD project, I utilized a DAC assay to detect circulating antibodies among COVID-19 patients with varying degrees of severity. Combining the results of two distinct COVID-19 cohorts, I could identify autoantigens associated with the disease and correlate them with the patient's phenotype. Aligning with previous studies, I detected several autoantibodies targeting IFN I signaling pathway proteins (anti-ILRAP, anti-IFIT1) (86), which are considered the hallmark of

severe COVID-19 leading to disruption of the IFN signaling pathway and hindering the antiviral response. Some other findings highlight the role of anti-C1q (SLE autoantigen), anti-β2GP1 (which is thrombogenic), anti-SERPINA10, and anti-SVEP1 are predicted to exacerbate COVID-19-related pathogenic processes, such as hyper coagulopathy and microvascular injury (102,206,227). Other detected putative autoantigens were various tissue-associated proteins, such as COLEC10, RELN, ST3GAL6, MFAP5, MMRN1, MMRN2, and correlations between these autoantibodies and clinical markers such as CRP, creatinine, liver damage markers (AST and ALT), as well as respiratory parameters in the Chicago cohort, signal about the potential involvement of these autoantibodies in the extensive tissue damage. Moreover, total levels of autoreactivity for each patient were correlated to prolonged ICU stays and increased susceptibility to secondary bacterial infections. Importantly, my study partially explained the origin of specific autoantigens targeted in severe COVID-19 patients. Most of the newly triggered autoantigens result from severe disease with high levels of pro-inflammatory cytokines and chemokines, active spread of the virus, and associated tissue injury.

Moreover, in the case of severe COVID-19 infection, increased levels of autoantibodies are not a consequence of total immunoglobulin production, as they represent only a proportion of the overall antibody pool. In my study, the detection of a various number of autoantigens targeted in individual patients, together with the presence of a B cell phenotype resembling one in SLE and other canonical autoimmune diseases, supports the hypothesis of loss of self-tolerance in contrast to global increase in autoantibody production.

Multiple reports cover the hypothesis of the underlying autoimmune pathology in severe COVID-19 cases. Our study examined the impact of COVID-19 on autoantibody production, identifying putative antigens specific to mild and severe COVID-19 cases and following their behavior throughout the disease. This project contributes to our understanding of the role of autoantibodies in COVID-19 pathogenesis and suggests that reducing the autoreactive background could prevent the development of severe disease courses and lead to more favorable clinical outcomes. This aspect might benefit translational medicine and requires further investigation. Concerning the project's perspectives, it is important to consider implementing the results obtained from the study of acute COVID-19 patients in the independent cohort of long COVID-19 patients with pulmonary and extrapulmonary manifestations based on the existing theory that autoreactive aspects of long COVID-19 emerge as a result of an unresolved acute phase of the infection.

Appendix

Table A1: Baseline characteristics of the Chicago cohort on the initial day of the intubation

	COVID-19 n=13	**Non-pneumonia control n=7**	**Bacterial pneumonia n=6**	**Influenza n=7**
Age	61.2±11.3	66.5±4.9	57.1±13.7	56.2±10.6
Sex	10 male (77%), 3 female (23%)	3 male (43%), 4 female (57%)	4 male (67%), 2 female (33%)	4 male (57%), 3 female (43%)
Day of intubation [days]	5.1±7.3	5.6±6.2	20.5±16.4	7.4±8.5
ARDS	13 (100%)	7 (100%)	6 (100%)	7 (100%)
Deceased	2 (15%)	3 (43%)	4 (67%)	4 (57%)
Superinfection	3 (23%)	NA	NA	0 (0%)
Smoking status	4 never smokers (31%), 4 past smokers (31%), 5 NA (38%)	5 never smokers (71%), 2 past smokers (29%)	3 never smokers (50%), 1 past smoker (17%), 2 NA (33%)	5 never smokers (71%), 2 past smokers (29%)
Cumulative ICU days [days]	30.2±26	11.7±5.65	28.5±13.7	16.9±8.67
PaO2/FIO2 ratio	148±52.2	248±105	212±60.1	209±68.9
SOFA score	11.8±3.7	10.6±4	11.8±5	11.4±3.5

Data is presented as mean (±SD) or n (%). Abbreviations: ARDS- acute respiratory distress syndrome, SOFA score- Sequential Organ Failure Assessment score.

Table A2: Baseline characteristics of the Munich cohort at the first time window (0-11 days)

	Mild **n=7**	**Severe** **n=16**
Age	66.3±19	66.4±11.1
Sex	6 male (86%), 1 female (14%)	13 male (81%), 3 female (19%)
ARDS	0 (0%)	16 (100%)
ECMO	0 (0%)	3 (18.8%)
Deceased	0 (0%)	6 (37.5%)
Immunosuppression	2 (28.6%)	9 (56.2%)
Acute Kidney Injury	2 (28.6%)	12 (75%)
Length of hospitalization [days]	33.4±12.9	32.6±11.9
CRP [mg/dl]	7.0±6.8	13.3±9.0
Interleukin 6 [pg/ml]	52.9±32.6	602.2±1188.0

Data are presented as mean (±SD) or n (%). Abbreviations: ARDS-acute respiratory distress syndrome, ECMO - extracorporeal membrane oxygenation, CRP- C-reactive protein.

Acknowledgments

Upon completing this thesis, I wish to express my utmost appreciation to my supervisors, Dr. Herbert Schiller and Dr. Theodoros Kapellos, for entrusting me with this project and enabling me to further my knowledge in the field. Furthermore, I would like to extend my gratitude to the esteemed members of my TAC committee, particularly Prof. Jürgen Behr, Prof. Nikolaus Kneidinger, and Prof. Andreas Pichlmair, for their invaluable guidance and oversight throughout the project.

I would also like to acknowledge the CPC Research School, specifically Dr. Claudia Staab-Weijnitz and Melanie Penning, for their exceptional training and support, as well as for facilitating a comprehensive training program.

Additionally, I am indebted to my colleagues from the CPC Helmholtz Munich and MPI Proteomics and signal transduction departments for their unwavering support and assistance during challenging situations, as well as for fostering a comfortable and welcoming atmosphere in the office.

Lastly, I am deeply grateful to my parents and grandparents for their unwavering support of my studies abroad and for instilling in me a passion for science and medicine, as I come from a family of doctors. In closing, I would like to convey my appreciation to my partner Andre and my dear friend Katy for their unwavering support throughout my PhD and for taking a keen interest in my day-to-day work.

List of publications

1. **Mass spectrometry-based autoimmune profiling reveals predictive autoantigens in idiopathic pulmonary fibrosis**
   Leuschner, ***Semenova***, Mayer et al., iScience 2023 • November 2023
2. **Spatial single-cell mass spectrometry defines zonation of the hepatocyte proteome**
   Rosenberger et al., Nature Methods 2023 • October 2023

LMU LUDWIG-MAXIMILIANS-UNIVERSITÄT MÜNCHEN

Dean's Office Medical Faculty
Faculty of Medicine

Affidavit

Semenova, Anna

Surname, first name

I hereby declare, that the submitted thesis entitled

Clinical proteomics of pneumonia — antibody-mediated immunopathology in COVID-19

is my own work. I have only used the sources indicated and have not made unauthorised use of services of a third party. Where the work of others has been quoted or reproduced, the source is always given.

I further declare that the dissertation presented here has not been submitted in the same or similar form to any other institution for the purpose of obtaining an academic degree.

München, 18.12.2024

Place, Date

Anna Semenova

Signature doctoral candidate

LMU LUDWIG-MAXIMILIANS-UNIVERSITÄT MÜNCHEN

Dean's Office Medical Faculty
Doctoral Office

Confirmation of congruency between printed and electronic version of the doctoral thesis

Semenova, Anna

Surname, first name

I hereby declare that the electronic version of the submitted thesis, entitled

Clinical proteomics of pneumonia — antibody-mediated immunopathology in COVID-19

is congruent with the printed version both in content and format.

München, 18.12.2024

Place, Date

Anna Semenova

Signature doctoral candidate

Bibliography

1. Pneumonia - What Is Pneumonia? | NHLBI, NIH [Internet]. [cited 2024 Mar 25]. Available from: https://www.nhlbi.nih.gov/health/pneumonia

2. Msemburi W, Karlinsky A, Knutson V, Aleshin-Guendel S, Chatterji S, Wakefield J. The WHO estimates of excess mortality associated with the COVID-19 pandemic. Nature. 2023 Jan;613(7942):130–7.

3. Arslan M, Xu B, Gamal El-Din M. Transmission of SARS-CoV-2 via fecal-oral and aerosols-borne routes: Environmental dynamics and implications for wastewater management in underprivileged societies. Sci Total Environ. 2020 Nov 15;743:140709.

4. Lauer SA, Grantz KH, Bi Q, Jones FK, Zheng Q, Meredith HR, et al. The Incubation Period of Coronavirus Disease 2019 (COVID-19) From Publicly Reported Confirmed Cases: Estimation and Application. Ann Intern Med. 2020 May 5;172(9):577–82.

5. Mizumoto K, Kagaya K, Zarebski A, Chowell G. Estimating the asymptomatic proportion of coronavirus disease 2019 (COVID-19) cases on board the Diamond Princess cruise ship, Yokohama, Japan, 2020. Euro Surveill. 2020 Mar;25(10).

6. Li J, Huang DQ, Zou B, Yang H, Hui WZ, Rui F, et al. Epidemiology of COVID-19: A systematic review and meta-analysis of clinical characteristics, risk factors, and outcomes. J Med Virol. 2021 Mar;93(3):1449–58.

7. Stokes EK, Zambrano LD, Anderson KN, Marder EP, Raz KM, El Burai Felix S, et al. Coronavirus Disease 2019 Case Surveillance - United States, January 22-May 30, 2020. MMWR Morb Mortal Wkly Rep. 2020 Jun 19;69(24):759–65.

8. Huang C, Wang Y, Li X, Ren L, Zhao J, Hu Y, et al. Clinical features of patients infected with 2019 novel coronavirus in Wuhan, China. Lancet. 2020 Feb 15;395(10223):497–506.

9. Su S, Zhao Y, Zeng N, Liu X, Zheng Y, Sun J, et al. Epidemiology, clinical presentation, pathophysiology, and management of long COVID: an update. Mol Psychiatry. 2023 Oct;28(10):4056–69.

10. Finelli L, Gupta V, Petigara T, Yu K, Bauer KA, Puzniak LA. Mortality Among US Patients Hospitalized With SARS-CoV-2 Infection in 2020. JAMA Netw Open. 2021 Apr 1;4(4):e216556.

11. Chakraborty S, Gonzalez J, Edwards K, Mallajosyula V, Buzzanco AS, Sherwood R, et al. Proinflammatory IgG Fc structures in patients with severe COVID-19. Nat Immunol. 2021 Jan;22(1):67–73.

12. Davies NG, Barnard RC, Jarvis CI, Russell TW, Semple MG, Jit M, et al. Association of tiered restrictions and a second lockdown with COVID-19 deaths and hospital admissions in England: a modelling study. Lancet Infect Dis. 2021;21(4):482–92.

13. Khlem R, Kannappan SR, Choudhury PP. Coronavirus disease-2019: Challenges, opportunities, and benefits in India. J Educ Health Promot. 2022 Mar 23;11:104.

14. Jiang S, Hillyer C, Du L. Neutralizing Antibodies against SARS-CoV-2 and Other Human Coronaviruses: (Trends in Immunology 41, 355-359; 2020). Trends Immunol. 2020 Jun;41(6):545.

15. Xu H, Zhong L, Deng J, Peng J, Dan H, Zeng X, et al. High expression of ACE2 receptor of 2019-nCoV on the epithelial cells of oral mucosa. Int J Oral Sci. 2020 Feb 24;12(1):8.

16. van Eijk LE, Binkhorst M, Bourgonje AR, Offringa AK, Mulder DJ, Bos EM, et al. COVID-19: immunopathology, pathophysiological mechanisms, and treatment options. J Pathol. 2021 Jul;254(4):307–31.

17. Hoffmann M, Kleine-Weber H, Schroeder S, Krüger N, Herrler T, Erichsen S, et al. SARS-CoV-2 Cell Entry Depends on ACE2 and TMPRSS2 and Is Blocked by a Clinically Proven Protease Inhibitor. Cell. 2020 Apr 16;181(2):271-280.e8.

18. Osipiuk J, Azizi S-A, Dvorkin S, Endres M, Jedrzejczak R, Jones KA, et al. Structure of papain-like protease from SARS-CoV-2 and its complexes with non-covalent inhibitors. Nat Commun. 2021 Feb 2;12(1):743.

19. Thoms M, Buschauer R, Ameismeier M, Koepke L, Denk T, Hirschenberger M, et al. Structural basis for translational shutdown and immune evasion by the Nsp1 protein of SARS-CoV-2. Science. 2020 Sep 4;369(6508):1249–55.

20. Cortese M, Lee J-Y, Cerikan B, Neufeldt CJ, Oorschot VMJ, Köhrer S, et al. Integrative Imaging Reveals SARS-CoV-2-Induced Reshaping of Subcellular Morphologies. Cell Host Microbe. 2020 Dec 9;28(6):853-866.e5.

21. Ricciardi S, Guarino AM, Giaquinto L, Polishchuk EV, Santoro M, Di Tullio G, et al. The role of NSP6 in the biogenesis of the SARS-CoV-2 replication organelle. Nature. 2022 Jun;606(7915):761–8.

22. Wang D, Jiang A, Feng J, Li G, Guo D, Sajid M, et al. The SARS-CoV-2 subgenome landscape and its novel regulatory features. Mol Cell. 2021 May 20;81(10):2135-2147.e5.

23. Yao H, Song Y, Chen Y, Wu N, Xu J, Sun C, et al. Molecular Architecture of the SARS-CoV-2 Virus. Cell. 2020 Oct 29;183(3):730-738.e13.

24. Lu S, Ye Q, Singh D, Cao Y, Diedrich JK, Yates JR, et al. The SARS-CoV-2 nucleocapsid phosphoprotein forms mutually exclusive condensates with RNA and the membrane-associated M protein. Nat Commun. 2021 Jan 21;12(1):502.

25. Ghosh S, Dellibovi-Ragheb TA, Kerviel A, Pak E, Qiu Q, Fisher M, et al. β-Coronaviruses Use Lysosomes for Egress Instead of the Biosynthetic Secretory Pathway. Cell. 2020 Dec 10;183(6):1520-1535.e14.

26. Steiner S, Kratzel A, Barut GT, Lang RM, Aguiar Moreira E, Thomann L, et al. SARS-CoV-2 biology and host interactions. Nat Rev Microbiol. 2024 Jan 15;

27. Altschul DJ, Unda SR, Benton J, de la Garza Ramos R, Cezayirli P, Mehler M, et al. A novel severity score to predict inpatient mortality in COVID-19 patients. Sci Rep. 2020 Oct 7;10(1):16726.

28. San I, Gemcioglu E, Baser S, Yilmaz Cakmak N, Erden A, Izdes S, et al. Brescia-COVID Respiratory Severity Scale (BRCSS) and Quick SOFA (qSOFA) score are most useful in showing severity in COVID-19 patients. Sci Rep. 2021 Nov 8;11(1):21807.

29. COVID-19 Treatment Guidelines [Internet]. [cited 2024 Feb 27]. Available from: https://www.covid19treatmentguidelines.nih.gov/

30. Palanidurai S, Phua J, Chan YH, Mukhopadhyay A. P/FP ratio: incorporation of PEEP into the PaO2/FiO2 ratio for prognostication and classification of acute respiratory distress syndrome. Ann Intensive Care. 2021 Aug 9;11(1):124.

31. Agrati C, Bordoni V, Sacchi A, Petrosillo N, Nicastri E, Del Nonno F, et al. Elevated P-Selectin in Severe Covid-19: Considerations for Therapeutic Options. Mediterr J Hematol Infect Dis. 2021 Mar 1;13(1):e2021016.

32. Ali N. Elevated level of C-reactive protein may be an early marker to predict risk for severity of COVID-19. J Med Virol. 2020 Nov;92(11):2409–11.

33. Tang N, Li D, Wang X, Sun Z. Abnormal coagulation parameters are associated with poor prognosis in patients with novel coronavirus pneumonia. J Thromb Haemost. 2020 Apr;18(4):844–7.

34. Connors JM, Brooks MM, Sciurba FC, Krishnan JA, Bledsoe JR, Kindzelski A, et al. Effect of Antithrombotic Therapy on Clinical Outcomes in Outpatients With Clinically Stable Symptomatic COVID-19: The ACTIV-4B Randomized Clinical Trial. JAMA. 2021 Nov 2;326(17):1703–12.

35. Perico L, Benigni A, Casiraghi F, Ng LFP, Renia L, Remuzzi G. Immunity, endothelial injury and complement-induced coagulopathy in COVID-19. Nat Rev Nephrol. 2021 Jan;17(1):46–64.

36. Purcell SC, Godula K. Synthetic glycoscapes: addressing the structural and functional complexity of the glycocalyx. Interface Focus. 2019 Apr 6;9(2):20180080.

37. Nagashima S, Mendes MC, Camargo Martins AP, Borges NH, Godoy TM, Miggiolaro AFRDS, et al. Endothelial Dysfunction and Thrombosis in Patients With COVID-19-Brief Report. Arterioscler Thromb Vasc Biol. 2020 Oct;40(10):2404–7.

38. Evans PC, Rainger GE, Mason JC, Guzik TJ, Osto E, Stamataki Z, et al. Endothelial dysfunction in COVID-19: a position paper of the ESC Working Group for Atherosclerosis and Vascular Biology, and the ESC Council of Basic Cardiovascular Science. Cardiovasc Res. 2020 Dec 1;116(14):2177–84.

39. El-Arif G, Farhat A, Khazaal S, Annweiler C, Kovacic H, Wu Y, et al. The Renin-Angiotensin System: A Key Role in SARS-CoV-2-Induced COVID-19. Molecules. 2021 Nov 17;26(22).

40. Bhoola KD, Figueroa CD, Worthy K. Bioregulation of kinins: kallikreins, kininogens, and kininases. Pharmacol Rev. 1992 Mar;44(1):1–80.

41. Marceau F, Bawolak M-T, Fortin J-P, Morissette G, Roy C, Bachelard H, et al. Bifunctional ligands of the bradykinin B2 and B1 receptors: An exercise in peptide hormone plasticity. Peptides. 2018 Jul;105:37–50.

42. Teuwen L-A, Geldhof V, Pasut A, Carmeliet P. COVID-19: the vasculature unleashed. Nat Rev Immunol. 2020 Jul;20(7):389–91.

43. Porto BN, Stein RT. Neutrophil extracellular traps in pulmonary diseases: too much of a good thing? Front Immunol. 2016 Aug 15;7:311.

44. Zhao X, Zhou L, Kou Y, Kou J. Activated neutrophils in the initiation and progression of COVID-19: hyperinflammation and immunothrombosis in COVID-19. Am J Transl Res. 2022 Mar 15;14(3):1454–68.

45. Afzali B, Noris M, Lambrecht BN, Kemper C. The state of complement in COVID-19. Nat Rev Immunol. 2022 Feb;22(2):77–84.

46. Holter JC, Pischke SE, de Boer E, Lind A, Jenum S, Holten AR, et al. Systemic complement activation is associated with respiratory failure in COVID-19 hospitalized patients. Proc Natl Acad Sci USA. 2020 Oct 6;117(40):25018–25.

47. Carvelli J, Demaria O, Vély F, Batista L, Chouaki Benmansour N, Fares J, et al. Association of COVID-19 inflammation with activation of the C5a-C5aR1 axis. Nature. 2020 Dec;588(7836):146–50.

48. Yu J, Yuan X, Chen H, Chaturvedi S, Braunstein EM, Brodsky RA. Direct activation of the alternative complement pathway by SARS-CoV-2 spike proteins is blocked by factor D inhibition. Blood. 2020 Oct 29;136(18):2080–9.

49. Ali YM, Ferrari M, Lynch NJ, Yaseen S, Dudler T, Gragerov S, et al. Lectin Pathway Mediates Complement Activation by SARS-CoV-2 Proteins. Front Immunol. 2021 Jul 5;12:714511.

50. Zaid Y, Puhm F, Allaeys I, Naya A, Oudghiri M, Khalki L, et al. Platelets Can Associate with SARS-Cov-2 RNA and Are Hyperactivated in COVID-19. Circ Res. 2020 Sep 17;127(11):1404–18.

51. Manne BK, Denorme F, Middleton EA, Portier I, Rowley JW, Stubben C, et al. Platelet gene expression and function in patients with COVID-19. Blood. 2020 Sep 10;136(11):1317–29.

52. Hottz ED, Azevedo-Quintanilha IG, Palhinha L, Teixeira L, Barreto EA, Pão CRR, et al. Platelet activation and platelet-monocyte aggregate formation trigger tissue factor expression in patients with severe COVID-19. Blood. 2020 Sep 10;136(11):1330–41.

53. Davizon-Castillo P, McMahon B, Aguila S, Bark D, Ashworth K, Allawzi A, et al. TNF-α-driven inflammation and mitochondrial dysfunction define the platelet hyperreactivity of aging. Blood. 2019 Aug 29;134(9):727–40.

54. Conway EM, Mackman N, Warren RQ, Wolberg AS, Mosnier LO, Campbell RA, et al. Understanding COVID-19-associated coagulopathy. Nat Rev Immunol. 2022 Oct;22(10):639–49.

55. Martinez-Rojas MA, Vega-Vega O, Bobadilla NA. Is the kidney a target of SARS-CoV-2? Am J Physiol Renal Physiol. 2020 Jun 1;318(6):F1454–62.

56. Nadim MK, Forni LG, Mehta RL, Connor MJ, Liu KD, Ostermann M, et al. COVID-19-associated acute kidney injury: consensus report of the 25th Acute Disease Quality Initiative (ADQI) Workgroup. Nat Rev Nephrol. 2020 Dec;16(12):747–64.

57. Pan X-W, Xu D, Zhang H, Zhou W, Wang L-H, Cui X-G. Identification of a potential mechanism of acute kidney injury during the COVID-19 outbreak: a study based on single-cell transcriptome analysis. Intensive Care Med. 2020 Jun;46(6):1114–6.

58. Su H, Yang M, Wan C, Yi L-X, Tang F, Zhu H-Y, et al. Renal histopathological analysis of 26 postmortem findings of patients with COVID-19 in China. Kidney Int. 2020 Jul;98(1):219–27.

59. Gupta A, Madhavan MV, Sehgal K, Nair N, Mahajan S, Sehrawat TS, et al. Extrapulmonary manifestations of COVID-19. Nat Med. 2020 Jul 10;26(7):1017–32.

60. Hessami A, Shamshirian A, Heydari K, Pourali F, Alizadeh-Navaei R, Moosazadeh M, et al. Cardiovascular diseases burden in COVID-19: Systematic review and meta-analysis. Am J Emerg Med. 2021 Aug;46:382–91.

61. Pathan N, Hemingway CA, Alizadeh AA, Stephens AC, Boldrick JC, Oragui EE, et al. Role of interleukin 6 in myocardial dysfunction of meningococcal septic shock. Lancet. 2004 Jan 17;363(9404):203–9.

62. Rydyznski Moderbacher C, Ramirez SI, Dan JM, Grifoni A, Hastie KM, Weiskopf D, et al. Antigen-Specific Adaptive Immunity to SARS-CoV-2 in Acute COVID-19 and Associations with Age and Disease Severity. Cell. 2020 Nov 12;183(4):996-1012.e19.

63. Grifoni A, Weiskopf D, Ramirez SI, Mateus J, Dan JM, Moderbacher CR, et al. Targets of T Cell Responses to SARS-CoV-2 Coronavirus in Humans with COVID-19 Disease and Unexposed Individuals. Cell. 2020 Jun 25;181(7):1489-1501.e15.

64. Le Bert N, Tan AT, Kunasegaran K, Tham CYL, Hafezi M, Chia A, et al. SARS-CoV-2-specific T cell immunity in cases of COVID-19 and SARS, and uninfected controls. Nature. 2020 Aug;584(7821):457–62.

65. Neidleman J, Luo X, George AF, McGregor M, Yang J, Yun C, et al. Distinctive features of SARS-CoV-2-specific T cells predict recovery from severe COVID-19. Cell Rep. 2021 Jul 20;36(3):109414.

66. Thieme CJ, Anft M, Paniskaki K, Blazquez-Navarro A, Doevelaar A, Seibert FS, et al. Robust T Cell Response Toward Spike, Membrane, and Nucleocapsid SARS-CoV-2 Proteins Is Not Associated with Recovery in Critical COVID-19 Patients. Cell Rep Med. 2020 Sep 22;1(6):100092.

67. Chioh FW, Fong S-W, Young BE, Wu K-X, Siau A, Krishnan S, et al. Convalescent COVID-19 patients are susceptible to endothelial dysfunction due to persistent immune activation. eLife. 2021 Mar 23;10.

68. Zheng H-Y, Zhang M, Yang C-X, Zhang N, Wang X-C, Yang X-P, et al. Elevated exhaustion levels and reduced functional diversity of T cells in peripheral blood may predict severe progression in COVID-19 patients. Cell Mol Immunol. 2020 May;17(5):541–3.

69. Qin C, Zhou L, Hu Z, Zhang S, Yang S, Tao Y, et al. Dysregulation of Immune Response in Patients With Coronavirus 2019 (COVID-19) in Wuhan, China. Clin Infect Dis. 2020 Jul 28;71(15):762–8.

70. Xu Z, Shi L, Wang Y, Zhang J, Huang L, Zhang C, et al. Pathological findings of COVID-19 associated with acute respiratory distress syndrome. Lancet Respir Med. 2020 Apr;8(4):420–2.

71. Tan L, Wang Q, Zhang D, Ding J, Huang Q, Tang Y-Q, et al. Lymphopenia predicts disease severity of COVID-19: a descriptive and predictive study. Signal Transduct Target Ther. 2020 Mar 27;5:33.

72. Zhou P, Yang X-L, Wang X-G, Hu B, Zhang L, Zhang W, et al. A pneumonia outbreak associated with a new coronavirus of probable bat origin. Nature. 2020 Mar;579(7798):270–3.

73. García-González P, Tempio F, Fuentes C, Merino C, Vargas L, Simon V, et al. Dysregulated Immune Responses in COVID-19 Patients Correlating With Disease Severity and Invasive Oxygen Requirements. Front Immunol. 2021 Oct 21;12:769059.

74. Feyaerts D, Hédou J, Gillard J, Chen H, Tsai ES, Peterson LS, et al. Integrated plasma proteomic and single-cell immune signaling network signatures demarcate mild, moderate, and severe COVID-19. Cell Rep Med. 2022 Jul 19;3(7):100680.

75. Janeway's Immunobiology von Kenneth M. Murphy | ISBN 978-0-393-88491-3 | Bei Lehmanns online kaufen - Lehmanns.de [Internet]. [cited 2024 Mar 26]. Available from: https://www.lehmanns.de/shop/naturwissenschaften/57284314-9780393884913-janeway-s-immunobiology

76. Gatto D, Brink R. The germinal center reaction. J Allergy Clin Immunol. 2010 Nov;126(5):898–907; quiz 908.

77. Long Q-X, Liu B-Z, Deng H-J, Wu G-C, Deng K, Chen Y-K, et al. Antibody responses to SARS-CoV-2 in patients with COVID-19. Nat Med. 2020 Jun;26(6):845–8.

78. Seow J, Graham C, Merrick B, Acors S, Pickering S, Steel KJA, et al. Longitudinal observation and decline of neutralizing antibody responses in the three months following SARS-CoV-2 infection in humans. Nat Microbiol. 2020 Dec;5(12):1598–607.

79. Sheikh-Mohamed S, Isho B, Chao GYC, Zuo M, Cohen C, Lustig Y, et al. Systemic and mucosal IgA responses are variably induced in response to SARS-CoV-2 mRNA vaccination and are associated with protection against subsequent infection. Mucosal Immunol. 2022 May;15(5):799–808.

80. Piccoli L, Park Y-J, Tortorici MA, Czudnochowski N, Walls AC, Beltramello M, et al. Mapping Neutralizing and Immunodominant Sites on the SARS-CoV-2 Spike Receptor-Binding Domain by Structure-Guided High-Resolution Serology. Cell. 2020 Nov 12;183(4):1024-1042.e21.

81. Nielsen SCA, Yang F, Jackson KJL, Hoh RA, Röltgen K, Jean GH, et al. Human B Cell Clonal Expansion and Convergent Antibody Responses to SARS-CoV-2. Cell Host Microbe. 2020 Oct 7;28(4):516-525.e5.

82. Zhao J, Yuan Q, Wang H, Liu W, Liao X, Su Y, et al. Antibody Responses to SARS-CoV-2 in Patients With Novel Coronavirus Disease 2019. Clin Infect Dis. 2020 Nov 19;71(16):2027–34.

83. Kaneko N, Kuo H-H, Boucau J, Farmer JR, Allard-Chamard H, Mahajan VS, et al. Loss of Bcl-6-Expressing T Follicular Helper Cells and Germinal Centers in COVID-19. Cell. 2020 Oct 1;183(1):143-157.e13.

84. Lei Q, Yu C-Z, Li Y, Hou H-Y, Xu Z-W, Yao Z-J, et al. Anti-SARS-CoV-2 IgG responses are powerful predicting signatures for the outcome of COVID-19 patients. J Advanc Res. 2022 Feb;36:133–45.

85. Muri J, Cecchinato V, Cavalli A, Shanbhag AA, Matkovic M, Biggiogero M, et al. Autoantibodies against chemokines post-SARS-CoV-2 infection correlate with disease course. Nat Immunol. 2023 Apr;24(4):604–11.

86. Bastard P, Rosen LB, Zhang Q, Michailidis E, Hoffmann H-H, Zhang Y, et al. Autoantibodies against type I IFNs in patients with life-threatening COVID-19. Science. 2020 Oct 23;370(6515).

87. Yang L, Liu S, Liu J, Zhang Z, Wan X, Huang B, et al. COVID-19: immunopathogenesis and Immunotherapeutics. Signal Transduct Target Ther. 2020 Jul 25;5(1):128.

88. Smatti MK, Cyprian FS, Nasrallah GK, Al Thani AA, Almishal RO, Yassine HM. Viruses and autoimmunity: A review on the potential interaction and molecular mechanisms. Viruses. 2019 Aug 19;11(8).

89. Chang R, Yen-Ting Chen T, Wang S-I, Hung Y-M, Chen H-Y, Wei C-CJ. Risk of autoimmune diseases in patients with COVID-19: A retrospective cohort study. EClinicalMedicine. 2023 Feb;56:101783.

90. Sharma C, Bayry J. High risk of autoimmune diseases after COVID-19. Nat Rev Rheumatol. 2023 Jul;19(7):399–400.

91. Tesch F, Ehm F, Vivirito A, Wende D, Batram M, Loser F, et al. Incident autoimmune diseases in association with SARS-CoV-2 infection: a matched cohort study. Clin Rheumatol. 2023 Oct;42(10):2905–14.

92. Nunez-Castilla J, Stebliankin V, Baral P, Balbin CA, Sobhan M, Cickovski T, et al. Potential Autoimmunity Resulting from Molecular Mimicry between SARS-CoV-2 Spike and Human Proteins. Viruses. 2022 Jun 28;14(7).

93. Jiang W, Johnson D, Adekunle R, Heather H, Xu W, Cong X, et al. COVID-19 is associated with bystander polyclonal autoreactive B cell activation as reflected by a broad autoantibody production, but none is linked to disease severity. J Med Virol. 2023 Jan;95(1):e28134.

94. Shrock E, Fujimura E, Kula T, Timms RT, Lee I-H, Leng Y, et al. Viral epitope profiling of COVID-19 patients reveals cross-reactivity and correlates of severity. Science. 2020 Nov 27;370(6520).

95. Balint E, Feng E, Giles EC, Ritchie TM, Qian AS, Vahedi F, et al. Bystander activated CD8+ T cells mediate neuropathology during viral infection via antigen-independent cytotoxicity. Nat Commun. 2024 Feb 5;15(1):896.

96. Bergamaschi L, Mescia F, Turner L, Hanson AL, Kotagiri P, Dunmore BJ, et al. Longitudinal analysis reveals that delayed bystander CD8+ T cell activation and early immune pathology distinguish severe COVID-19 from mild disease. Immunity. 2021 Jun 8;54(6):1257-1275.e8.

97. Lin YS, Lin CF, Fang YT, Kuo YM, Liao PC, Yeh TM, et al. Antibody to severe acute respiratory syndrome (SARS)-associated coronavirus spike protein domain 2 cross-reacts with lung epithelial cells and causes cytotoxicity. Clin Exp Immunol. 2005 Sep;141(3):500–8.

98. Pascolini S, Vannini A, Deleonardi G, Ciordinik M, Sensoli A, Carletti I, et al. COVID-19 and Immunological Dysregulation: Can Autoantibodies be Useful? Clin Transl Sci. 2021 Mar;14(2):502–8.

99. Wong AKH, Woodhouse I, Schneider F, Kulpa DA, Silvestri G, Maier CL. Broad auto-reactive IgM responses are common in critically ill patients, including those with COVID-19. Cell Rep Med. 2021 Jun 15;2(6):100321.

100. Cabral-Marques O, Halpert G, Schimke LF, Ostrinski Y, Vojdani A, Baiocchi GC, et al. Autoantibodies targeting GPCRs and RAS-related molecules associate with COVID-19 severity. Nat Commun. 2022 Mar 9;13(1):1220.

101. Fonseca DLM, Filgueiras IS, Marques AHC, Vojdani E, Halpert G, Ostrinski Y, et al. Severe COVID-19 patients exhibit elevated levels of autoantibodies targeting cardiolipin and platelet glycoprotein with age: a systems biology approach. npj Aging. 2023 Aug 24;9(1):21.

102. Zuo Y, Estes SK, Ali RA, Gandhi AA, Yalavarthi S, Shi H, et al. Prothrombotic autoantibodies in serum from patients hospitalized with COVID-19. Sci Transl Med. 2020 Nov 18;12(570):eabd3876.

103. Fagyas M, Nagy B, Ráduly AP, Mányiné IS, Mártha L, Erdősi G, et al. The majority of severe COVID-19 patients develop anti-cardiac autoantibodies. Geroscience. 2022 Oct;44(5):2347–60.

104. Wang EY, Mao T, Klein J, Dai Y, Huck JD, Jaycox JR, et al. Diverse functional autoantibodies in patients with COVID-19. Nature. 2021 Jul;595(7866):283–8.

105. Davies NG, Klepac P, Liu Y, Prem K, Jit M, CMMID COVID-19 working group, et al. Age-dependent effects in the transmission and control of COVID-19 epidemics. Nat Med. 2020;26(8):1205–11.

106. Liu Z, Liang Q, Ren Y, Guo C, Ge X, Wang L, et al. Immunosenescence: molecular mechanisms and diseases. Signal Transduct Target Ther. 2023 May 13;8(1):200.

107. Nakamura T, Morodomi Y, Kanaji S, Okamura T, Nagafuji K, Kanaji T. Detection of anti-GPIbα autoantibodies in a case of immune thrombocytopenia following COVID-19 vaccination. Thromb Res. 2022 Jan;209:80–3.

108. Greinacher A, Selleng K, Mayerle J, Palankar R, Wesche J, Reiche S, et al. Anti-platelet factor 4 antibodies causing VITT do not cross-react with SARS-CoV-2 spike protein. Blood. 2021 Oct 7;138(14):1269–77.

109. Cabral-Marques O, Marques A, Giil LM, De Vito R, Rademacher J, Günther J, et al. GPCR-specific autoantibody signatures are associated with physiological and pathological immune homeostasis. Nat Commun. 2018 Dec 6;9(1):5224.

110. Lutz HU, Binder CJ, Kaveri S. Naturally occurring auto-antibodies in homeostasis and disease. Trends Immunol. 2009 Jan;30(1):43–51.

111. Amendt T, Allies G, Nicolò A, El Ayoubi O, Young M, Röszer T, et al. Autoreactive antibodies control blood glucose by regulating insulin homeostasis. Proc Natl Acad Sci USA. 2022 Feb 8;119(6).

112. Cabral-Marques O, Riemekasten G. Functional autoantibodies targeting G protein-coupled receptors in rheumatic diseases. Nat Rev Rheumatol. 2017 Nov;13(11):648–56.

113. Nagele EP, Han M, Acharya NK, DeMarshall C, Kosciuk MC, Nagele RG. Natural IgG autoantibodies are abundant and ubiquitous in human sera, and their number is influenced by age, gender, and disease. PLoS ONE. 2013 Apr 2;8(4):e60726.

114. Ding Z, Wei X, Pan H, Shi H, Shi Y. Unveiling the intricacies ofCOVID -19: Autoimmunity, multi-organ manifestations and the role of autoantibodies. Scand J Immunol. 2023 Dec 10;

115. Post COVID-19 condition (Long COVID) [Internet]. [cited 2024 Feb 27]. Available from: https://www.who.int/europe/news-room/fact-sheets/item/post-covid-19-condition

116. Groff D, Sun A, Ssentongo AE, Ba DM, Parsons N, Poudel GR, et al. Short-term and Long-term Rates of Postacute Sequelae of SARS-CoV-2 Infection: A Systematic Review. JAMA Netw Open. 2021 Oct 1;4(10):e2128568.

117. Bell ML, Catalfamo CJ, Farland LV, Ernst KC, Jacobs ET, Klimentidis YC, et al. Post-acute sequelae of COVID-19 in a non-hospitalized cohort: Results from the Arizona CoVHORT. PLoS ONE. 2021 Aug 4;16(8):e0254347.

118. Klein J, Wood J, Jaycox JR, Dhodapkar RM, Lu P, Gehlhausen JR, et al. Distinguishing features of long COVID identified through immune profiling. Nature. 2023 Nov;623(7985):139–48.

119. Davis HE, Assaf GS, McCorkell L, Wei H, Low RJ, Re'em Y, et al. Characterizing long COVID in an international cohort: 7 months of symptoms and their impact. EClinicalMedicine. 2021 Aug;38:101019.

120. Michelen M, Manoharan L, Elkheir N, Cheng V, Dagens A, Hastie C, et al. Characterising long COVID: a living systematic review. BMJ Glob Health. 2021 Sep;6(9).

121. Munblit D, Nicholson T, Akrami A, Apfelbacher C, Chen J, De Groote W, et al. A core outcome set for post-COVID-19 condition in adults for use in clinical practice and research: an international Delphi consensus study. Lancet Respir Med. 2022 Jul;10(7):715–24.

122. Davis HE, McCorkell L, Vogel JM, Topol EJ. Long COVID: major findings, mechanisms and recommendations. Nat Rev Microbiol. 2023 Mar;21(3):133–46.

123. Cheung CCL, Goh D, Lim X, Tien TZ, Lim JCT, Lee JN, et al. Residual SARS-CoV-2 viral antigens detected in GI and hepatic tissues from five recovered patients with COVID-19. Gut. 2022 Jan;71(1):226–9.

124. Chertow D, Stein S, Ramelli S, Grazioli A, Chung J-Y, Singh M, et al. SARS-CoV-2 infection and persistence throughout the human body and brain. Res Sq. 2021 Dec 20;

125. Peluso MJ, Lu S, Tang AF, Durstenfeld MS, Ho H-E, Goldberg SA, et al. Markers of immune activation and inflammation in individuals with postacute sequelae of severe acute respiratory syndrome coronavirus 2 infection. J Infect Dis. 2021 Dec 1;224(11):1839–48.

126. Joy G, Artico J, Kurdi H, Seraphim A, Lau C, Thornton GD, et al. Prospective Case-Control Study of Cardiovascular Abnormalities 6 Months Following Mild COVID-19 in Healthcare Workers. JACC Cardiovasc Imaging. 2021 Nov;14(11):2155–66.

127. Murata N, Yamada A, Fujito H, Hashimoto N, Nagao T, Tanaka Y, et al. Cardiovascular manifestations identified by multi-modality imaging in patients with long COVID. Front Cardiovasc Med. 2022 Sep 23;9:968584.

128. Remy-Jardin M, Duthoit L, Perez T, Felloni P, Faivre J-B, Fry S, et al. Assessment of pulmonary arterial circulation 3 months after hospitalization for SARS-CoV-2 pneumonia: Dual-energy CT (DECT) angiographic study in 55 patients. EClinicalMedicine. 2021 Apr;34:100778.

129. Dennis A, Wamil M, Alberts J, Oben J, Cuthbertson DJ, Wootton D, et al. Multiorgan impairment in low-risk individuals with post-COVID-19 syndrome: a prospective, community-based study. BMJ Open. 2021 Mar 30;11(3):e048391.

130. Visvabharathy L, Hanson BA, Orban ZS, Lim PH, Palacio NM, Jimenez M, et al. T cell responses to SARS-CoV-2 in people with and without neurologic symptoms of long COVID. medRxiv. 2022 Oct 21;

131. Woodruff MC, Ramonell RP, Nguyen DC, Cashman KS, Saini AS, Haddad NS, et al. Extrafollicular B cell responses correlate with neutralizing antibodies and morbidity in COVID-19. Nat Immunol. 2020 Dec;21(12):1506–16.

132. Arish M, Qian W, Narasimhan H, Sun J. COVID-19 immunopathology: From acute diseases to chronic sequelae. J Med Virol. 2023 Jan;95(1):e28122.

133. Grant RA, Morales-Nebreda L, Markov NS, Swaminathan S, Querrey M, Guzman ER, et al. Circuits between infected macrophages and T cells in SARS-CoV-2 pneumonia. Nature. 2021 Feb;590(7847):635–41.

134. Acute Respiratory Distress Syndrome Network, Brower RG, Matthay MA, Morris A, Schoenfeld D, Thompson BT, et al. Ventilation with lower tidal volumes as compared with traditional tidal volumes for acute lung injury and the acute respiratory distress syndrome. N Engl J Med. 2000 May 4;342(18):1301–8.

135. Guérin C, Reignier J, Richard J-C, Beuret P, Gacouin A, Boulain T, et al. Prone positioning in severe acute respiratory distress syndrome. N Engl J Med. 2013 Jun 6;368(23):2159–68.

136. Geyer PE, Arend FM, Doll S, Louiset M-L, Virreira Winter S, Müller-Reif JB, et al. High-resolution serum proteome trajectories in COVID-19 reveal patient-specific seroconversion. EMBO Mol Med. 2021 Aug 9;13(8):e14167.

137. Leuschner G, Semenova A, Mayr CH, Kapellos TS, Ansari M, Seeliger B, et al. Mass spectrometry-based autoimmune profiling reveals predictive autoantigens in idiopathic pulmonary fibrosis. iScience. 2023 Nov 17;26(11):108345.

138. Geyer PE, Kulak NA, Pichler G, Holdt LM, Teupser D, Mann M. Plasma proteome profiling to assess human health and disease. Cell Syst. 2016 Mar 23;2(3):185–95.

139. Batth TS, Tollenaere MX, Rüther P, Gonzalez-Franquesa A, Prabhakar BS, Bekker-Jensen S, et al. Protein aggregation capture on microparticles enables multipurpose proteomics sample preparation. Mol Cell Proteomics. 2019 May;18(5):1027–35.

140. Bouyssié D, Gonzalez de Peredo A, Mouton E, Albigot R, Roussel L, Ortega N, et al. Mascot file parsing and quantification (MFPaQ), a new software to parse, validate, and quantify proteomics data generated by ICAT and SILAC mass spectrometric analyses: application to the proteomics study of membrane proteins from primary human endothelial cells. Mol Cell Proteomics. 2007 Sep;6(9):1621–37.

141. Cox J, Hein MY, Luber CA, Paron I, Nagaraj N, Mann M. Accurate proteome-wide label-free quantification by delayed normalization and maximal peptide ratio extraction, termed MaxLFQ. Mol Cell Proteomics. 2014 Sep;13(9):2513–26.

142. Cox J, Mann M. MaxQuant enables high peptide identification rates, individualized p.p.b.-range mass accuracies and proteome-wide protein quantification. Nat Biotechnol. 2008 Dec;26(12):1367–72.

143. Demichev V, Messner CB, Vernardis SI, Lilley KS, Ralser M. DIA-NN: neural networks and interference correction enable deep proteome coverage in high throughput. Nat Methods. 2020 Jan;17(1):41–4.

144. Messner CB, Demichev V, Wendisch D, Michalick L, White M, Freiwald A, et al. Ultra-High-Throughput Clinical Proteomics Reveals Classifiers of COVID-19 Infection. Cell Syst. 2020 Jul 22;11(1):11-24.e4.

145. Oestreich M, Holsten L, Agrawal S, Dahm K, Koch P, Jin H, et al. hCoCena: horizontal integration and analysis of transcriptomics datasets. Bioinformatics. 2022 Oct 14;38(20):4727–34.

146. Bigaret S, Hodgett RE, Meyer P, Mironova T, Olteanu A-L. Supporting the multi-criteria decision aiding process: R and the MCDA package. EURO J Decis Process. 2017 Apr 3;

147. Seifikar M, Farzi S, Barati M. C-Blondel: An Efficient Louvain-Based Dynamic Community Detection Algorithm. IEEE Trans Comput Soc Syst. 2020 Apr;7(2):308–18.

148. Wu T, Hu E, Xu S, Chen M, Guo P, Dai Z, et al. clusterProfiler 4.0: A universal enrichment tool for interpreting omics data. Innovation (Camb). 2021 Aug 28;2(3):100141.

149. Croft D, O'Kelly G, Wu G, Haw R, Gillespie M, Matthews L, et al. Reactome: a database of reactions, pathways and biological processes. Nucleic Acids Res. 2011 Jan;39(Database issue):D691-7.

150. Hänzelmann S, Castelo R, Guinney J. GSVA: gene set variation analysis for microarray and RNA-seq data. BMC Bioinformatics. 2013 Jan 16;14:7.

151. Tyanova S, Temu T, Sinitcyn P, Carlson A, Hein MY, Geiger T, et al. The Perseus computational platform for comprehensive analysis of (prote)omics data. Nat Methods. 2016 Sep;13(9):731–40.

152. Stephenson E, Reynolds G, Botting RA, Calero-Nieto FJ, Morgan MD, Tuong ZK, et al. Single-cell multi-omics analysis of the immune response in COVID-19. Nat Med. 2021 Apr 20;

153. Finak G, McDavid A, Yajima M, Deng J, Gersuk V, Shalek AK, et al. MAST: a flexible statistical framework for assessing transcriptional changes and characterizing heterogeneity in single-cell RNA sequencing data. Genome Biol. 2015 Dec 10;16:278.

154. Oelen R, de Vries DH, Brugge H, Gordon MG, Vochteloo M, single-cell eQTLGen consortium, et al. Single-cell RNA-sequencing of peripheral blood mononuclear cells reveals widespread, context-specific gene expression regulation upon pathogenic exposure. Nat Commun. 2022 Jun 7;13(1):3267.

155. Morgan D, Tergaonkar V. Unraveling B cell trajectories at single cell resolution. Trends Immunol. 2022 Mar;43(3):210–29.

156. Mulè MP, Martins AJ, Tsang JS. Normalizing and denoising protein expression data from droplet-based single cell profiling. Nat Commun. 2022 Apr 19;13(1):2099.

157. Baumgarth N. The double life of a B-1 cell: self-reactivity selects for protective effector functions. Nat Rev Immunol. 2011 Jan;11(1):34–46.

158. Heumos L, Schaar AC, Lance C, Litinetskaya A, Drost F, Zappia L, et al. Best practices for single-cell analysis across modalities. Nat Rev Genet. 2023 Aug;24(8):550–72.

159. Su CT-T, Ling W-L, Lua W-H, Poh J-J, Gan SK-E. The role of Antibody Vκ Framework 3 region towards Antigen binding: Effects on recombinant production and Protein L binding. Sci Rep. 2017 Jun 19;7(1):3766.

160. Yaari G, Vander Heiden JA, Uduman M, Gadala-Maria D, Gupta N, Stern JNH, et al. Models of somatic hypermutation targeting and substitution based on synonymous mutations from high-throughput immunoglobulin sequencing data. Front Immunol. 2013 Nov 15;4:358.

161. Gupta NT, Vander Heiden JA, Uduman M, Gadala-Maria D, Yaari G, Kleinstein SH. Change-O: a toolkit for analyzing large-scale B cell immunoglobulin repertoire sequencing data. Bioinformatics. 2015 Oct 15;31(20):3356–8.

162. Geyer PE, Voytik E, Treit PV, Doll S, Kleinhempel A, Niu L, et al. Plasma Proteome Profiling to detect and avoid sample-related biases in biomarker studies. EMBO Mol Med. 2019 Nov 7;11(11):e10427.

163. Saifi MA, Bansod S, Godugu C. COVID-19 and fibrosis: Mechanisms, clinical relevance, and future perspectives. Drug Discov Today. 2022 Nov;27(11):103345.

164. Mayr CH, Simon LM, Leuschner G, Ansari M, Schniering J, Geyer PE, et al. Integrative analysis of cell state changes in lung fibrosis with peripheral protein biomarkers. EMBO Mol Med. 2021 Apr 9;13(4):e12871.

165. García-Abellán J, Padilla S, Fernández-González M, García JA, Agulló V, Andreo M, et al. Antibody Response to SARS-CoV-2 is Associated with Long-term Clinical Outcome in Patients with COVID-19: a Longitudinal Study. J Clin Immunol. 2021 Oct;41(7):1490–501.

166. Xu S-W, Ilyas I, Weng J-P. Endothelial dysfunction in COVID-19: an overview of evidence, biomarkers, mechanisms and potential therapies. Acta Pharmacol Sin. 2023 Apr;44(4):695–709.

167. Taeschler P, Cervia C, Zurbuchen Y, Hasler S, Pou C, Tan Z, et al. Autoantibodies in COVID-19 correlate with antiviral humoral responses and distinct immune signatures. Allergy. 2022 Aug;77(8):2415–30.

168. LeBien TW, Tedder TF. B lymphocytes: how they develop and function. Blood. 2008 Sep 1;112(5):1570–80.

169. Murphy K, Weaver C. Janeway's Immunobiology, 9th Edition. Berlin, Heidelberg: Springer Berlin Heidelberg; 2018.

170. Souroujon M, White-Scharf ME, Andreschwartz J, Gefter ML, Schwartz RS. Preferential autoantibody reactivity of the preimmune B cell repertoire in normal mice. J Immunol. 1988 Jun 15;140(12):4173–9.

171. Nemazee D. Does immunological tolerance explain the waste in the B-lymphocyte immune system? Experiment and theory. Ann N Y Acad Sci. 1995 Sep 29;764:397–401.

172. Merrell KT, Benschop RJ, Gauld SB, Aviszus K, Decote-Ricardo D, Wysocki LJ, et al. Identification of anergic B cells within a wild-type repertoire. Immunity. 2006 Dec;25(6):953–62.

173. Goodnow CC, Vinuesa CG, Randall KL, Mackay F, Brink R. Control systems and decision making for antibody production. Nat Immunol. 2010 Aug;11(8):681–8.

174. Nemazee D. Mechanisms of central tolerance for B cells. Nat Rev Immunol. 2017 May;17(5):281–94.

175. Nemazee DA, Bürki K. Clonal deletion of B lymphocytes in a transgenic mouse bearing anti-MHC class I antibody genes. Nature. 1989 Feb 9;337(6207):562–6.

176. Gay D, Saunders T, Camper S, Weigert M. Receptor editing: an approach by autoreactive B cells to escape tolerance. J Exp Med. 1993 Apr 1;177(4):999–1008.

177. Cooke MP, Heath AW, Shokat KM, Zeng Y, Finkelman FD, Linsley PS, et al. Immunoglobulin signal transduction guides the specificity of B cell-T cell interactions and is blocked in tolerant self-reactive B cells. J Exp Med. 1994 Feb 1;179(2):425–38.

178. Fulcher DA, Basten A. Reduced life span of anergic self-reactive B cells in a double-transgenic model. J Exp Med. 1994 Jan 1;179(1):125–34.

179. Erikson J, Radic MZ, Camper SA, Hardy RR, Carmack C, Weigert M. Expression of anti-DNA immunoglobulin transgenes in non-autoimmune mice. Nature. 1991 Jan 24;349(6307):331–4.

180. Aplin BD, Keech CL, de Kauwe AL, Gordon TP, Cavill D, McCluskey J. Tolerance through indifference: autoreactive B cells to the nuclear antigen La show no evidence of tolerance in a transgenic model. J Immunol. 2003 Dec 1;171(11):5890–900.

181. Fulcher DA, Lyons AB, Korn SL, Cook MC, Koleda C, Parish C, et al. The fate of self-reactive B cells depends primarily on the degree of antigen receptor engagement and availability of T cell help. J Exp Med. 1996 May 1;183(5):2313–28.

182. Shlomchik MJ. Sites and stages of autoreactive B cell activation and regulation. Immunity. 2008 Jan;28(1):18–28.

183. Martínez-Riaño A, Delgado P, Tercero R, Barrero S, Mendoza P, Oeste CL, et al. Recreation of an antigen-driven germinal center in vitro by providing B cells with phagocytic antigen. Commun Biol. 2023 Apr 20;6(1):437.

184. Setliff I, Shiakolas AR, Pilewski KA, Murji AA, Mapengo RE, Janowska K, et al. High-Throughput Mapping of B Cell Receptor Sequences to Antigen Specificity. Cell. 2019 Dec 12;179(7):1636-1646.e15.

185. Allard-Chamard H, Kaneko N, Bertocchi A, Sun N, Boucau J, Kuo H-H, et al. Extrafollicular IgD-CD27-CXCR5-CD11c- DN3 B cells infiltrate inflamed tissues in autoimmune fibrosis and in severe COVID-19. Cell Rep. 2023 Jun 27;42(6):112630.

186. Meednu N, Rangel-Moreno J, Zhang F, Escalera-Rivera K, Corsiero E, Prediletto E, et al. Dynamic spectrum of ectopic lymphoid B cell activation and hypermutation in the RA synovium characterized by NR4A nuclear receptor expression. Cell Rep. 2022 May 3;39(5):110766.

187. Tan C, Hiwa R, Mueller JL, Vykunta V, Hibiya K, Noviski M, et al. NR4A nuclear receptors restrain B cell responses to antigen when second signals are absent or limiting. Nat Immunol. 2020 Oct;21(10):1267–79.

188. Tsukumo S-I, Subramani PG, Seija N, Tabata M, Maekawa Y, Mori Y, et al. AFF3, a susceptibility factor for autoimmune diseases, is a molecular facilitator of immunoglobulin class switch recombination. Sci Adv. 2022 Aug 26;8(34):eabq0008.

189. Willis SN, Tellier J, Liao Y, Trezise S, Light A, O'Donnell K, et al. Environmental sensing by mature B cells is controlled by the transcription factors PU.1 and SpiB. Nat Commun. 2017 Nov 10;8(1):1426.

190. Mackay F, Woodcock SA, Lawton P, Ambrose C, Baetscher M, Schneider P, et al. Mice transgenic for BAFF develop lymphocytic disorders along with autoimmune manifestations. J Exp Med. 1999 Dec 6;190(11):1697–710.

191. Kremlitzka M, Mácsik-Valent B, Polgár A, Kiss E, Poór G, Erdei A. Complement receptor type 1 suppresses human B cell functions in SLE patients. J Immunol Res. 2016 Nov 17;2016:5758192.

192. Bhamidipati K, Silberstein JL, Chaichian Y, Baker MC, Lanz TV, Zia A, et al. CD52 Is Elevated on B cells of SLE Patients and Regulates B Cell Function. Front Immunol. 2020;11:626820.

193. Bernardes JP, Mishra N, Tran F, Bahmer T, Best L, Blase JI, et al. Longitudinal Multi-omics Analyses Identify Responses of Megakaryocytes, Erythroid Cells, and Plasmablasts as Hallmarks of Severe COVID-19. Immunity. 2020 Dec 15;53(6):1296-1314.e9.

194. Land WG. The Role of Damage-Associated Molecular Patterns in Human Diseases: Part I - Promoting inflammation and immunity. Sultan Qaboos Univ Med J. 2015 Feb;15(1):e9–21.

195. Bell SA, Faust H, Schmid A, Meurer M. Autoantibodies to C-reactive protein (CRP) and other acute-phase proteins in systemic autoimmune diseases. Clin Exp Immunol. 1998 Sep;113(3):327–32.

196. Piaggi S, Lorenzini E, Pratesi F, Migliorini P, Pompella A, Bruschi F, et al. Anti-glutathione S-transferase omega 1-1 (GSTO1-1) antibodies are increased during acute and chronic inflammation in humans. Clin Exp Immunol. 2022 Sep 29;209(3):305–10.

197. Matola AT, Józsi M, Uzonyi B. Overview on the role of complement-specific autoantibodies in diseases. Mol Immunol. 2022 Nov;151:52–60.

198. Jung I-H, Elenbaas JS, Alisio A, Santana K, Young EP, Kang CJ, et al. SVEP1 is a human coronary artery disease locus that promotes atherosclerosis. Sci Transl Med. 2021 Mar 24;13(586).

199. Qian W, Zhao M, Wang R, Li H. Fibrinogen-like protein 1 (FGL1): the next immune checkpoint target. J Hematol Oncol. 2021 Sep 15;14(1):147.

200. Le Voyer T, Parent AV, Liu X, Cederholm A, Gervais A, Rosain J, et al. Autoantibodies against type I IFNs in humans with alternative NF-κB pathway deficiency. Nature. 2023 Nov 8;623(7988):803–13.

201. Zaborek-Łyczba M, Łyczba J, Mertowska P, Mertowski S, Hymos A, Podgajna M, et al. The HLA-G Immune Checkpoint Plays a Pivotal Role in the Regulation of Immune Response in Autoimmune Diseases. Int J Mol Sci. 2021 Dec 12;22(24).

202. Schwiebert C, Kühnen P, Becker N-P, Welsink T, Keller T, Minich WB, et al. Antagonistic Autoantibodies to Insulin-Like Growth Factor-1 Receptor Associate with Poor Physical Strength. Int J Mol Sci. 2020 Jan 11;21(2).

203. Koether K, Besnard V, Sandig H, Carruthers A, Miranda E, Grootenboer-Mignot S, et al. Autoantibodies are associated with disease progression in idiopathic pulmonary fibrosis. Eur Respir J. 2023 May 18;61(5).

204. Kattah NH, Kattah MG, Utz PJ. The U1-snRNP complex: structural properties relating to autoimmune pathogenesis in rheumatic diseases. Immunol Rev. 2010 Jan;233(1):126–45.

205. Wichmann I, Montes-Cano MA, Respaldiza N, Alvarez A, Walter K, Franco E, et al. Clinical significance of anti-multiple nuclear dots/Sp100 autoantibodies. Scand J Gastroenterol. 2003 Sep;38(9):996–9.

206. Knight JS, Kanthi Y. Mechanisms of immunothrombosis and vasculopathy in antiphospholipid syndrome. Semin Immunopathol. 2022 May;44(3):347–62.

207. Serrano M, Espinosa G, Serrano A, Cervera R. COVID-19 and the antiphospholipid syndrome. Autoimmun Rev. 2022 Dec;21(12):103206.

208. Sun Q, Oltra E, Dijck-Brouwer DAJ, Chillon TS, Seemann P, Asaad S, et al. Autoantibodies to selenoprotein P in chronic fatigue syndrome suggest selenium transport impairment and acquired resistance to thyroid hormone. Redox Biol. 2023 Sep;65:102796.

209. Thibord F, Song C, Pattee J, Rodriguez BAT, Chen M-H, O'Donnell CJ, et al. FGL1 as a modulator of plasma D-dimer levels: Exome-wide marker analysis of plasma tPA, PAI-1, and D-dimer. J Thromb Haemost. 2021 Aug;19(8):2019–28.

210. Piaggi S, Marchi E, Carnicelli V, Zucchi R, Griese M, Hector A, et al. Airways glutathione S-transferase omega-1 and its A140D polymorphism are associated with severity of inflammation and respiratory dysfunction in cystic fibrosis. J Cyst Fibros. 2021 Nov;20(6):1053–61.

211. Elenbaas JS, Pudupakkam U, Ashworth KJ, Kang CJ, Patel V, Santana K, et al. SVEP1 is an endogenous ligand for the orphan receptor PEAR1. Nat Commun. 2023 Feb 15;14(1):850.

212. Winkler MJ, Müller P, Sharifi AM, Wobst J, Winter H, Mokry M, et al. Functional investigation of the coronary artery disease gene SVEP1. Basic Res Cardiol. 2020 Nov 13;115(6):67.

213. Zhang M, Jing Y, Xu W, Shi X, Zhang W, Chen P, et al. The C-type lectin COLEC10 is predominantly produced by hepatic stellate cells and involved in the pathogenesis of liver fibrosis. Cell Death Dis. 2023 Nov 30;14(11):785.

214. Di Cataldo I, Proietto A, Coppolino I, Cannavò MF, Cotroneo A, Bello FL, et al. Bacterial infections in the lungs of patients with systemic autoimmune diseases. Infections in systemic autoimmune diseases: risk factors and management. Elsevier; 2020. p. 1–11.

215. Sadeghi Dousari A, Hosseininasab SS, Sadeghi Dousari F, Fuladvandi M, Satarzadeh N. The impact of COVID-19 on liver injury in various age. World J Virol. 2023 Mar 25;12(2):91–9.

216. Zhang Q, Bastard P, Liu Z, Le Pen J, Moncada-Velez M, Chen J, et al. Inborn errors of type I IFN immunity in patients with life-threatening COVID-19. Science. 2020 Oct 23;370(6515).

217. Charles A Janeway J, Travers P, Walport M, Shlomchik MJ. The Humoral Immune Response. 2001;

218. Damoiseaux J, Dotan A, Fritzler MJ, Bogdanos DP, Meroni PL, Roggenbuck D, et al. Autoantibodies and SARS-CoV2 infection: The spectrum from association to clinical implication: Report of the 15th Dresden Symposium on Autoantibodies. Autoimmun Rev. 2022 Mar;21(3):103012.

219. Castleman MJ, Stumpf MM, Therrien NR, Smith MJ, Lesteberg KE, Palmer BE, et al. SARS-CoV-2 infection relaxes peripheral B cell tolerance. J Exp Med. 2022 Jun 6;219(6).

220. Kuri-Cervantes L, Pampena MB, Meng W, Rosenfeld AM, Ittner CAG, Weisman AR, et al. Comprehensive mapping of immune perturbations associated with severe COVID-19. Sci Immunol. 2020 Jul 15;5(49).

221. Wardemann H, Yurasov S, Schaefer A, Young JW, Meffre E, Nussenzweig MC. Predominant autoantibody production by early human B cell precursors. Science. 2003 Sep 5;301(5638):1374–7.

222. Davis CW, Jackson KJL, McElroy AK, Halfmann P, Huang J, Chennareddy C, et al. Longitudinal analysis of the human B cell response to ebola virus infection. Cell. 2019 May 30;177(6):1566-1582.e17.

223. Lau CM, Broughton C, Tabor AS, Akira S, Flavell RA, Mamula MJ, et al. RNA-associated autoantigens activate B cells by combined B cell antigen receptor/Toll-like receptor 7 engagement. J Exp Med. 2005 Nov 7;202(9):1171–7.

224. Jenks SA, Cashman KS, Zumaquero E, Marigorta UM, Patel AV, Wang X, et al. Distinct Effector B Cells Induced by Unregulated Toll-like Receptor 7 Contribute to Pathogenic Responses in Systemic Lupus Erythematosus. Immunity. 2018 Oct 16;49(4):725-739.e6.

225. Marshak-Rothstein A, Rifkin IR. Immunologically active autoantigens: the role of toll-like receptors in the development of chronic inflammatory disease. Annu Rev Immunol. 2007;25:419–41.

226. Woodruff MC, Ramonell RP, Haddad NS, Anam FA, Rudolph ME, Walker TA, et al. Dysregulated naive B cells and de novo autoreactivity in severe COVID-19. Nature. 2022 Nov;611(7934):139–47.

227. Dema B, Charles N. Autoantibodies in SLE: specificities, isotypes and receptors. Antibodies (Basel). 2016 Jan 4;5(1):2.